The optimal patient-specific placement of the reverse total shoulder component

by

Sven Delport

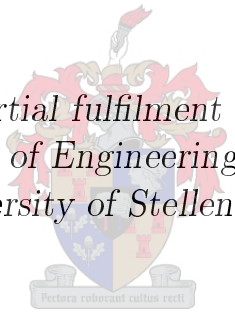

Thesis presented in partial fulfilment of the requirements for the degree of Master of Engineering (Mechanical) at the University of Stellenbosch

Supervisor: Prof. C. Scheffer

March 2015

Declaration

By submitting this thesis electronically, I declare that the entirety of the work contained therein is my own, original work, that I am the sole author thereof (save to the extent explicitly otherwise stated), that reproduction and publication thereof by Stellenbosch University will not infringe any third party rights and that I have not previously in its entirety or in part submitted it for obtaining any qualification.

Signature: .....
S. Delport

Date: November 2014 .....

Abstract

The optimal patient-specific placement of the reverse total shoulder component

S. Delport

Thesis: MEng Research (Mechanical)

March 2015

Reverse total shoulder arthroplasty is used as the treatment for arthritic rotator cuff deficient shoulders. Some of the most common complications of a reverse shoulder arthroplasty are scapular notching, glenoid dissociations, glenohumeral dislocation, loosening or dissociation of the humeral component and nerve injury. Clinical outcomes are dependent on the preoperative diagnosis, the function of the deltoid and remaining rotator cuff muscles, biomechanical design of the prosthesis, and the orientation and placement of the reverse shoulder component. This study aims to optimize the patient-specific placement of a reverse shoulder component. A simulation software package was developed that can be used to determine the optimal placement of the reverse shoulder prosthesis for a specific patient. This is achieved by maximizing the humerothoracic range of motion and minimizing the adduction deficit. The motion of the simulation model is driven by shoulder complex motion equations adjusted for each patient. This data was obtained from literature with the motion of the arm fixed to the coronal, scapular and sagittal elevation planes. The influence of the various components of the Tornier Aequalis® - Reversed II system, together with changing the glenoid component inclination and humeral component retroversion, was investigated. This allowed the simulation software to be verified and validated, as well as applying the insight and knowledge gained to a case study. Further simulations evaluated a design change of the humeral component neck-shaft angle from the standard 155° to 145° or 165°. The reverse shoulder simulation software provides accurate patient-specific Three Dimensional (3D) pre-operative planning and shoulder complex motion simulation.

Uittreksel

Die optimale pasiënt-spesifieke plasing van die prostesekomponent by 'n omgekeerde volledige skouervervanging

S. Delport

Tesis: MIng Navorsing (Meganies)
Maart 2015

Omgekeerde volledige skouerartoplastie word as behandeling van ontsteking in gewrigsomhulsel-aangetaste skouers gebruik. Onder die algemeenste komplikasies van 'n omgekeerde skouergewrig-operasie is kepe in die skouerblad (skapulier), lostrekkings of onthegting van die gewrigskom (glenoïede), ontwrigting van die boarm/skouergewrig, die loskom of onthegting van die boarmbeen en beskadiging van senuwees. Mediese resultate is afhanklik van diagnose voor die operasie, die werking van die driehoekspier (deltoïede) en oorblywende draaispiere, die biomeganiese ontwerp van die prostese en die oriëntasie en plasing van die omgekeerde skouerkomponent. Hierdie studie is gemik op die beste pasiënt-spesifieke plasing van die omgekeerde skouerkomponent. Die simulasie-sagtewarepakket wat ontwikkel is, kan gebruik word om die optimale plasing van die omgekeerde skouerprostese in die geval van 'n spesifieke pasiënt te bepaal. Dit word gedoen deur die bewegingsvermoë van die bo-armbeen te maksimaliseer en die gebrekkige werking van die trekspiere te minimaliseer. Die werking van die simulasiemodel word gedryf deur die beweging van skouerkomponente te vergelyk, aangepas vir elke pasiënt. Hierdie data is verkry uit literatuur en die koppeling van die arm se beweging aan die belangrikste, skouerblad- en sagittale elevasievlakke. Die invloed van die onderskeie komponente van die Tornier Aequalis® - Reversed II-stelsel is saam met die verandering van die gewrigskom-komponent se helling en bo-armkomponent se terugstoting ondersoek. Sodoende kon die simulasie-sagteware nagegaan, bevestig en geldig verklaar word; en die insig en kennis wat verkry is op 'n gevallestudie toegepas word. Met verdere simulasies is 'n ontwerpwysiging geëvalueer waar die skouerkomponent se beenpyphoek vanaf die standaard van 155° na 145° of 165° verander is. Die omgekeerde skouersimulasiesagteware

maak akkurate pasiëntspesifieke driedimensionele (3D) beplanning voor 'n operasie en simulasie van die bewegings skouerdele moontlik.

Acknowledgements

I would like to express my sincerest gratitude to the following people who have contributed to the completion of this study:

- To my supervisor, Prof. Cornie Scheffer for his constant guidance, advice and motivation throughout the year.
- To Dr. Joe De Beer, for his invaluable clinical experience and collaboration to obtain useful clinical data.

Dedications

Honour and glory to Jesus Christ for His support and guidance

Contents

List of Figures

List of Tables

Nomenclature

Abbreviations

2D	Two Dimensional
3D	Three Dimensional
AA	Angulus Acromialis
AC	Acromioclavicular
AI	Angulus Inferior
ANOVA	Analysis Of Variance
C7	7^{th} Cervical Vertebra
CAD	Computer Assisted Design
COR	Centre Of Rotation
CT	Computed Tomography
DICOM	Digital Imaging and Communication
GH	Glenohumeral Rotation Centre
GUI	Graphical User Interface
GUIDE	Graphical User Interface Design Environment
HCS	Humerus Coordinate System
IJ	Incisura Jugularis
ISB	International Society of Biomechanics
LE	Lateral Epicondyle
ME	Medial Epicondyle
PSI	Patient-Specific Instrumentation

PX Processus Xiphoideus

R^2 Coefficient of Determination

ROM Range Of Motion

RS^3 Reverse Shoulder Simulation Software

RSA Reverse Shoulder Arthroplasty

SC Sternoclavicular

SCS Scapula Coordinate System

STL Stereolithography

T8 8^{th} Thoracic Vertebra

TS Trigonum Spinae Scapulae

TSA Total Shoulder Arthroplasty

WCS World Coordinate System

Subscripts

APR_a Coronal Plane Anterior/Posterior Rotation

APR_b Scapula Plane Anterior/Posterior Rotation

APR_c Sagittal Plane Anterior/Posterior Rotation

APT_a Coronal Plane Anterior/Posterior Tilting

APT_b Scapula Plane Anterior/Posterior Tilting

APT_c Sagittal Plane Anterior/Posterior Tilting

ED_a Coronal Plane Elevation/Depression

ED_b Scapula Plane Elevation/Depression

ED_c Sagittal Plane Elevation/Depression

IER_a Coronal Plane Internal/External Rotation

IER_b Scapula Plane Internal/External Rotation

IER_c Sagittal Plane Internal/External Rotation

PR_a Coronal Plane Protraction/Retraction

PR_b Scapula Plane Protraction/Retraction

PR_c Sagittal Plane Protraction/Retraction

UDR_a Coronal Plane Upward/Downward Rotation

UDR_b Scapula Plane Upward/Downward Rotation

UDR_c Sagittal Plane Upward/Downward Rotation

Symbols

γ	Humeral Component Neck-shaft Angle	[°]
ψ	Humeral Component Retroversion Angle	[°]
φ	Glenoid Component Inclination Angle	[°]

1. Introduction

1.1 Background

Current shoulder arthroplasty can be attributed to Charles Neer II, who introduced a hemiarthroplasty in 1955 for fractures and dislocations of the humeral head (NeerII, 1955). This was later on also applied to arthritic shoulders and in 1974 Neer developed a polyethylene glenoid component (NeerII, 1974) to introduce the unconstrained Total Shoulder Arthroplasty (TSA). The TSA has since then been used in the management and treatment of many traumatic and arthritic conditions of the shoulder.

However, treatment of an arthritic rotator cuff deficient shoulder has proven a surgical challenge. A hemiarthroplasty for cuff deficient arthritis of the shoulder has produced somewhat unpredictable results (Williams and Rockwood, 1996; Favard *et al.*, 2000; Sanchez-Sotelo *et al.*, 2001). Furthermore, TSA has been abandoned for such cases due to proximal migration of the prosthesis with eventual superior impingement, as well as early glenoid component loosening.

Between 1970 and 1980 many, including Neer, attempted to develop a prosthesis that would stabilize a rotator cuff deficient shoulder. Several constrained reverse shoulder implants were developed, yet none showed any promising results and were later abandoned. It was only in 1985 when Professor Paul Grammont conceptualized the idea of medialization and lowering of the Centre Of Rotation (COR) of the reverse shoulder implant. He developed a semi-contrained reverse shoulder prosthesis that had a hemispherical glenosphere, which was placed inferiorly on the glenoid (Grammont and Baulot, 1993). Grammont's design demonstrated promising early results with an improvement in functionality (Grammont *et al.*, 1987).

Further studies, involving 261 shoulders and an overall average duration of 3 years of follow-up, have shown improvement after a Reverse Shoulder Arthroplasty (RSA) in abduction, forward flexion and in pain relief. Despite these positive short-term results, there have been a relatively high number of complications (mean, 24.4 %, range, 6.25 % to 50 %) (Sperling *et al.*, 2012). Sperling *et al.* (2012) listed some of the most common complications of a RSA to be scapular notching, glenoid dissociations, glenohumeral dislocation, loosening or dissociation of the humeral component and nerve injury.

Recent studies were aimed at better understanding the various factors in-

volved in a RSA and how to improve the impact by said factors in order to achieve better long-term clinical outcomes. Clinical outcomes are dependent on the preoperative diagnosis, the function of the deltoid and remaining rotator cuff muscles, biomechanical design of the prosthesis, and the orientation and placement of the reverse shoulder component (DeFranco and Walch, 2011).

1.2 Motivation

The author has previous experience in the orthopaedic, especially arthroplasty, field. His previous work includes the design of Patient-Specific Instrumentation (PSI) used by orthopaedic surgeons to quickly and accurately perform the required cuts and/or insert the K-wire in the desired orientation during arthroplasties for the hip, knee or shoulder. This enables the surgeon to place the prosthesis at the desired pre-determined orientation. A hip clinical trial and a shoulder cadaver trial have shown very promising results with the accuracy obtained by these PSI.

However, it was found that due to the relatively recent development of the reverse shoulder prosthesis there is a limited understanding of its long-term effects. Previous studies looked at the effects of the placement of the glenoid and humeral component on the functionality and survival rate of the prosthesis (Nyffeler *et al.*, 2005; Gutiérrez *et al.*, 2008; Favre *et al.*, 2010; Gulotta *et al.*, 2012). These studies only looked at glenohumeral motion. This simplified their approach, but ignored the effects of the scapulohumeral rhythm. In most of these studies only a single elevation plane was considered when determining the Range Of Motion (ROM). They also attempted to standardize the effects of the placement of the prosthesis for all scapulae and humeri.

Dr. Joe De Beer[1] acted as consultant on this study. With the author's background in patient-specific designs and the support of Dr De Beer, it was believed that an optimal prosthesis placement can be determined for each patient undergoing a RSA, which will improve functionality and increase prosthesis lifetime. The complete shoulder complex motion and not only the glenohumeral motion, as well as three distinct elevation planes would be included in order to determine said placement.

1.3 Objectives

This study will aim to optimize the patient-specific placement of a reverse shoulder component. A simulation software package is to be developed that will determine the optimal placement of such a prosthesis for a specific patient.

[1] One of the leading shoulder specialists in South Africa and director of the Cape Shoulder Institute.

This is achieved by maximizing the combined humerothoracic ROM and minimizing the combined adduction deficit within specified prosthesis placement constraints. Literature, as well as the experience and contribution from Dr De Beer will be used to determine these constraints, ultimately determining the allowable placement range within which the optimal placement of the reverse shoulder prosthesis is to be found. The simulation software will also be used to determine the general influence of the placement and design of the reverse shoulder components on the humerothoracic ROM and adduction deficit.

The objectives of this study can therefore be summarised as:

- Develop a software simulation package to determine the optimal patient-specific placement of the reverse shoulder component.
- Investigate and determine the influence of the placement of the reverse shoulder glenoid components and the reverse shoulder humeral components on humerothoracic ROM and adduction deficit.
- Investigate and determine the influence of the design of the reverse shoulder glenoid components and the reverse shoulder humeral components on humerothoracic ROM and adduction deficit.

The expected contributions of this study will allow surgeons to quickly and accurately determine the optimal positioning of the reverse shoulder components. More inexperienced surgeons will be able to attempt a RSA with greater confidence. Improved pre-operative planning will reduce surgery time and cost. Finally, it is expected that the results of this study may improve prosthesis survival rates and long-term clinical outcomes.

1.4 Thesis Outline

Chapter 2 discusses the shoulder complex and provides the relevant anatomical terms and definitions required by later chapters. A review is also given of the history of reverse shoulder arthroplasty. This consists of the evolution of the reverse shoulder prosthesis, its current complications and the previous work performed to understand and mitigate these problems. The chapter concludes with related work conducted to optimize the patient-specific placement of the reverse shoulder component.

Chapter 3 presents the development of the reverse shoulder simulation software. The shoulder complex motion used by the software is defined and the work required to generate the necessary input data is also outlined. Lastly, an in-depth discussion of the work flow and functionality of the software is provided.

The effects of the Tornier Aequalis® - Reversed II components, as well as proposed design changes, on the shoulder complex motion are assessed in

Chapter 4. The findings are used to verify and validate the simulation software. The simulation results are also applied to a case study to determine the optimal placement of the reverse shoulder component.

Finally, Chapter 5 contains an outline of the research that was done, results that were obtained and recommendations made for future work.

2. Literature Review

In this chapter a review is presented of a reverse shoulder arthroplasty. Attention is specifically given to the anatomy and biomechanics of the shoulder complex, the history and development of the reverse shoulder components, the complications experienced with the RSA up to date and finally, previous work completed with respect to obtaining the objectives mentioned in Chapter 1.

2.1 Shoulder Complex

The shoulder is one of the most complex joints in the human body. It consists of the clavicle, scapula, and humerus; the glenohumeral and Acromioclavicular (AC) joints that unite them and lastly, the Sternoclavicular (SC) joint, which is the only connection of the complex to the axial skeleton. The scapulothoracic joint is also included in the anatomical description of the shoulder complex.

The shoulder complex contains muscles that stabilize the scapula and muscles that help move the arm. The rhomboid, trapezius and serratus anterior muscles are a few of the scapular stabilizing muscles. The pectoralis major, the deltoid and the rotator cuff muscles are some of the muscles that move the arm at the glenohumeral joint.

Complete shoulder motion is dependent on coordinated, synchronous motion in all joints of the shoulder complex (Culham and Peat, 1993).

2.1.1 Shoulder Anatomy

Figure 2.1 illustrates the various bones of the shoulder complex. The joints are more clearly illustrated in Figure 2.2.

The glenohumeral joint is formed where the humeral head of the humerus (upper arm bone) fits onto the glenoid of the scapula (shoulder blade), like a ball and socket. The AC joint is the junction between the acromion of the scapula and the distal end of the clavicle (collar bone). The SC joint occurs between the proximal end of the clavicle and the clavicular notch at the top of the sternum (breast bone).

For the purpose of this work, attention is given to the four rotator cuff muscles, which are the subscapularis, supraspinatus, infraspinatus and teres minor, and the deltoid muscle. These are depicted in Figure 2.3.

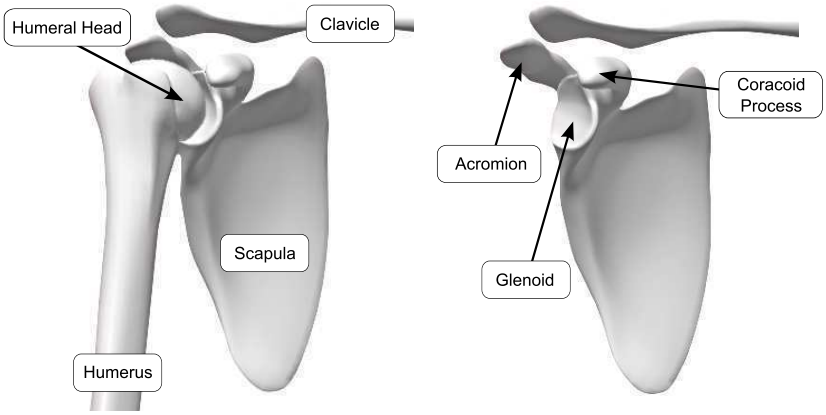

Figure 2.1: Bones of the Shoulder Complex

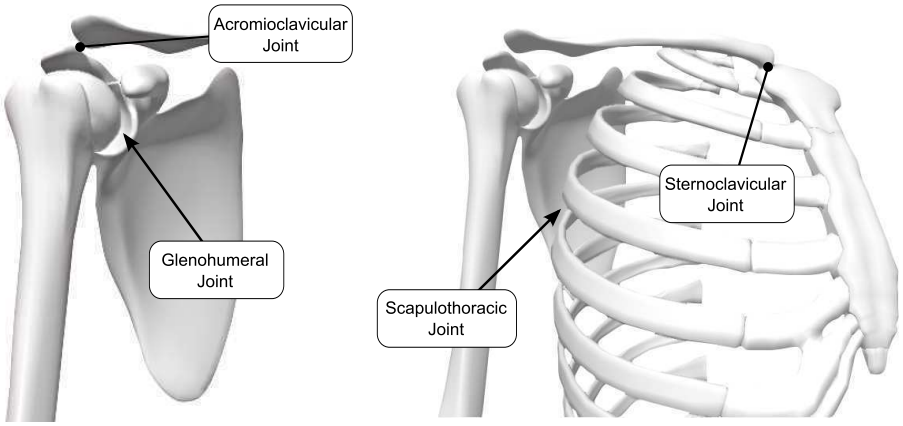

Figure 2.2: Joints of the Shoulder Complex

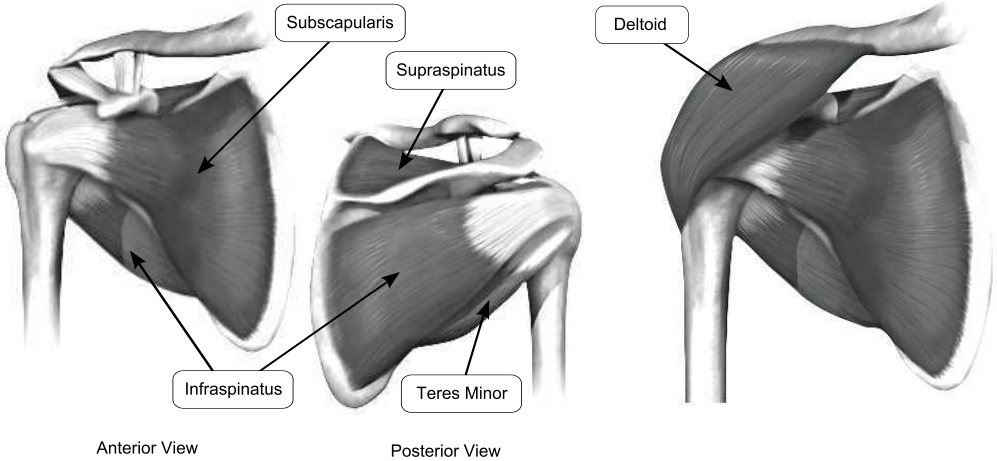

Figure 2.3: Muscles of the Shoulder Complex

The scapula is connected to the axial skeleton through the SC and AC joints. The scapula plane, the yz-plane of the second Scapula Coordinate System (SCS) described in Section 2.1.3, is approximately perpendicular to the plane of the glenoid surface. At rest, the scapula lies obliquely between the coronal and sagittal planes, rotated internally between 30 ° to 45 °, anterior to the coronal plane (Figure 2.4(a)). It also has a slight anterior tilt in the sagittal plane (Figure 2.4(b)).

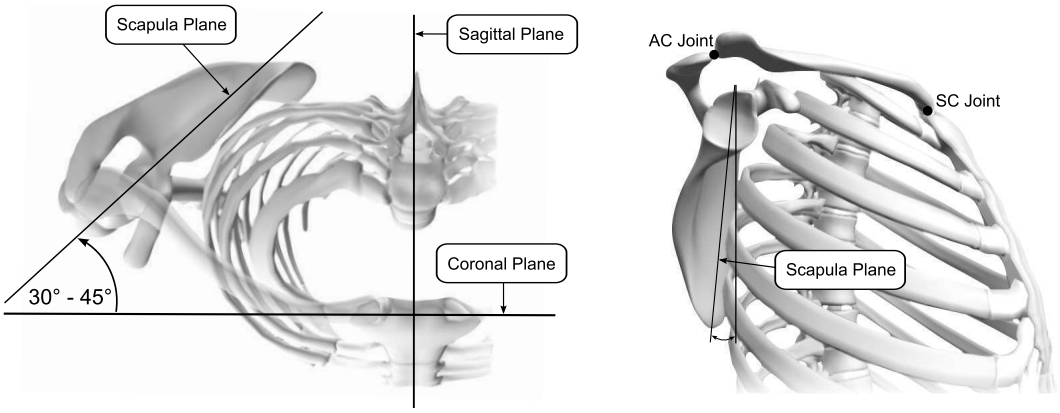

(a) Internal Rotation at Rest (b) Anterior Tilt at Rest

Figure 2.4: Scapula Rest Position

2.1.2 Anatomic References

Before any motion of the shoulder complex can accurately be described the anatomic reference terms are explained.

The anatomic references used throughout this work are listed in Table 2.1 and illustrated in Figures 2.5 and 2.6.

In order to facilitate communication among researchers and ensure the repeatability of experimental work, it is important that the definitions of the coordinate systems used are clearly stated and are consistent with the definitions used in previous work. Figures 2.7, 2.9 and 2.10 show the definition of the coordinate systems of the thorax, scapula and humerus, respectively, and are described below.

Table 2.1: Anatomic Reference Terms

	Term	Definition
Planes	Coronal	Vertical plane dividing the body into front and back
	Sagittal	Vertical plane dividing the body into left and right
	Transverse	Horizontal plane dividing the body into upper and lower
Translations	Anterior	Forwards
	Posterior	Backwards
	Medial	Toward the middle or inside
	Lateral	Toward the outside, left or right
	Superior	Above
	Inferior	Below
	Proximal	Towards the beginning or torso
	Distal	Further from the beginning or torso
Rotations	Abduction	Motion away from mid-line of body
	Adduction	Motion towards mid-line of body
	Flexion	Motion decreasing joint angle
	Extension	Motion increasing joint angle
	Internal	Inward rotation
	External	Outward rotation

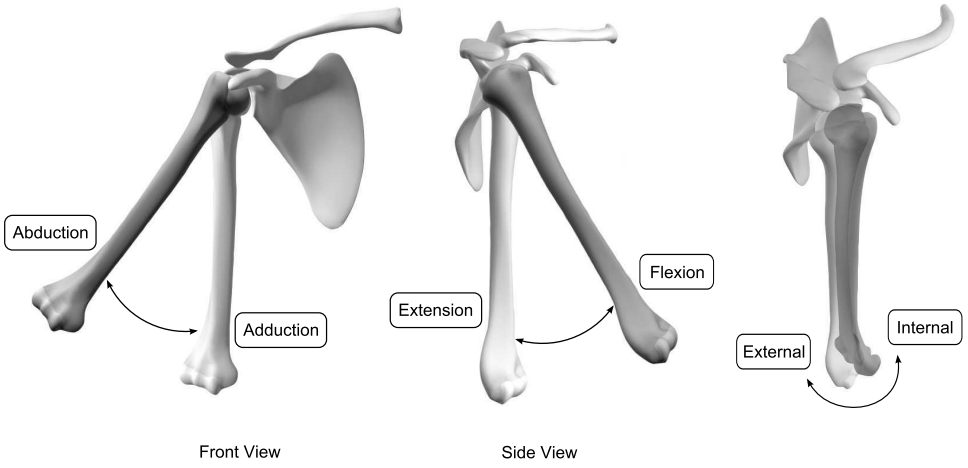

Figure 2.5: Anatomic Reference Rotations of the Shoulder

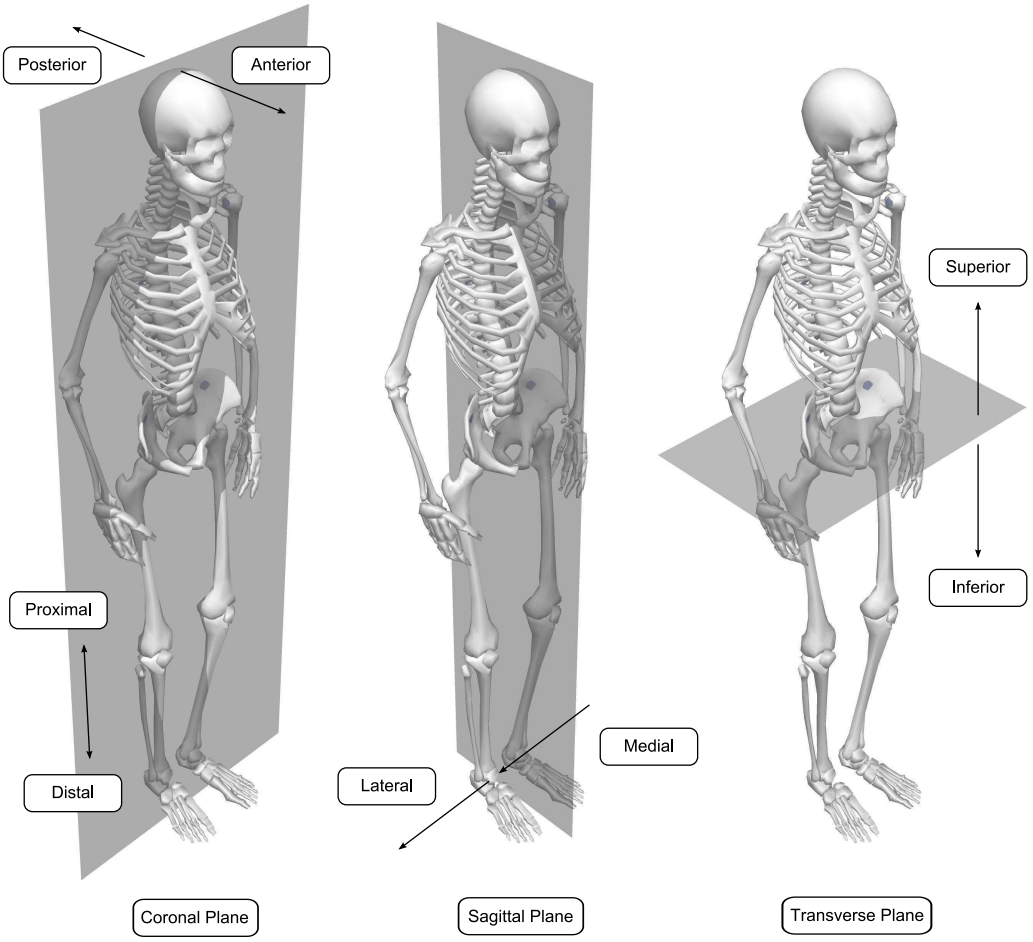

Figure 2.6: Anatomic Reference Planes and Translations of the Human Body (Illustration: Van der Merwe (2013))

2.1.3 Shoulder Coordinate Systems

The various relevant skeletal coordinate systems used throughout this work are defined and described below.

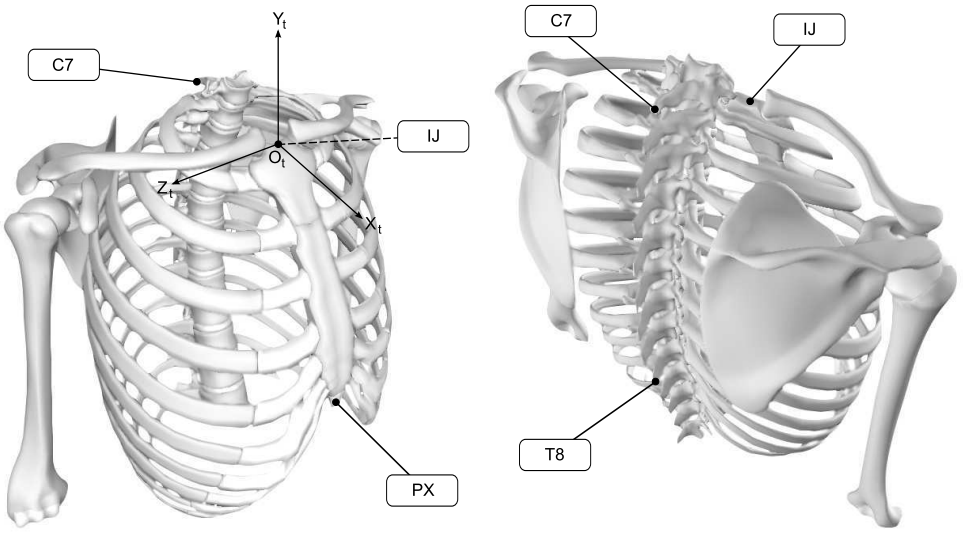

Figure 2.7: Thorax Coordinate System

Thorax Coordinate System (TCS):

Terminology:

IJ: Deepest point of the Incisura Jugularis (suprasternal notch).

PX: Processus Xiphoideus (xiphoid process), the most caudal point on the sternum.

$C7$: Processus Spinosus (spinous process) of the 7^{th} cervical vertebra.

$T8$: Processus Spinosus (spinous process) of the 8^{th} thoracic vertebra.

TCS definition:

O_t: The origin coincident with IJ.

Y_t: The line connecting the midpoint between PX and T8 and the midpoint between IJ and C7, pointing superiorly.

Z_t: The line perpendicular to the plane formed by IJ, C7, and the midpoint between PX and T8, pointing laterally.

X_t: The line perpendicular to the Z_t- and Y_t-axis, pointing anteriorly.

The TCS is assumed to be static with respect to the motion of the scapula and the humerus.

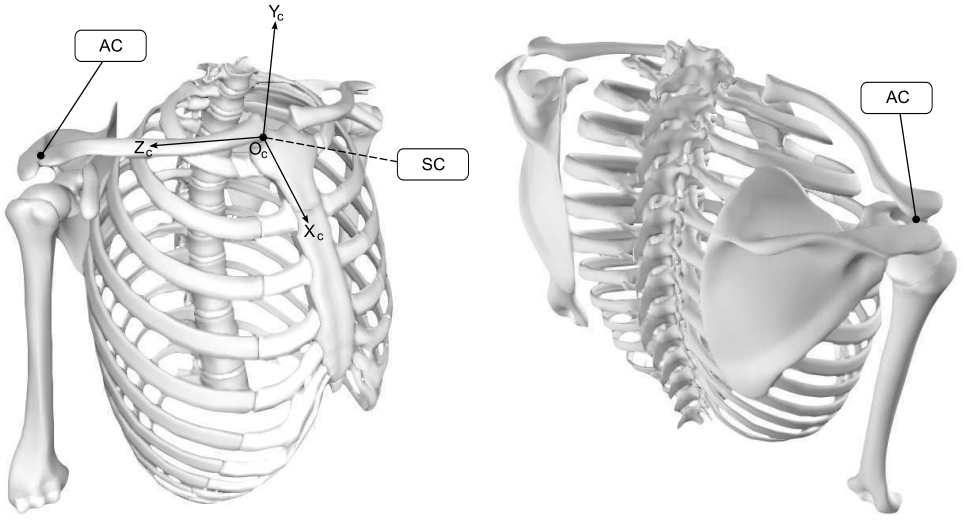

Figure 2.8: Clavicle Coordinate System (Right)

Clavicle Coordinate System (CCS):

Terminology:

SC: The most ventral point on the sternoclavicular joint.

AC: The most dorsal point on the acromioclavicular joint (shared with the scapula).

CCS definition:

O_c: The origin coincident with SC.

Z_c: The line connecting SC and AC, pointing to AC.

X_c: The line perpendicular to Z_c and Y_t, pointing anteriorly.

Y_c: The line perpendicular to the X_c- and Z_c-axis, pointing superiorly.

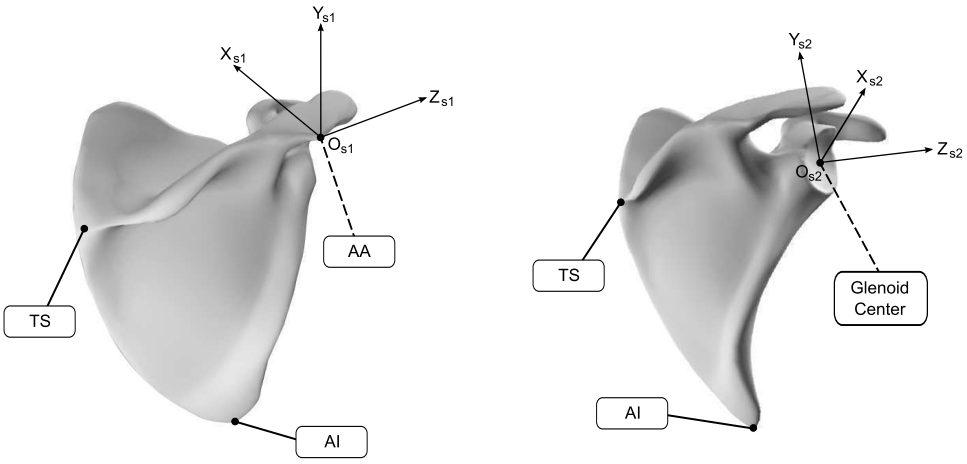

(a) SCS_1 (b) SCS_2

Figure 2.9: Scapula Coordinate Systems (Right)

Scapula Coordinate Systems (SCSs):

Terminology:

AA: Angulus Acromialis (acromial angle), the most laterodorsal point of the scapula.

TS: Trigonum Spinae Scapulae (root of the spine), the midpoint of the triangular surface on the medial border of the scapula in line with the scapula spine.

AI: Angulus Inferior (inferior angle), the most caudal point of the scapula.

Glenoid centre: The centre point of the glenoid surface.

SCS_1 definition:

O_{s1}: The origin coincident with AA.

Z_{s1}: The line connecting TS and AA, pointing to AA.

X_{s1}: The line perpendicular to the plane formed by AI, AA, and TS, pointing anteriorly.

Y_{s1}: The line perpendicular to the X_{s1}- and Z_{s1}-axis, pointing superiorly.

The first SCS is consistent with the coordinate system as defined by the International Society of Biomechanics (ISB) (Wu *et al.*, 2005).

SCS_2 definition:

O_{s2}: The origin coincident with the glenoid centre.

Z_{s2}: The line connecting TS and the glenoid centre, pointing to the glenoid centre.

X_{s2}: The line perpendicular to the plane formed by AI, TS, and the glenoid centre, pointing anteriorly.

Y_{s2}: The line perpendicular to the X_{s2}- and Z_{s2}-axis, pointing superiorly.

The second SCS is consistent with the coordinate system as defined by Friedman *et al.* (1992) for Two Dimensional (2D) Computed Tomography (CT) slices, which was later on more accurately defined by Kwon *et al.* (2005) for 3D space.

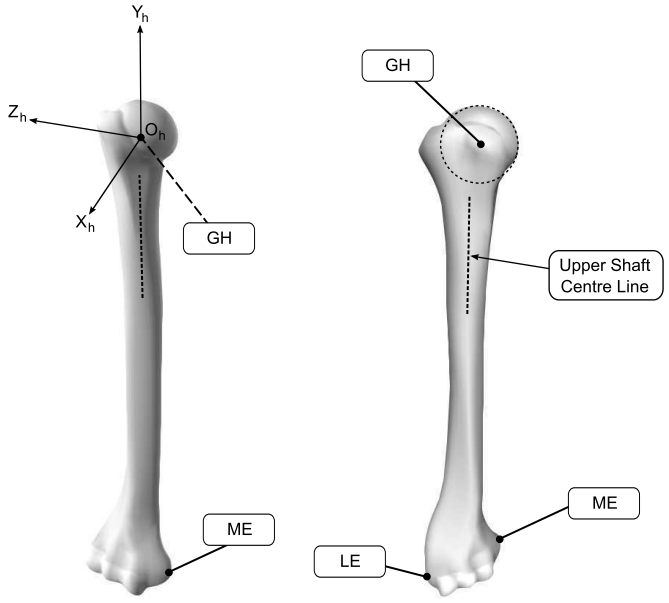

Figure 2.10: Humerus Coordinate System (Right)

Humerus Coordinate System (HCS):

Terminology:

GH: Glenohumeral rotation centre.

LE: Lateral Epicondyle, the most caudal point on the lateral epicondyle.

ME: Medial Epicondyle, the most caudal point on the medial epicondyle.

HCS definition:

O_h: The origin coincident with GH.

Y_h: The line parallel to the centre line of the upper shaft, pointing superiorly.

X_h: The line produced by the cross product between the line from LE to ME and the upper shaft centre line, pointing anteriorly.

Z_h: The line perpendicular to the X_h- and Y_h-axis, pointing laterally.

The HCS is consistent with the coordinate system used by Boileau and Walch (1997).

2.1.4 Shoulder Anatomical Angles

The shoulder anatomical angles referenced throughout this study are the glenoid and humerus anatomical angles.

2.1.4.1 Glenoid Anatomical Angles

The glenoid has a mean length and width of 37.8 mm (range, 32.5 mm to 43.1 mm) and 26.8 mm (range, 21.8 mm to 31.8 mm), respectively. It has an average anteversion of 1.1° (range, −6.2° to 4°) and an average inclination of 4.2° (range, −7° to 15.8°) (Kwon *et al.*, 2005).

The glenoid anatomical version and inclination angles are calculated as the angles between the glenoid surface normal and the planes of the SCS_2. Figures 2.11(a) and 2.11(b) demonstrate the glenoid version and inclination angles, respectively. Anteversion is when the glenoid surface faces more anteriorly, whereas retroversion is when the glenoid surface faces more posteriorly. Superior inclination is found when the glenoid surface points more superiorly

and conversely, inferior inclination is when the glenoid surface points more inferiorly.

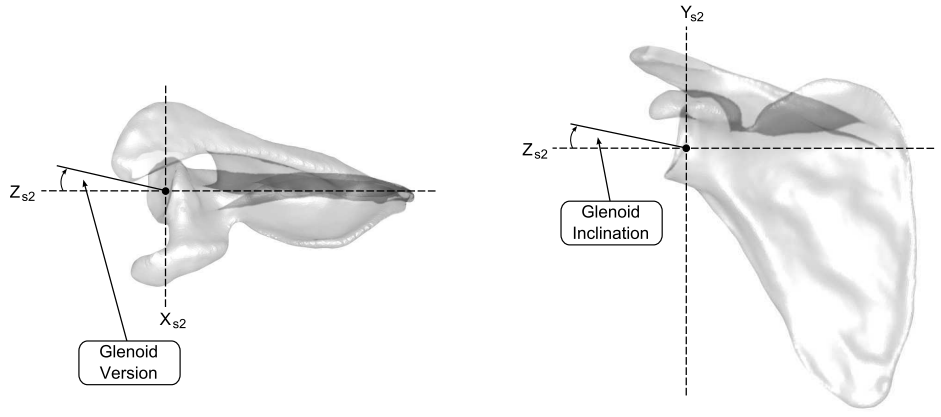

(a) Glenoid Version (b) Glenoid Inclination

Figure 2.11: Glenoid Anatomical Angles

2.1.4.2 Humerus Anatomical Angles

The humerus articular surface has a radius of curvature between 35 mm to 55 mm. The joint surface has a neck-shaft angle between 130° to 150° with the upper shaft of the humerus (Figure 2.12(a)) and is retroverted about 15° to 25° (Boileau *et al.*, 2008) (Figure 2.12(b)).

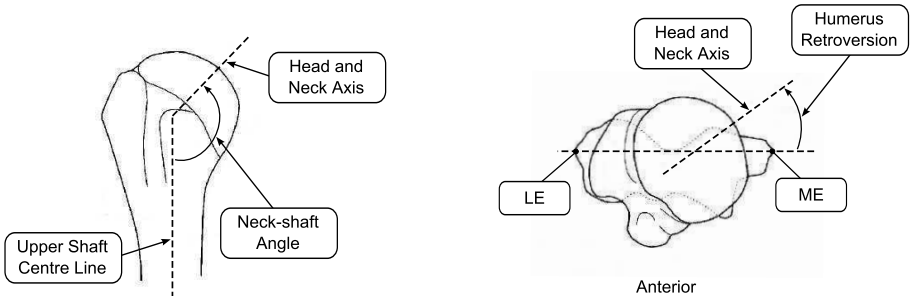

(a) Humerus Neck-shaft Angle (b) Humerus Retroversion

Figure 2.12: Humerus Anatomical Angles

2.1.5 Shoulder Complex Motion

Shoulder complex motion can be described by the sternoclavicular, the scapulothoracic and the humerothoracic motion of the shoulder.

2.1.5.1 Sternoclavicular Motion

Motion of the clavicle relative to the sternum was defined as protraction/ retraction about the superior axis, elevation/depression about the anterior axis, and anterior/posterior rotation about the lateral axis of the TCS (Ebaugh *et al.*, 2005). All rotations occur around the SC joint. Figure 2.13 depicts the directions for protraction (a) (superior view), elevation (b) (anterior view) and posterior rotation (c) (anterior view), respectively. Rotations of the clavicle are used to describe the position of the scapula on the thorax.

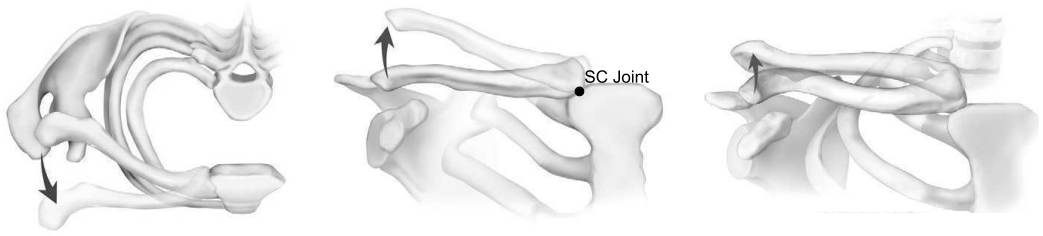

(a) Protraction (b) Elevation (c) Posterior Rotation

Figure 2.13: Rotation of the Clavicle (Illustration: Ludewig *et al.* (2009))

2.1.5.2 Scapulothoracic Motion

Motion of the scapula relative to the thorax is described by three rotary motions around the various TCS axes.

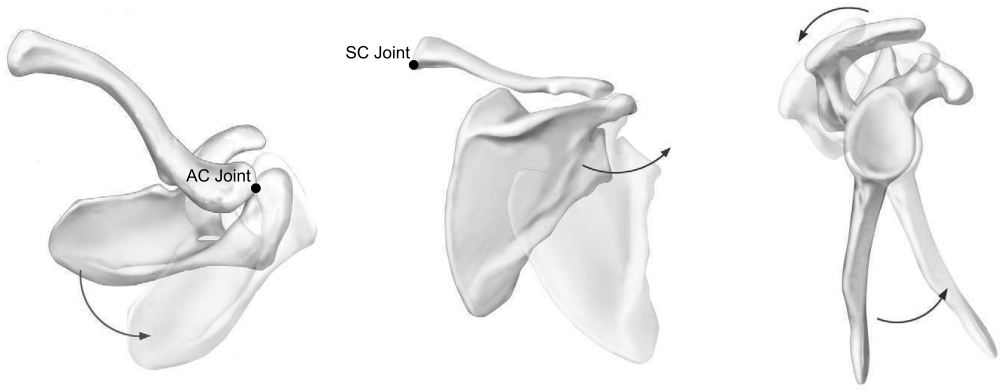

(a) Internal Rotation (b) Upward Rotation (c) Posterior Tilting

Figure 2.14: Rotation of the Scapula (Illustration: Ludewig *et al.* (2009))

Firstly, external/internal rotation occurs around a superior axis at the AC joint. Secondly, rotation about an anterior axis results in an upward/downward

rotation. This occurs at the AC and SC joints. Lastly, rotation of the scapula around a lateral axis at the AC joint results in posterior/anterior tilting of the scapula (Culham and Peat, 1993). Figure 2.14 indicates the directions for internal rotation (a) (superior view), upward rotation (b) (posterior view) and posterior tilting (c) (lateral view), respectively.

With abduction of the arm the scapula rotates upwardly, rotates externally and tilts posteriorly and the clavicle retracts and elevates (McClure *et al.*, 2001). For coronal plane abduction , Bourne *et al.* (2007) determined that the scapula rotated upwardly by 49° (range, 42° to 56°), rotated externally by 27° (range, 16° to 38°), and tilted posteriorly by 44° (range, 55° to 33°). For scapular plane abduction, McClure *et al.* (2001) found that the scapula rotated upwardly by 50° (range, 45.2° to 54.8°), rotated externally by 24° (range, 11.2° to 36.8°), and tilted posteriorly by 30° (range, 17° to 43°).

2.1.5.3 Humerothoracic Motion

Humerothoracic motion is the motion of the humerus relative to the thorax. It is described as having three degrees of freedom, namely abduction/adduction, flexion/extension and external/internal rotation around GH. Humerothoracic abduction or elevation is measured as the angle created by the humeral shaft and the superior thorax axis as the arm is being lifted. Figure 2.15 desribes the possibility of varying planes of humerothoracic elevation (a) and also explains humerothoracic elevation (b) in the second part of the figure.

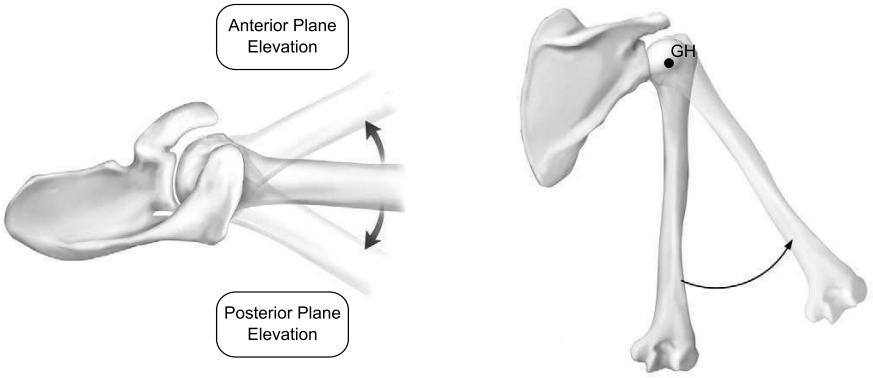

(a) Plane of Elevation (b) Humerothoracic Elevation

Figure 2.15: Rotation of the Scapula (Illustration: Ludewig *et al.* (2009))

The amount of humerothoracic abduction in the coronal plane is between 90° to 120° with the humerus externally rotated. The humerothoracic abduction decreases to 60° to 90°, if the humerus is internally rotated. This decrease is due to the impingement of the greater tubercle of the humerus on the acromion of the scapula. Elevation of the humerus in the sagittal plane

is accompanied by medial rotation of the humerus. Elevation in the scapular plane, scapular plane abduction, is such that the deltoid and the suptraspinatus muscles are optimally aligned to lift the humerus. With scapular plane abduction no lateral rotation is required by the humerus to prevent impingement of the humerus on the acromion. The humeral head remains centred on the glenoid surface throughout scapular plane abduction. At full elevation of the humerus the end position is always the same, regardless of the abduction plane. The humerus is then positioned in the scapular plane with its medial epicondyle facing forward (Culham and Peat, 1993).

2.2 History of Reverse Shoulder Arthroplasty

2.2.1 Background

TSA is the surgical procedure that involves the replacement of the humeral head with a metal ball and the glenoid with either a polyethylene or metal cup (Figure 2.16(a)). This, however, has been abandoned as a surgical treatment for arthritic rotator cuff deficient shoulders, because the excessive shearing forces produce what is known as the 'rocking-horse' phenomenon, which leads to glenoid component loosening (Franklin *et al.*, 1988; Pollock *et al.*, 1992). This phenomenon results from cyclic, eccentric loading of the humeral head on the glenoid. A torque is produced about the fixation surface that causes tensile stresses at the implant-bone interface. Repetitive eccentric loading may ultimately lead to glenoid component failure. Consequently, hemiarthroplasty has become the recommended treatment option for arthritic shoulders with cuff deficiencies. This procedure involves only replacing the humeral head (Figure 2.16(b)). This provides a smooth surface for articulation with the native glenoid. Yet, the biomechanical stabilization of the fulcrum for elevation is still deficient. The results have shown to provide limited function and inconsistent pain relief (Williams and Rockwood, 1996; Favard *et al.*, 2000; Sanchez-Sotelo *et al.*, 2001).

(a) Total Shoulder Prosthesis - *In-Vivo* (b) Hemi-Shoulder Prosthesis - *In-Vivo*

Figure 2.16: Total Shoulder Arthroplasty and Hemiarthroplasty (Illustration: Medical MultiMEDIA Group, LLC (2009))

Constrained and semiconstrained reverse shoulder prostheses were introduced between 1970 and 1980 in order to provide a fixed centre of rotation for the humerus relative to the scapula and to convert the upward-directed force of the deltoid muscle into a rotational movement, which would allow for elevation of the arm. A RSA consists of placing the ball on the glenoid and the articulating cup on the humerus. The initial reverse shoulder component designs failed, because their centre of rotation remained lateral to the glenoid and created excessive torque and shear forces at the glenoid component-bone interface, leading to component loosening.

In 1985 Paul Grammont designed a reverse shoulder prosthesis based on two biomechanical concepts: medialization of the COR of the glenoid component and lowering of the humerus. This design, shown in Figure 2.17(b), decreases mechanical torque at the glenoid component-bone interface and allows tensioning of the deltoid to increase its functional strength (Grammont and Baulot, 1993). The reverse shoulder components, illustrated in Figure 2.17(a), consist out of humeral and glenoid components. The humeral components are made up of the humeral stem and the polyethylene insert, whereas the glenoid components consist of the glenoid baseplate or metaglene, the glenosphere and the fixation screws.

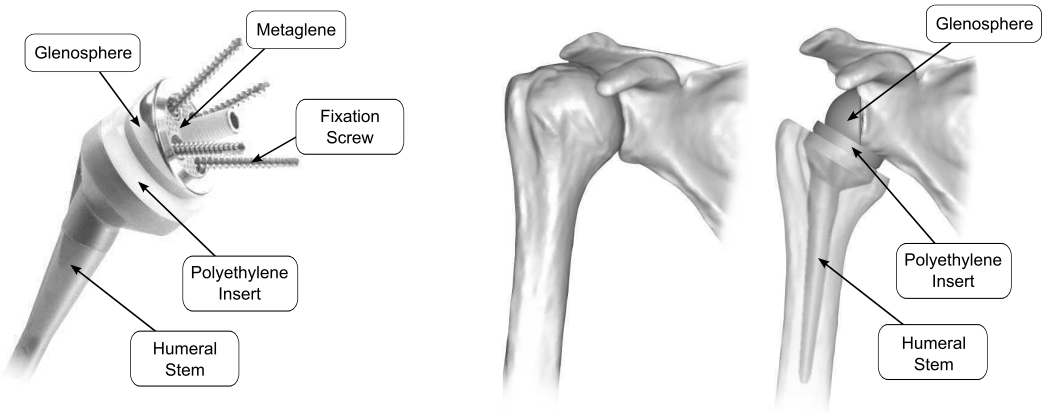

(a) Tornier Aequalis® - Reversed II (Photo: Tornier, Inc)

(b) Reverse Shoulder Prosthesis - *In-Vivo*

Figure 2.17: Reverse Shoulder Arthroplasty

Early results of the first series of RSA with Grammont's reverse shoulder prosthesis with at least two years follow-up showed excellent functional outcome and stable glenoid fixation (Baulot *et al.*, 1995; Boulahia *et al.*, 2002). Mid-to-long-term follow-up studies have, however, shown complication rates as high as 71 % and revision rates of up to 33 %. These complications include scapular notching, glenoid dissociations, loosening or dissociation of the humeral component, glenohumeral dislocation and nerve injury (Sirveaux *et al.*, 2004; Boileau *et al.*, 2006).

2.2.2 Complications

Scapular notching is a common problem in patients treated with a reverse shoulder prosthesis. Impingement of the reverse humeral cup against the inferior part of the scapular neck creates the onset of a notch. This case is depicted in Figure 2.18(a). In a retrospective study Sirveaux *et al.* (2004) found a scapular notch in 50 of 77 patients (65 %) at a mean follow-up of 44.5 months. Glenoid component positioning influences the mechanical impingement between the humeral prosthesis and the glenoid, as well as the glenohumeral ROM. Nyffeler *et al.* (2005) showed that the mechanical contact at the inferior scapular neck correlated with the position of the glenosphere. Lateralizing the baseplate reduces impingement, but shear and torque forces at the glenoid component-bone interface will increase due to the 'rocking horse' phenomenon. This could possibly lead to component failure (Boileau *et al.*, 2005). In his study, Nyffeler *et al.* (2005) concluded that by placing the baseplate flush with the inferior margin of the glenoid, the glenosphere extends beyond the scapular neck, as shown in Figure 2.18(b).

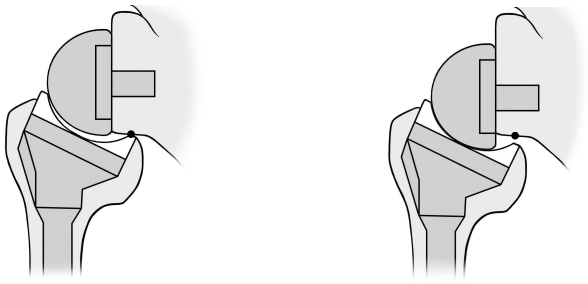

(a) Onset of a Scapular Notch (b) Inferior Glenosphere Overhang

Figure 2.18: Scapular Notching

This allows for better clearance and complete adduction of the arm without abutment of the polyethylene cup against the scapular neck. Retrospective observations made from previous clinical studies recommended that a glenoid component with some inferior tilt decreases scapular notching (Sirveaux *et al.*, 2004; Lévigne *et al.*, 2008). The investigation conducted by Edwards *et al.* (2012), however, produced no evidence that placing the glenoid component with a 10° inferior tilt has any clinical benefit. Additionally, an investigation by Simovitch *et al.* (2007) found increased scapular notching with an inferiorly tilt of the glenoid component.

Glenoid component complications have been attributed to excessive force placed across the glenoid baseplate-bone interface producing failure of baseplate fixation. The key factors contributing to long-term glenoid fixation in RSA include bone-implant contact, screw fixation/engagement, and, ultimately, bone ingrowth (Hopkins and Hansen, 2009). Initial rigid fixation of reverse glenoid baseplates is dependent on the surgical placement of the screws and the quality of the glenoid bone stock (Harman *et al.*, 2005). Biomechanical studies reflecting the actual loads seen at the baseplate-bone interface are currently lacking, therefore optimal screw fixation in the field of spine surgery is assumed. This means that a longer screw provides better fixation than a shorter screw and a bicortical screw provides better fixation than a unicortical screw. Stable screw fixation has been correlated with an increase in screw surface area within the bone (Hopkins *et al.*, 2008). In a study of reversed glenoid components, Hopkins and Hansen (2009) demonstrated that using a convex-backed baseplate would allow screws to be placed further apart than with a flat-backed design, thereby resulting in greater resistance to interface motion. A study has shown a direct relationship between increased screw pull-out strength with increased cortical thickness (Huja *et al.*, 2005). A previous cadaver-based anatomical study has established that cortical thickness is greatest in the medial and lateral borders of the scapula body, scapular spine and acromion (Burke *et al.*, 2006). Other anatomic considerations must also be taken into account when placing the screws, specifically, screw impinge-

ment on adjacent neural and vascular structures. Of particular concern is the suprascapular nerve, which runs through the suprascapular and spino-glenoid notches. The superior locking screw is aimed at the base of the coracoid. The exit point is just anterior and inferior to the suprascapular nerve. This allows safe penetration of the screw into the medial cortex. The scapular spine is the aim point for the anterior screw. The scapular pillar is a prominent, thick column of bone and is the aim point for the inferior screw. The posterior screw is drilled anteriorly and inferiorly toward the anterior prominence of the pillar. The suprascapular nerve is put at risk if the posterior screw is not drilled anteriorly. Fixing the baseplate with 3 rather than 4 screws has not been reported to lead to early failure. Whether fixation strength of an in-out-in course compared to the fixation strength of a screw simply exiting at the far cortex is stronger, weaker or similar is unknown (Humphrey *et al.*, 2008). In contrast, the load to failure of glenoid component fixation is significantly reduced if any of the 4 screws fails to achieve good purchase in the bone. Fixation is strongest when the 2 locking screws (superior and inferior screws) are in line with the applied load (Chebli *et al.*, 2008).

A biomechanical prerequisite for successful osseous integration for cementless fixation is to provide a stable interface between the bone and the prosthetic implant during initial healing. Baseplate motion of more than 150µm inhibits effective bony ingrowth into the reverse shoulder components (Virani *et al.*, 2008). To minimize any motion of the baseplate, proper purchase of bone stock is required by the fixation of the screws and the centre peg. Error in glenoid component version alignment can result in a suboptimal position with increased potential for perforation of the centre peg, which can lead to failure (Iannotti *et al.*, 2012). The 'rocking horse' phenomenon has accompanied TSA of cuff-deficient shoulders as well as a too lateralized COR of a reverse shoulder component. Glenospheres with a lateralized eccentric COR allow a greater abduction and adduction of the arm. Conversely, lateralization requires increased deltoid force to abduct the arm (Henninger *et al.*, 2012). An inferior tilt of the glenoid component allows more even distribution of forces along the superior and inferior screws, which promotes the fixation of the baseplate to the glenoid surface (Gutiérrez *et al.*, 2011).

The reverse shoulder prosthesis is considered a semi-constrained implant, yet dislocation is a relatively common complication. Studies by Molé and Favard (2007) and Wall *et al.* (2007) have shown that dislocation rates were 3.4 % and 7.5 %, respectively. Glenoid and humeral component malposition and impingement increase the risk of dislocation (Molé and Favard, 2007). In case of a dislocation due to malpositioned components a revision surgery is required.

2.2.3 Orientation of the Reverse Shoulder Components

The estimation of the anatomical glenoid version and inclination, as well as anatomical humeral retroversion is becoming increasingly important in shoulder replacement surgery. Accurate determination of the natural version and inclination of the shoulder complex is vital in the survivorship of shoulder replacement prostheses. Initially, X-rays were used to determine glenoid and humeral orientation. Randelli and Gambrioli (1986) noted that the position of the scapula throughout an X-ray is very important when glenoid version is assessed. With minor rotation of the scapula in the coronal plane, glenoid version can vary up to 10.5°. Currently, CT scans are used to determine glenoid and humeral orientations. Although an improvement on conventional X-ray methods there remain limitations to this technique in that the results are still scanning orientation dependent (Bokor *et al.*, 1999).

Furthermore, glenoid component version seems to play an important role in the stability and loading of the glenohumeral joint. Abnormalities of component version have been associated with glenohumeral instability. Recent reports have suggested that excessive glenoid component version is associated with poor clinical results (Nyffeler *et al.*, 2005). As previously mentioned, there is an increased potential of perforation of the centre peg due to a malposition of the glenoid components. This may lead to failure (Iannotti *et al.*, 2012). Previous studies show controversial results regarding the effect that an inferior tilt has on scapular notching. Studies have shown that placing the glenoid component with an inferior tilt decreases scapular notching (Sirveaux *et al.*, 2004; Lévigne *et al.*, 2008). A study by Simovitch *et al.* (2007) showed that an inferior tilt of the glenoid component increased scapular notching and lastly an investigation by Edwards *et al.* (2012) produced no evidence that an inferior tilt of the glenoid component had a clinical benefit regarding scapular notching.

Gutiérrez *et al.* (2011) showed that for concentric and lateral glenospheres, an inferior tilt provides the most even distribution of forces between the superior and inferior screws and a superior tilt provides the most uneven distribution of forces. For inferior eccentric glenospheres, an inferior tilt produced the most uneven distribution of forces and a neutral tilt produced the most even distribution of forces. An uneven distribution of forces promotes the 'rocking horse' motion of the baseplate. The most desirable to least desirable tilt positions for the different glenospheres with regard to superior and inferior screw force distribution are illustrated in Figure 2.19.

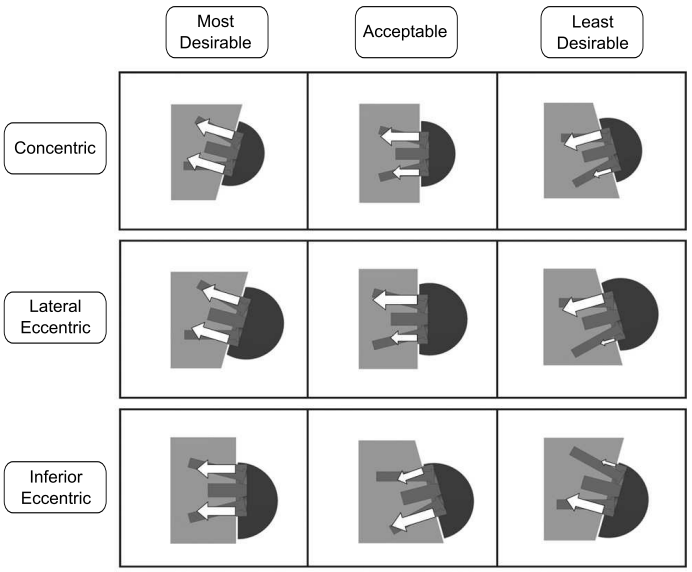

Figure 2.19: Force Distribution for Different Glenospheres and Tilt Positions (Illustration: Gutiérrez *et al.* (2011))

Version of the humeral component plays a role in ROM and impingement in RSA. Humeral component anteversion can significantly decrease the amount of external rotation achievable after RSA. Increasing humeral component retroversion increased the amount of external rotation before impingement on the scapular border and decreased the amount of internal rotation before impingement. Stephenson *et al.* (2011) found that for the Tornier Aequalis® Reversed shoulder prosthesis, the optimal version for the humeral component appears to be between 20° and 40° of retroversion. From the results of Dedy *et al.* (2011), posterior offset humeral components for the uncemented PROMOS RSA do not appear to affect ROM with regard to abduction and external rotation. Greater retroversion allows for easier dislocation and may even lead to anterior scapular notching.

2.2.4 Prosthesis Design

Glenospheres with a lateralized COR allow a greater ROM of the arm. The inferior edge of the humeral component does not impinge on the scapula as readily as it would have with a more medial COR. The force required to lift the arm is increased by the lateralized COR. Inferior eccentric glenosphere designs increase the deltoid tension. It also allows for a smaller adduction deficit. Larger glenospheres have shown to have a greater ROM, but there are little biomechanical/clinical results to motivate the use of the larger glenosphere design.

Hopkins and Hansen (2009) demonstrated that using a convex-backed baseplate would allow screws to be placed further apart than with a flat-backed

design, which resulted in greater resistance to component-bone interface motion.

A Morse taper is used to attach the glenosphere to the baseplate, which prevents postoperative loosening of the glenosphere.

Introducing a posterior offset in the humeral components did not appear to affect ROM with regard to abduction and external rotation (Dedy *et al.*, 2011). The current standard neck-shaft angle of the humeral component is 155°. Oh *et al.* (2014) found that decreasing the neck-shaft angle allowed an increased adduction of the humerus before scapular impingement.

2.3 Related Work

In 2006, Krekel *et al.* (2006) developed a prototype pre-operative planning software for total shoulder and hemi-shoulder replacements. Collision detection, using bounding boxes, is used to predict bone-determined glenohumeral ROM. The prosthesis placement parameters can be adjusted interactively to determine the effect the alterations have on the ROM.

To calculate the ROM, he represented the glenohumeral joint as a generally accepted, simplified bio-mechanical model, a ball-joint (Meskers *et al.*, 1997; van der Glas *et al.*, 2002).

Furthermore, in 2010, Krekel *et al.* (2010) investigated visualisation techniques to enhance the analysis of multi-joint kinematic data, specifically of the upper extremity, i.e. the shoulder and arm joints.

2.4 Summary

The shoulder is one of the most complex joints of the human body. To accurately describe the motion of the shoulder joint requires an understanding of the anatomic reference planes, translations and rotations, as well as the shoulder coordinate systems (thorax, clavicle, scapula and humerus) involved, which are defined in this chapter. The shoulder complex motion is described as the combination of the sternoclavicular, the scapulothoracic and the humerothoracic motion.

TSA is the surgical procedure that involves the replacement of the humeral head with a metal ball and the glenoid with either a polyethylene or metal cup. Whereas, RSA consists of placing the ball on the glenoid and the articulating cup on the humerus. Early results of RSA showed excellent functional outcome and stable glenoid fixation for arthritic rotator cuff deficient shoulders. Mid-to-long-term follow-up studies have, however, shown high complication rates. These complications include scapular notching, glenoid dissociation, loosening or dissociation of the humeral component, glenohumeral dislocation and nerve injury. Clinical outcomes are dependent on the preoperative diagnosis,

the function of the deltoid and remaining rotator cuff muscles, biomechanical design of the prosthesis, and the orientation and placement of the reverse shoulder component.

Krekel *et al.* (2006) developed pre-operative planning glenohumeral motion software for total and hemi-shoulder replacements.

3. Reverse Shoulder Simulation Software

This section comprises of the development of the Reverse Shoulder Simulation Software (RS^3). Firstly, the shoulder complex motion data used to drive the simulation is provided and analyzed. Secondly, the generation of the implant and patient data used in the RS^3 is explained. Finally, a closer look is taken at the work flow of the RS^3, as well as its Graphical User Interface (GUI).

3.1 Shoulder Complex Motion Data

Ludewig *et al.* (2009) analysed the shoulder complex motion, as described in Section 2.1.5, for the coronal, scapular and sagittal elevation planes. The 3D motion of the shoulder complex of 12 subjects without any shoulder abnormality was recorded with the use of direct bone measurement during elevation of the arm. The subjects were between twenty-two and forty-one years old, with average height and weight of 1.74 m and 77.5 kg, respectively. Electromagnetic motion sensors were fixed to the clavicle, scapula and humerus using transcortical pins (Figure 3.1). Bone-fixed tracking, as an alternative to skin sensors, is the current gold standard for precise shoulder motion measurement (Koh *et al.*, 1998). Subjects were asked to elevate their non-dominant arm to a maximum of 120° in the respective elevation planes, while keeping light fingertip contact on a planar board to maintain the motion in the desired elevation plane. Motion capturing of scapula plane elevation of the arm of one of the subjects is shown in Figure 3.1. Note that for all elevation planes the thumb pointed upwards, ensuring minimal external/internal rotation of the humerus. Scapula plane abduction was performed at a plane 40° anterior to the coronal plane.

The various bone segment axes alignments used throughout the study made by Ludewig *et al.* (2009) were consistent with the TCS, CCS, SCS_1 and HCS defined in Section 2.1.3. Clavicular, scapular and humeral motions were described relative to the thorax with use of Euler angles. Euler angles enable the 3D angular rotations of the shoulder complex to be described as sequential rotations about each of the three anatomical axes of the respective bones

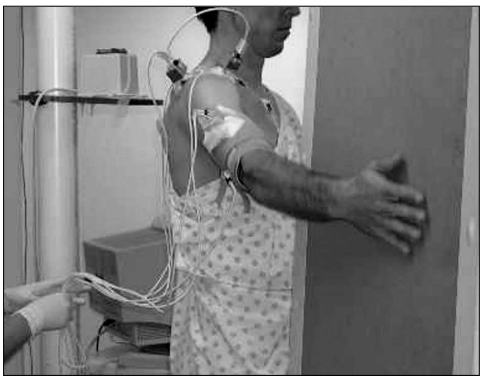

Figure 3.1: Scapula Elevation Plane Motion Capturing (Photo: Ludewig *et al.* (2009))

of the shoulder complex. This is the current standard for shoulder motion description in research testing (Wu *et al.*, 2005).

The Euler angles for the sternoclavicular motion were obtained using the sequence depicted in Figure 2.13. Firstly, protraction/retraction about the superior axis, secondly, elevation/depression about the anterior axis, and lastly, anterior/posterior rotation about the lateral axis of the TCS were determined. The Euler angles for the scapulothoracic motion were obtained using the sequence depicted in Figure 2.14. Firstly, internal/external rotation about the superior axis, then, upward/downward rotation about the anterior axis, and finally, anterior/posterior tilting about the lateral axis of the TCS were determined. Humerothoracic motion angles were obtained by determining the elevation angle about the anterior axis and then determining the plane of elevation about the superior axis of the TCS.

The average sternoclavicular and scapulothoracic motion data obtained by Ludewig *et al.* (2009) is provided in Appendix A.1 and A.2. This data was selected as it represents motion in three different elevation planes compared to other studies that only tested motion in a single elevation plane. It is, therefore, also a fairly good representation of the achievable shoulder complex ROM.

With the use of this data a best fit polynomial line was fitted to each set of motion data using a least squares fitting method. The order of polynomial chosen was based on two criteria. The first criterion was to obtain a coefficient of determination, R^2, which minimized the proportion of variability between the data set and the best fit line. The proportion of variability decreases as R^2 approaches a value of 1. The second criterion required that the y-intercept of the polynomial approaches the respective angular joint position with the arm at the side, at 0° humerothoracic elevation. The resting angular joint positions are contained in Table 3.1. Figure 3.2 below shows an example of the motion data, best fit lines and R^2 values for the coronal elevation plane.

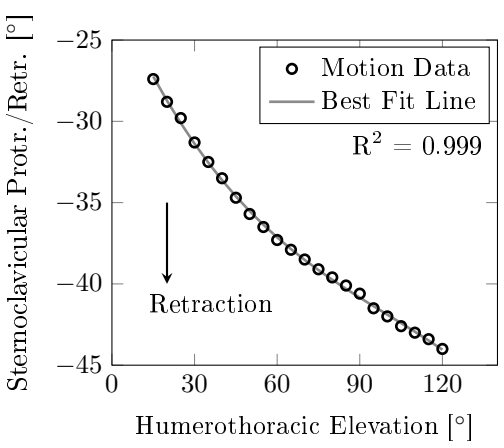

(a) Sternoclavicular Protraction/Retraction Data and Best Fit Line

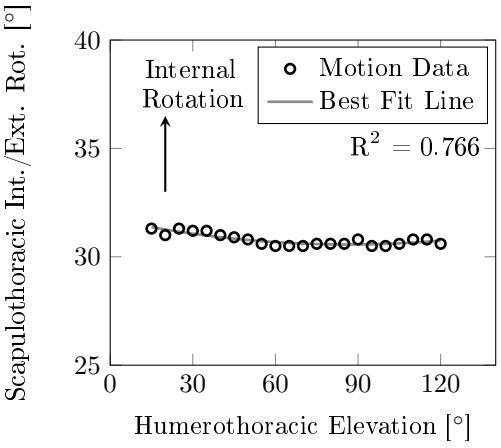

(b) Scapulothoracic Internal/External Rotation Data and Best Fit Line

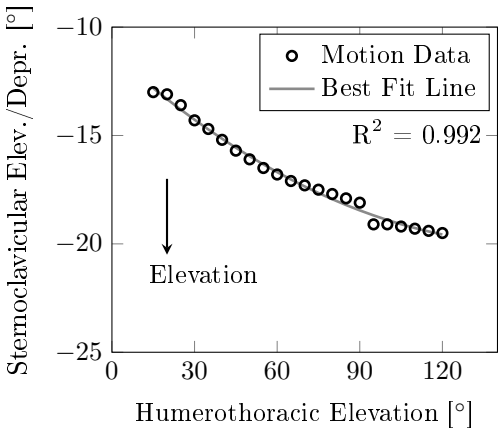

(c) Sternoclavicular Elevation/Depression Data and Best Fit Line

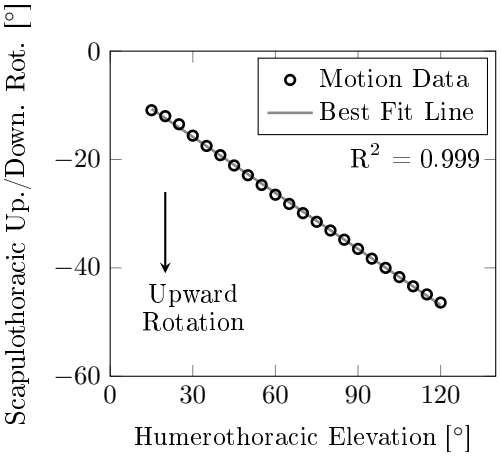

(d) Scapulothoracic Upward/Downward Rotation Data and Best Fit Line

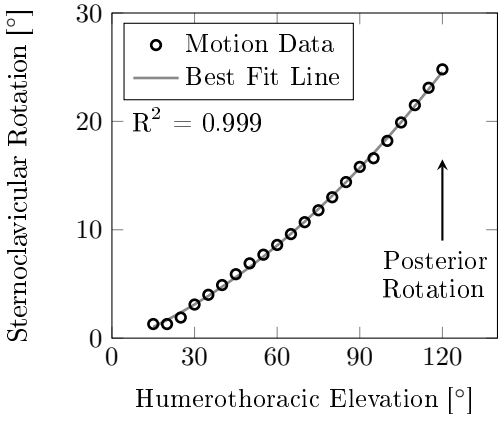

(e) Sternoclavicular Anterior/Posterior Rotation Data and Best Fit Line

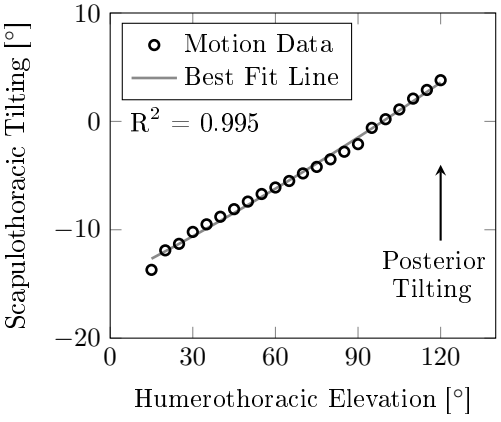

(f) Scapulothoracic Anterior/Posterior Tilting Data and Best Fit Line

Figure 3.2: Coronal Plane Elevation - Sternoclavicular and Scapulothoracic Motion

Table 3.1: Resting Angular Joint Positions with the Arm at the Side and Corresponding y-intercept Values (Adapted from Ludewig *et al.* (2009))

		Elevation Plane								
		Coronal			Scapula			Sagittal		
Joint	**Position [°]**	c_1	c_2	c_3	c_4	c_5	c_6	c_7	c_8	c_9
Sternoclavicular joint										
Retraction	19.2 ± 2	22			19.8			19.7		
Elevation	5.9 ± 1		11.2			8.41			9.13	
Posterior rotation	0.1 ± 1			0.628			1.62			3.21
		c_{10}	c_{11}	c_{12}	c_{13}	c_{14}	c_{15}	c_{16}	c_{17}	c_{18}
Scapulothoracic joint										
Internal rotation	41.1 ± 2	31.7			37.6			42.8		
Upward rotation	5.4 ± 1		5.49			4.56			7.27	
Anterior tilting	13.5 ± 2			14.7			14.9			13.9

Appendix A.3 shows the figures describing the motion data for the coronal, scapula and sagittal elevation planes, respectively, together with the best fit lines and R^2 values. The equations of the best fit lines determined for the various elevation planes are listed in Appendix A.3, from Equation A.1 - A.18. The constant term values for the equations are shown in Table 3.1. All equations, except two, achieved an R^2 value greater than 0.9. This, however, does not affect the motion equations, because these equations are overpowered by the remaining seven equations that did achieve an R^2 value close to unity. The y-intercept (constant term) values mostly corresponded well with the desired resting position values.

The shoulder complex motion equations approximate the average motion data recorded by Ludewig *et al.* (2009). Changing the constant term values of the equations will either move the line up or down. The RS^3 is patient-specific and uses the resting angular joint positions of a specific patient (calculated in Sections 3.4.3.3 and 3.4.3.4) to update the constant term values of the motion equations. This ensures that the simulation is unique to that patient. The motion equations, with the patient-specific constant terms, are used by the RS^3 to calculate the ROM and to run the simulation in Sections 3.4.5.1 and 3.4.5.3, respectively.

3.2 Data Preparation

The preparation work required for the RS^3 consisted of generating the desired implant files and performing the necessary steps to produce good patient data.

3.2.1 Implant Data Generation

The case study performed in Section 4.2 formed part of Dr. De Beer's pre-operative planning procedure. The implants used in the RS^3 were, therefore, generated according to the Tornier Aequalis® - Reversed II implants (Figure 3.3), as this is consistent with what is used by Dr. De Beer.

Dr. De Beer provided the necessary Tornier Aequalis® - Reversed II implants. These were scanned with the NextEngine 3D Laser Scanner (Santa Monica, California, USA) to obtain initial 3D model files. These files were imported into the Computer Assisted Design (CAD) software package Autodesk Inventor® (San Rafael, California, USA), which provided sufficient information to accurately generate 3D models of the implants in Inventor®. Finally, the implants were exported as Stereolithography (STL) files, as is required by the RS^3. This format approximates the surfaces of a 3D object with triangles. A STL file contains the xyz-coordinates of the vertices and normals for the triangles that describe a 3D object.

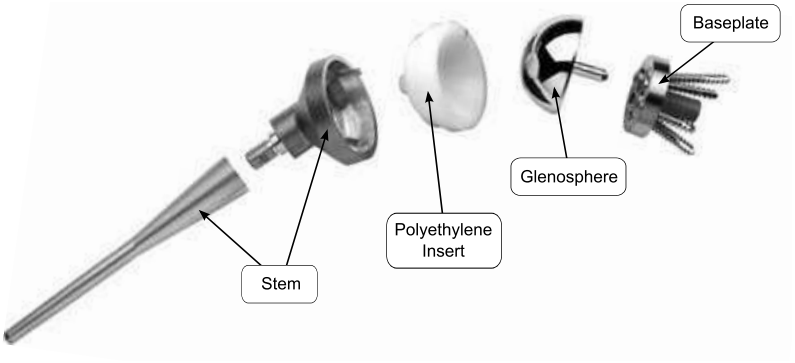

Figure 3.3: Tornier Aequalis® - Reversed II (expanded)(Photo: Tornier, Inc)

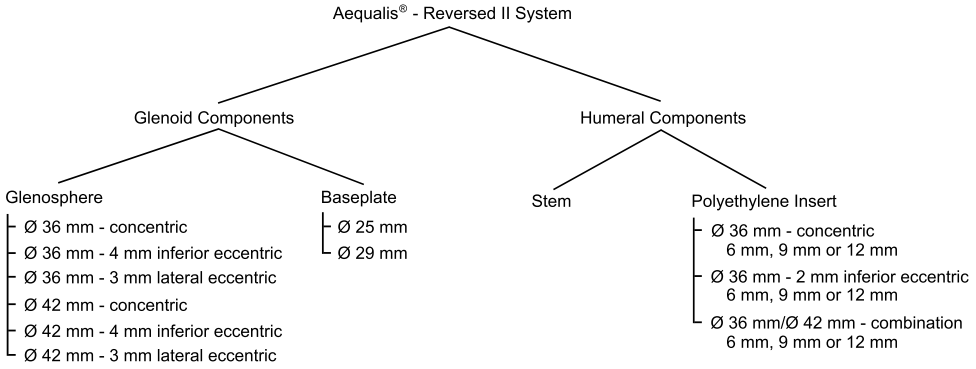

Figure 3.4: Component Possibilities of the Aequalis® - Reversed II System

Figure 3.3 shows an expanded view of the different components of the Tornier Aequalis® - Reversed II system and how these fit into one another. The Reversed II system allows extensive and interchangeable combinations between the glenoid and humeral components. The possible options available for each component are listed in Figure 3.4. All of them were included in the RS^3 implant data.

Figure 3.5 contains an example of the ∅ 29 mm baseplate and the 3 types of ∅ 42 mm glenospheres. Similarly, an example of the humeral stem and the 3 types of 6 mm poyethylene inserts can be seen in Figure 3.6.

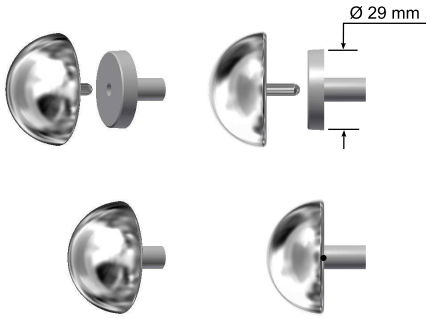

(a) Baseplate (∅ 29 mm) and Glenosphere (∅ 42 mm - concentric)

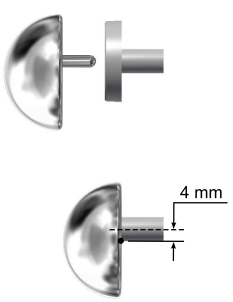

(b) Baseplate (∅ 29 mm) and Glenosphere (∅ 42 mm - 4 mm inferior eccentric)

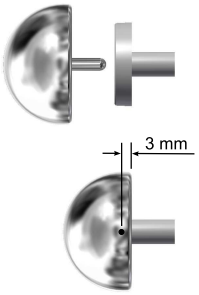

(c) Baseplate (∅ 29 mm) and Glenosphere (∅ 42 mm - 3 mm lateral eccentric)

Figure 3.5: Glenoid Components

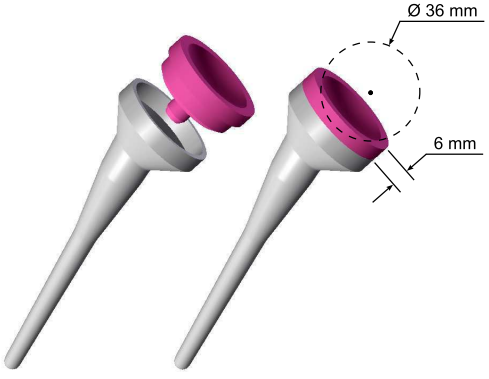

(a) Stem and Polyethylene Insert (∅ 36 mm - concentric (6 mm))

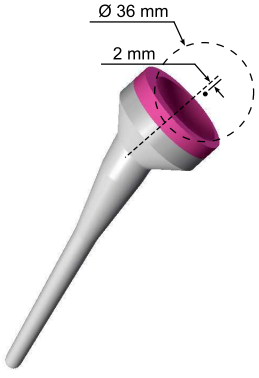

(b) Stem and Polyethylene Insert (∅ 36 mm - inferior eccentric (6 mm))

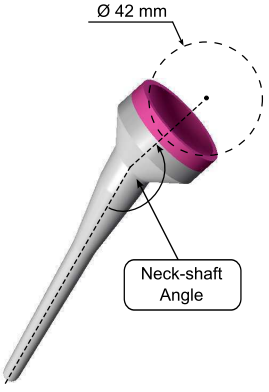

(c) Stem and Polyethylene Insert (∅ 36 mm/∅ 42 mm - combination (6 mm))

Figure 3.6: Humeral Components

3.2.2 Patient Data Preparation

Any patient undergoing a RSA requires a CT scan. Conventionally, an arthroplasty shoulder CT scan is taken from above the clavicle to about 15 cm inferior to the humeral head. The CT scan data required by the RS^3 consists of a scan taken from above the clavicle to below the elbow joint line. This ensures that the anatomical landmarks required by the RS^3 are scanned. The patients have to lie flat on their back with their arms next to their bodies. This resembles a relaxed upright standing position with the arms hanging down at the sides of the body. The scan settings have to be set to use a bone kernel window and to use 1 mm axial slice thickness. A CT scan produces Digital Imaging and Communication (DICOM) images, which are imported into Mimics (Materialise, Leuven, Belgium) software. The patient's clavicle, scapula, humerus, C7 and T8 vertebrae, and sternum are segmented in Mimics and exported separately as STL files. A final check is performed in 3-Matic (Materialise, Leuven, Belgium) software to ensure the quality of the STL mesh. Any irregularities can be corrected using the fixing function in 3-Matic before exporting the files.

3.3 Work Flow

The flow charts in Figure 3.7 and Figure 3.8 illustrate the work flow and logic of the processes in the RS^3.

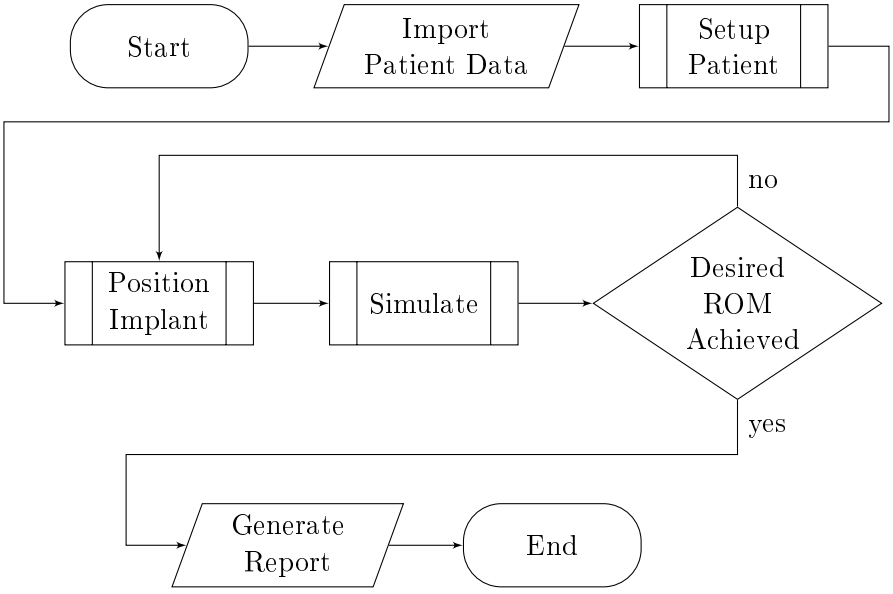

Figure 3.7: Overview of the RS^3 Work Flow

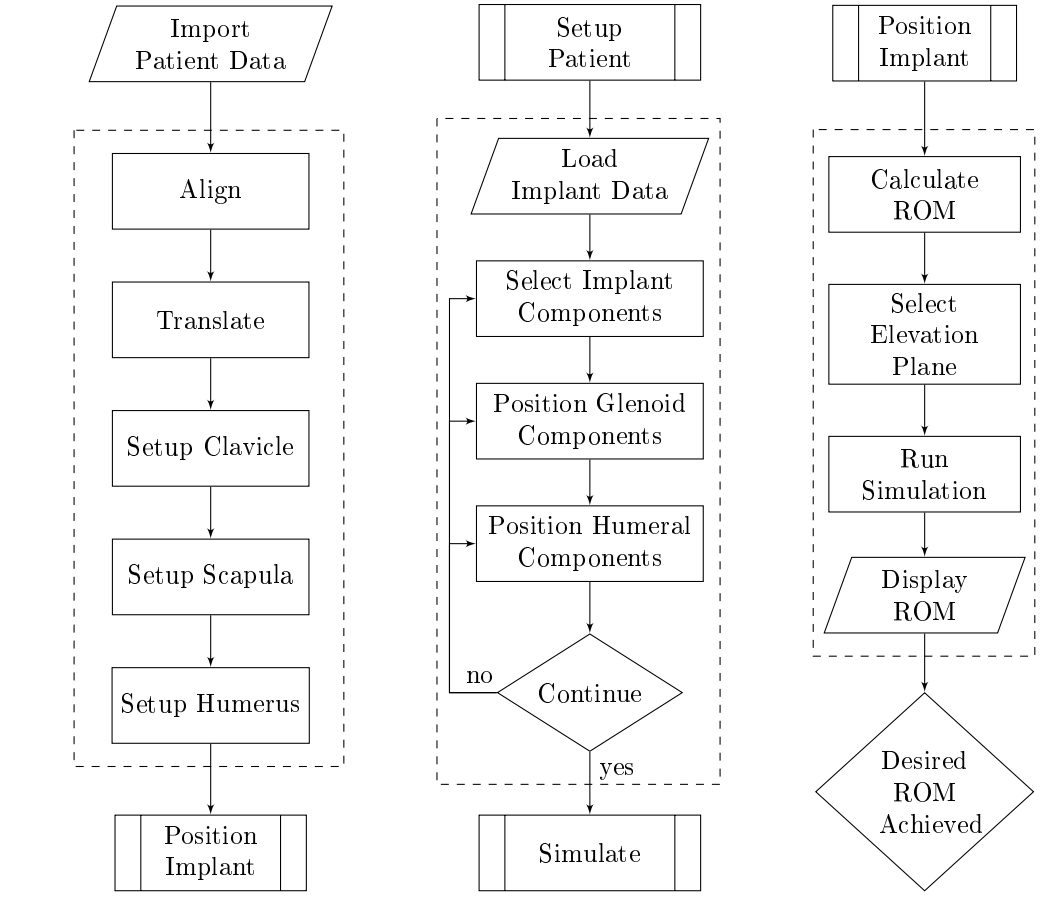

(a) Setup Patient Subroutine (b) Position Implant Subroutine (c) Simulate Subroutine

Figure 3.8: RS^3 Subroutine Flow Charts

The work flow of the RS^3 starts with an orthopaedic surgeon, an orthopaedic representative or an engineer (hereafter referred to as the user) importing the specific patient data. This is followed by the three main subroutine processes, which are performing the patient setup, positioning the implant and running the simulation process (Figure 3.8). The user can then decide to generate a report with the pre-operative planning details or to reselect and reposition the implant and repeat the simulation process.

3.4 GUI

The RS^3 was developed in Matlab (MathWorks, Natick, MA, USA) software using its Graphical User Interface Design Environment (GUIDE) tools.

This section describes the layout and functionality of the GUI and how this pertains to the above-mentioned work flow processes.

3.4.1 Layout

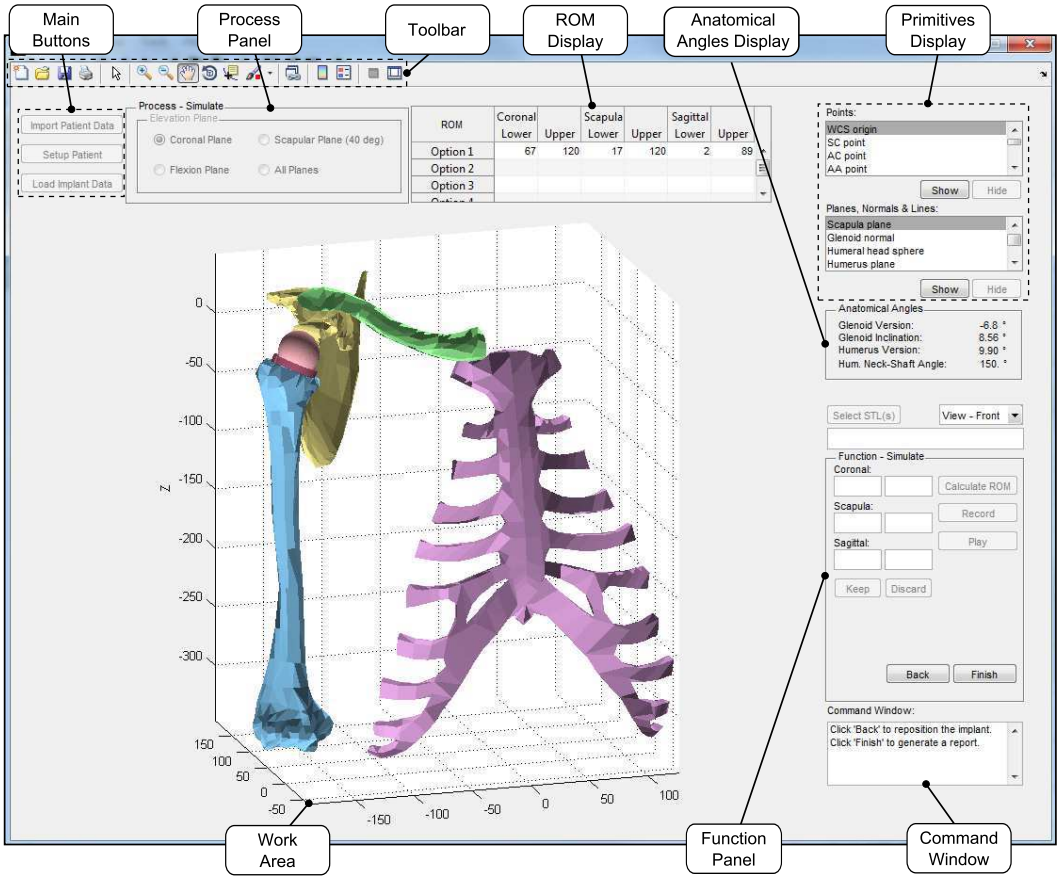

Figure 3.9: GUI Layout

The GUI layout consists of several buttons, panels, areas, displays, windows and a toolbar. Figure 3.9 illustrates these clearly. The main buttons are the *Import Patient Data*, the *Setup Patient* and the *Load Implant Data* buttons. The *Process Panel* indicates to the user, which process is currently active. The processes coincide with the subroutines found in Figures 3.7 and 3.8, namely the *Setup Patient*, the *Position Implant* and the *Simulate* processes (Figure 3.10). The *Function Panel* is dependent on the currently active process. For each process, there are a number of different function panels that allow the user to perform the required tasks within the given process. The *Work Area* is Matlab's World Coordinate System (WCS). This is the area that displays the patient and implant data. All interaction between the user and the patient data occurs within this area. The shoulder complex motion simulation is also displayed here. The *ROM Display* is a table that displays the ROM for the different implant components and positions selected as preferable by the user. The anatomical glenoid version and inclination, as well as the anatomical

humeral version and neck-shaft angle are displayed in the *Anatomical Angles Display*. Important anatomical landmarks, planes, normal directions and centre lines are displayed and accessed in the *Primitives Display*. The *Command Window* instructs the user what to do while operating the RS^3. Finally, the *Toolbar* provides the user the functionality to select, zoom, pan or rotate the WCS in the *Work Area*.

For the following sections refer to the flow charts in Figure 3.7 and Figure 3.8.

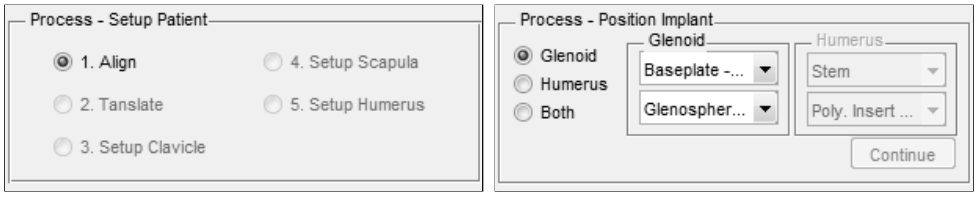

(a) Setup Patient Process Panel (b) Position Implant Process Panel

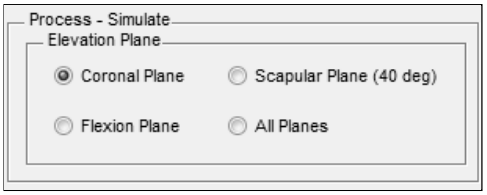

(c) Simulate Process Panel

Figure 3.10: Process Panels

3.4.2 Import Patient Data

The patient data required is the clavicle, the scapula, the humerus, the C7 and T8 vertebrae and the sternum. These must all be in STL format and orientated in the positions as found on the CT scan described in Section 3.2.2.

Once the RS^3 is started, the user is instructed to click on the *Import Patient Data* button. This opens a standard dialog box that allows the user to select and import the different patient STL files. The imported files are each given a unique colour, which help to distinguish them, and are displayed in the *Work Area*. After all the required patient files are imported, the user can continue with the patient setup process by clicking on the *Setup Patient* button.

3.4.3 Setup Patient

The RS^3 is patient-specific. The patient setup process is comprised of identifying and allocating anatomical landmarks. The anatomical landmarks are used to determine the various shoulder coordinate systems previously described in Section 2.1.3. Additionally, the patient setup process provides the required

information for the implant positioning and simulation processes to function. Lastly, the glenoid and humerus anatomical angles are also calculated in the patient setup process. The surgeon uses the anatomical angles during the pre-operative planning procedure to determine the implant placement required to restore the current anatomical angles to a healthy orientation.

An intra and inter subject analysis was performed to determine the repeatability and sensitivity of identifying the anatomical landmarks required to define the various shoulder coordinate systems. The anatomical landmarks identification process was repeated 10 times for a right and left shoulder, respectively. The coordinate systems were used to calculate the shoulder anatomical angles. The angles obtained did not vary more than 2°, with a maximum variation of 1.8°.

Clicking on the *Setup Patient* button activates the *Setup Patient Process Panel* (Figure 3.10(a)). The patient setup process consists of the *Align and Translate*, *Setup Clavicle*, *Setup Scapula* and *Setup Humerus* functions. The function panels for each of these functions are shown below in Figure 3.11.

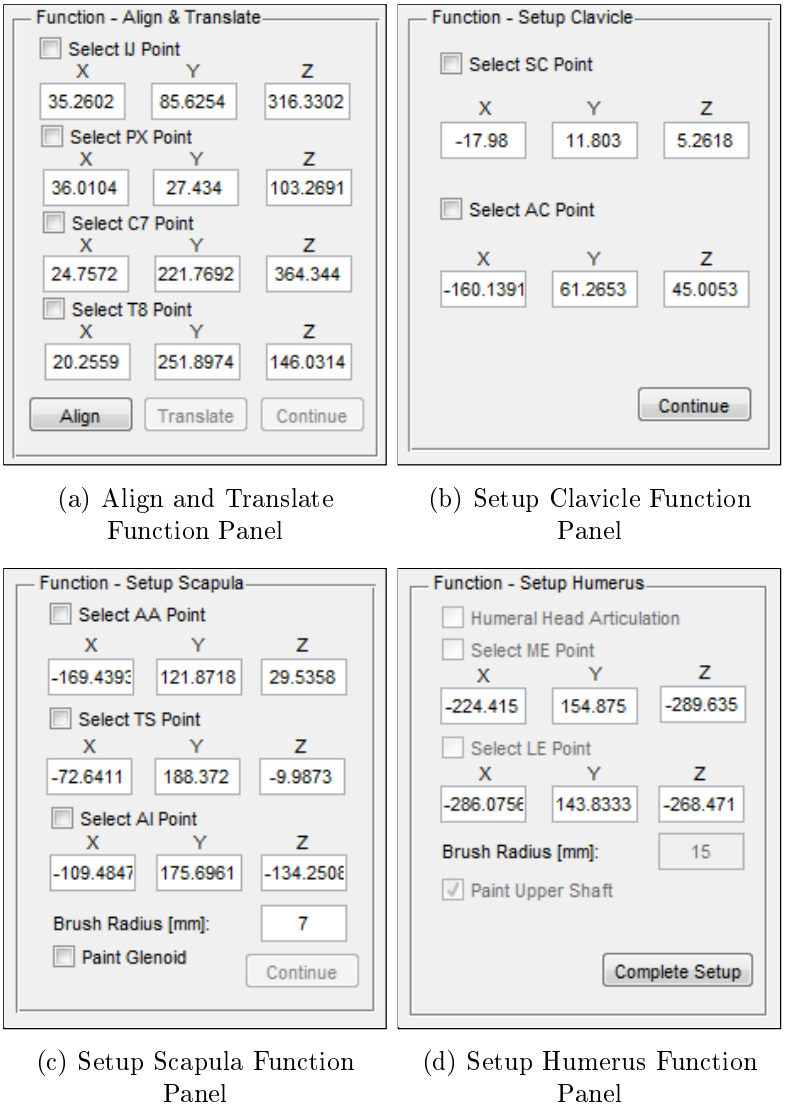

(a) Align and Translate Function Panel

(b) Setup Clavicle Function Panel

(c) Setup Scapula Function Panel

(d) Setup Humerus Function Panel

Figure 3.11: Setup Patient Process Function Panels

3.4.3.1 Align

In the *Align* function, the TCS is orientated such that its axes are aligned with Matlab's WCS. This requires the selection of the anatomical landmarks, IJ, PX, C7 and T8, used to define the TCS.

The *Align and Translate Function Panel* (Figure 3.11(a)) allows the user to interactively select the required anatomical landmarks in the *Work Area*.

3.4.3.2 Translate

After aligning the patient data with the WCS, the STLs are translated so that the IJ point is coincident with the origin of the WCS. The TCS is now

coincident with the WCS.

The *Align and Translate* functions ensure that all the calculations (resting position and motion) of the CCS, SCS and HCS are relative to the TCS.

3.4.3.3 Setup Clavicle

To determine the CCS requires the selection of the SC and AC points (Figure 3.11(b)), which are again interactively selected by the user in the *Work Area*. These two anatomical landmarks are used as rotation centres in the simulation process. The SC and AC points are listed in the *Primitives Display*.

Furthermore, the resting angular sternoclavicular joint position is calculated as the angular differences between the axes of the CCS and the TCS. The calculated angles are used as the input values for the constant terms in the Equations A.1 - A.3, A.7 - A.9 and A.13 - A.15.

3.4.3.4 Setup Scapula

The AA, TS, AI and glenoid centre points are needed to determine the two SCSs. The AA, TS and AI points are interactively selected by the user (Figure 3.11(c)). To determine the glenoid centre point the user is instructed to paint the faces of the triangles that make up the glenoid surface. The selected points and painted glenoid surface are indicated in Figure 3.12(a). The glenoid centre point is then calculated as the mean coordinate of all the vertices of the faces that were painted. Additionally, a plane is fitted, in a least squares sense, to the selected vertices in order to determine the normal to this plane as illustrated in Figure 3.12(b).

The SCS_1 is used to calculate the resting angular scapulothoracic joint position relative to the TCS. These angles are used as the input values for the constant terms in the Equations A.4 - A.6, A.10 - A.12 and A.16 - A.18.

The SCS_2 is used to determine the glenoid anatomical version and inclination angles. The glenoid anatomical version is calculated as the angle between the glenoid surface plane normal and the yz-plane (scapula plane) of the SCS_2. The glenoid anatomical inclination is calculated as the angle between the glenoid surface plane normal and the xz-plane of the SCS_2 (Section 2.1.4). Secondly, the SCS_2 acts as the reference coordinate system when loading and positioning the glenoid components.

The AA, TS, AI and glenoid centre points, as well as the scapula plane and glenoid normal are listed in the *Primitives Display*. The glenoid anatomical version and inclination are shown in the *Anatomical Angles Display*.

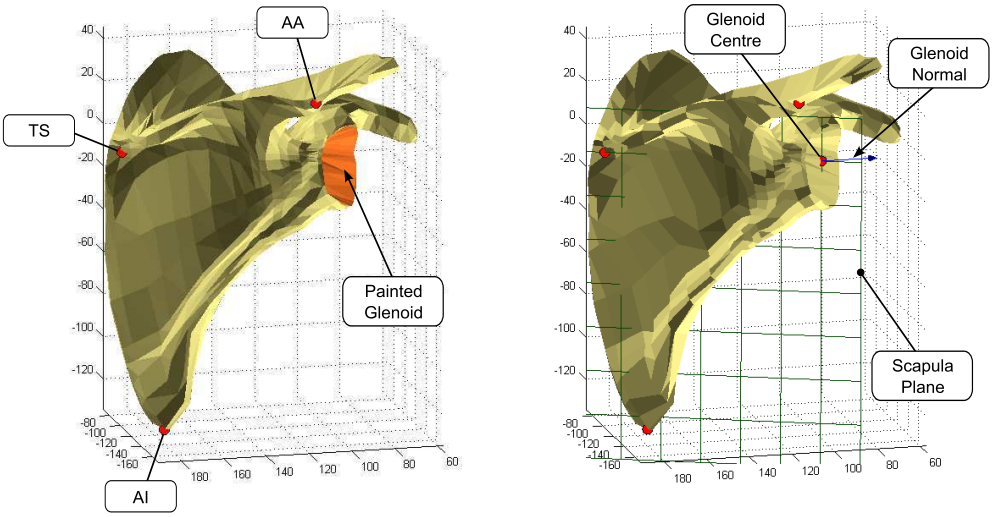

(a) (b)

Figure 3.12: Setup Scapula Functions

3.4.3.5 Setup Humerus

The GH, ME and LE points are required to describe the HCS. The LE and ME points are anatomical landmarks that can be identified (Figure 3.11(d)). The GH, however, is determined by selecting the articulating surface of the humeral head and calculating its COR. Lastly, the humeral upper shaft centre line is determined as the midline running through a selected section of the upper humerus. All of this information is used to calculate the humeral anatomical retroversion.

Figure 3.13 depicts the different functions throughout the humerus setup. Figure 3.13(a) shows how five points are selected on the rim of the articulating cartilage of the humeral head. The RS^3 fits a plane through these points and calculates the plane normal, illustrated in Figure 3.13(b). A sphere is then fitted to the vertices that make up the selected articulating surface. The humeral upper shaft centre line is taken as the cylinder axis after a cylinder is fitted to the vertices of the painted faces (Figure 3.13(b)).

The humeral anatomical retroversion is calculated as the angle formed between the articulating surface plane normal and the yz-plane of the HCS (Section 2.1.4).

The GH, ME and LE points, and the humeral head sphere, upper shaft centre line and articulating surface plane normal are listed in the *Primitives Display*. The humeral anatomical version and neck-shaft angle are shown in the *Anatomical Angles Display*.

The HCS is used as the reference coordinate system when loading and positioning the humeral components.

After the *Setup Patient* process has been completed, the user proceeds to the *Position Implant* process.

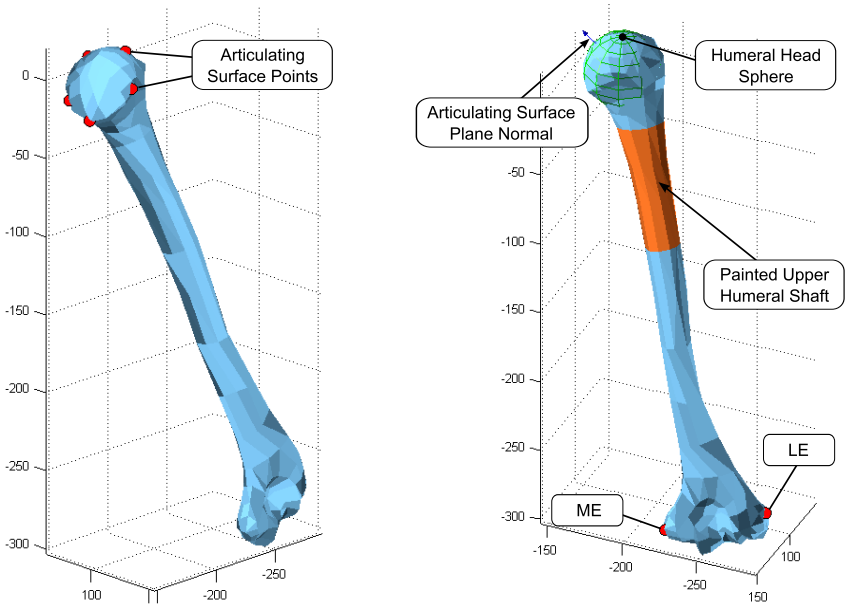

(a) (b)

Figure 3.13: Setup Humerus Functions

3.4.4 Position Implant

The implant positioning process includes the uploading of the implant data and the implant component selection and positioning.

3.4.4.1 Load Implant Data

The *Position Implant Process Panel* (Figure 3.10(b)) is activated by clicking on the *Load Implant Data* button. The Tornier Aequalis® - Reversed II implant components are then uploaded into the RS^3. The glenoid components are aligned with the SCS_2 and the humeral components are aligned with the HCS.

3.4.4.2 Select Implant Components

After the implant components are uploaded, the user can choose to view, select and position the glenoid components (Figure 3.14(a)) or to view, select and position the humeral components (Figure 3.14(b)). Figure 3.4 lists the glenoid and humeral component possibilities. For each of these two views, a different function panel is activated, shown in Figure 3.15. Moreover, the user can select to view the selected implant components correctly positioned relative to one

another and the shoulder joint, as seen in Figure 3.14(c). The various views and component selections are chosen in the *Position Implant Process Panel*.

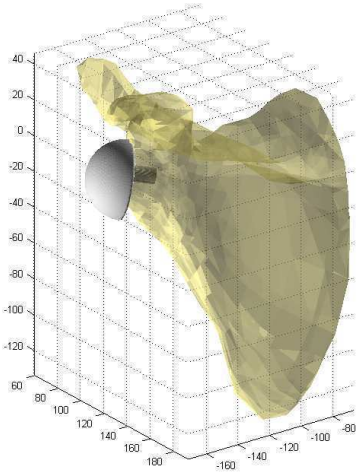

(a) Position Glenoid Components View

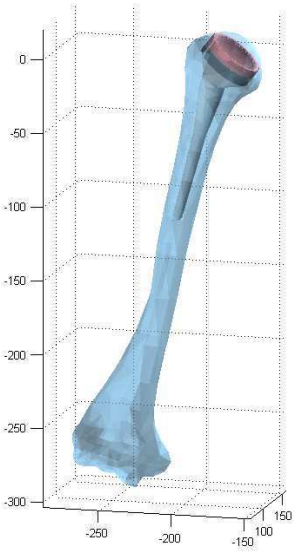

(b) Position Humeral Components View

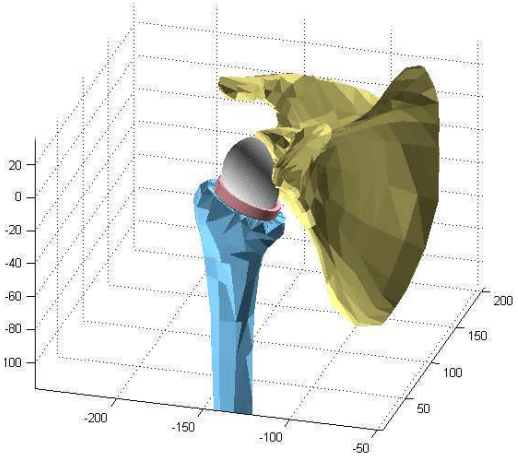

(c) Glenoid and Humeral Components View

Figure 3.14: Implant Component Views

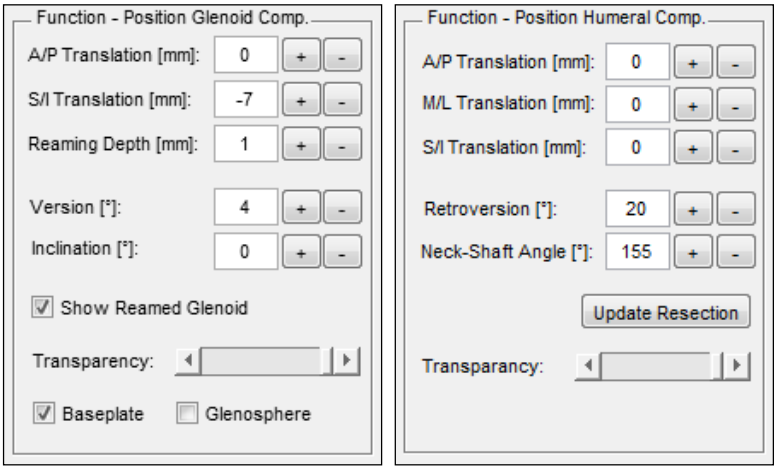

(a) Position Glenoid Components Function Panel

(b) Position Humeral Components Function Panel

Figure 3.15: Position Implant Process Function Panels

3.4.4.3 Position Glenoid Components

The glenoid components (baseplate and glenosphere) can interactively be translated and rotated as the user desires (Figure 3.15(a)). The translations and rotations are relative to the SCS_2. The function panel allows the user to toggle between a scapula that is reamed and one that is not yet reamed. This enables the user to determine how much bone has to be reamed away and whether the baseplate is fully seated on the glenoid. The user can also enable or disable the baseplate or glenosphere, allowing the user to accurately assess the correct placement of the baseplate. The transparency of the scapula can be changed from opaque to fully transparent. This function provides the user the capability to view the baseplate centre peg direction, as well as bone purchase quality.

3.4.4.4 Position Humeral Components

The user can interactively translate and rotate the humeral components (humeral stem and polyethylene insert) (Figure 3.15(b)). The translations and rotations are relative to the HCS. The humeral head resection is performed at the Aequalis® - Reversed II stem neck-shaft angle of 155°. After any translations and/or rotations of the humeral components have been performed, the humeral head resection can be updated. Lastly, by changing the transparency of the humerus, the user can ensure the correct stem placement.

3.4.4.5 Continue

The implant component selection and placement are interchangeable, which allows the user to make any desired changes throughout the implant positioning process before eventually continuing to the simulation process. Clicking on the *Continue* button of the *Position Implant Process Panel* (Figure 3.10(b)), activates the *Simulate Process Panel* and the *Simulate Function Panel* shown in Figures 3.10(c) and 3.16, respectively.

3.4.5 Simulate

The simulation process displays the possible humerothoracic ROM for the selected implant and placement option. Furthermore, it simulates the shoulder complex motion for the calculated ROM. The user can reselect and reposition the implant components (Sections 3.4.4.2 - 3.4.4.5) and then repeat the simulation process. Once the user is satisfied with the attainable ROM, a report can be generated containing the pre-operative planning details.

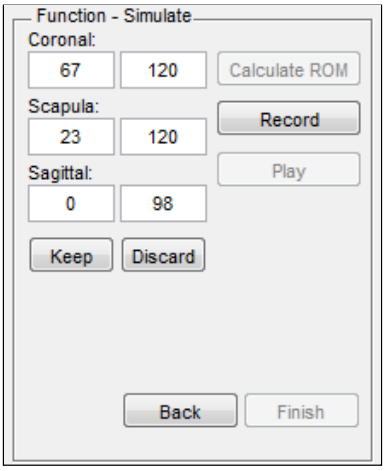

Figure 3.16: Simulate Function Panel

3.4.5.1 Calculate ROM

During the simulation process the RS^3 initially calculates, using the shoulder complex motion equations described in Section 3.1, the upper and lower boundaries of the humerothoracic ROM, to the nearest degree, for the selected implant components and positions. The upper boundary of the ROM is reached when the humerus or one of the humeral components impinges on any part of the scapula, while lifting the arm. If the humerus and its components reach an elevation of 120° without impinging on the scapula, this is taken as the upper boundary. The shoulder complex motion data and equations (Section 3.1) only accurately describe elevation of the arm up to 120°. Similarly,

the lower boundary of the ROM is determined when the humerus or one of its components impinges on the scapula, while lowering the arm. If the humerus and its components can be lowered to 0° without impinging on the scapula, this is taken as the lower boundary. This is performed for all elevation planes.

The adduction deficit for a specific elevation plane is its lower boundary value. The humerothoracic ROM is calculated as the difference between the upper and the lower boundary values.

Figure 3.17 shows the adduction deficit and humerothoracic ROM determined in the scapula elevation plane for an arbitrary implant component placement.

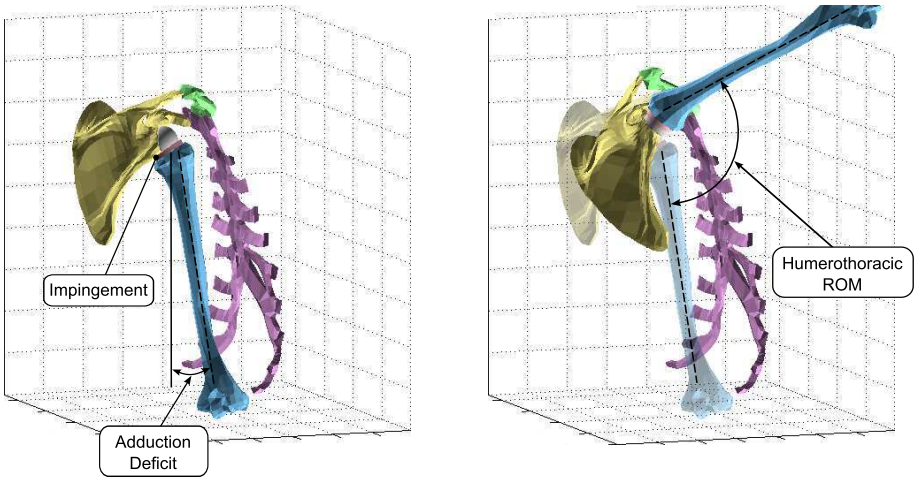

(a) Adduction Deficit (b) Humerothoracic ROM

Figure 3.17: Adduction Deficit and Humerothoracic ROM

3.4.5.2 Select Elevation Plane

The desired elevation plane for the shoulder complex motion simulation, either coronal, scapula, sagittal or all planes can be selected in the *Simulate Process Panel*. The selected elevation plane determines the set of motion equations to be used in the shoulder complex motion simulation. The coronal elevation plane uses the Equations A.1 - A.6. The scapula elevation plane uses the Equations A.7 - A.12 and the sagittal elevation plane uses the Equations A.13 - A.18.

3.4.5.3 Run Simulation

The shoulder complex motion simulation for the selected elevation plane is performed for the current implant components and position.

The SC and AC points and the glenosphere COR are used as the rotation centres for the clavicle, scapula and humerus, respectively. These points are dynamically updated throughout the lifting and lowering of the arm.

The simulation is displayed in the *Work Area* and can be viewed from any orientation.

3.4.5.4 Display ROM

The user can choose to *Keep* or *Discard* the selected implant components and placement option. When keeping the current option, the RS^3 stores the selected implant components and placement and displays the ROM in the *ROM Display*. Conversely, when discarding the current option, the RS^3 allows the user to reselect and reposition the implant components.

3.4.6 Desired ROM Achieved

After the simulation process, the user can choose to generate a report for one of the stored options or to return to the implant positioning process.

3.4.7 Generate Report

A report is generated of the implant components and placement option selected by the user. The report contains the glenoid anatomical version and inclination angles, the humeral anatomical retroversion angle and the humeral anatomical neck-shaft angle. It also contains the glenoid and humeral components selected, as well as their translations and rotations with respect to the SCS_2 and HCS. Lastly, the report shows the ROM possible for the implant components and placement.

3.5 Summary

The RS^3 uses shoulder complex motion equations obtained by fitting polynomials to the motion data of Ludewig *et al.* (2009). The motion equations are patient-specific and describe sternoclavicular and scapulothoracic motion in the coronal, scapula and sagittal elevation planes.

The Tornier Aequalis® - Reversed II implants are used in the software. The software also requires STL files of the patient's clavicle, scapula, humerus, C7 and T8 vertebrae, and sternum, which are created in Mimics software from the patient's CT data.

The functionality and work flow of the GUI is presented in detail. Firstly, the user performs the patient setup process (setup patient process). This is comprised of the alignment and translation of the patient data and the setup of the clavicle, scapula and humerus. Secondly, the user selects and positions

the desired implant components (position implant process). Lastly, the ROM of the selected implant components and placement can be calculated and simulated (simulate process). The position implant and simulate process can be repeated until a satisfactory ROM has been achieved. A report containing the anatomical angles, the selected implant components, the implant positions and the achievable ROM is then generated.

4. Optimal Reverse Shoulder Component Placement

Before determining the optimal reverse shoulder component placement for a specific patient, the simulation software has to be verified and validated. Furthermore, the influence of component combinations and orientations on humerothoracic ROM and adduction deficit has to be better understood. To address these points, a complete series of simulations was performed.

The simulation results and insight gained were then applied in a pre-operative planning simulation case study.

4.1 Simulations

The RS^3 simulations consisted of obtaining the humerothoracic ROM for the different elevation planes and component combinations, by incrementally changing the glenoid component inclination from $-10\,^\circ$ to $10\,^\circ$. For every inclination simulated the glenoid components were placed at the desired inferior or superior inclination and the baseplate was placed flush with the inferior margin of the glenoid rim. This coincided with the surgical technique recommendations, Dr De Beer's preference and the findings of Nyffeler *et al.* (2005). Reaming was then performed until the entire back of the baseplate was fully seated on the glenoid.

Throughout the simulations the glenoid component version was held constant at $0\,^\circ$. This restores the anatomical glenoid version angle and ensures centralized placement of the baseplate's centre peg within the scapular neck, which allows proper bone purchase and also prevents perforation of the centre peg. For every inclination simulated, the humerothoracic ROM and adduction deficit was determined for increasing humeral component retroversion angles, ranging from $0\,^\circ$ to $50\,^\circ$.

Additionally, proposed prosthesis design changes were simulated. Incorporating inferior and lateral eccentricity into a glenosphere was evaluated. The effect of using a humeral component with a neck-shaft angle of $145\,^\circ$ and $165\,^\circ$, compared to the standard $155\,^\circ$ neck-shaft angle, was also investigated.

The optimal component placement was determined by maximizing the combined humerothoracic ROM across the coronal, scapula and sagittal elevation

planes, as well as minimizing the combined adduction deficit across the said elevation planes.

Lastly, descriptive statistics were performed using an Analysis Of Variance (ANOVA). A significance level of $p < 0.05$ was used.

4.1.1 Shoulder Model Validation

The results shown were obtained for a shoulder model with a glenoid height and width of 37.2 mm and 28.9 mm, and superior inclination and retroversion of 6.7° and 7.3°, respectively. The humeral head radius was 24.4 mm. These measurements compared agreeably with the anatomical measurements taken by Gutiérrez *et al.* (2008) of patients that have undergone a RSA (Table 4.1).

At resting position, the shoulder model sternoclavicular joint was retracted, elevated and anteriorly rotated with 26.5°, 16.3° and 0°, respectively. Additionally, at resting position, the shoulder model scapulothoracic joint was internally rotated, upwardly rotated and anteriorly tilted with 33.3°, 19.1° and 4.2°, respectively.

Table 4.1: Comparison of the Shoulder Model with Anatomical Measurements (Adapted from Gutiérrez *et al.* (2008))

Anatomical Measurements	**Shoulder Model**	**95 % Confidence Interval in Population of Patients with RSA**
Glenoid Height [mm]	37.2	33.0 - 38.2
Glenoid Width [mm]	28.9	24.2 - 29.4
Glenoid Superior Inclination [°]	6.7	2.5 - 11.5
Glenoid Retroversion [°]	7.3	6.1 - 13.3
Humeral Head Radius [mm]	24.4	20.9 - 24.7

4.1.2 Results

The simulations were two-fold. Firstly, the Aequalis® - Reversed II components were simulated as previously explained. Secondly, implementing the prosthesis design changes was also simulated.

All the simulation data can be found in Appendix B. This data is summarized and presented in this section.

4.1.2.1 Aequalis® - Reversed II System

The 25 mm baseplate and 36 mm glenosphere (concentric) placement for the different inclination angles (φ) is shown in Figure 4.1. This figure also shows the reaming required to place the baseplate flush with the inferior rim of the glenoid and to ensure that the back of the baseplate is fully seated on the glenoid surface.

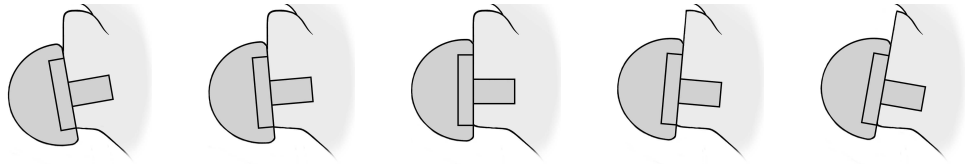

(a) $-10°$ (b) $-5°$ (c) $0°$ (d) $5°$ (e) $10°$

Figure 4.1: Glenoid Component Inclination (φ)

Table 4.2 shows the humeral component retroversion angle (ψ) that produced the smallest combined (coronal, scapula and sagittal elevation plane) adduction deficit for each of the component combinations and φ simulated. The frequency distribution of this table is depicted in Figure 4.2.

Table 4.2: ψ that Minimizes the Combined Adduction Deficit for Different φ

	φ				
Component Combination	**-10**	**-5**	**0**	**5**	**10**
36 mm glenopshere (concentric)					
25 mm baseplate; 6 mm poly. (con.)	35	35	35	35	30
25 mm baseplate; 6 mm poly. (inf.)	35	35	35	30	30
29 mm baseplate; 6 mm poly. (con.)	30	25;30	30	25	25
29 mm baseplate; 6 mm poly. (inf.)	25;30	25;30	30	20	20
36 mm glenopshere (inferior eccentric)					
25 mm baseplate; 6 mm poly. (con.)	40	40	*40	*35	*30
25 mm baseplate; 6 mm poly. (inf.)	45	40	*35;*40	*30	*20;*25
29 mm baseplate; 6 mm poly. (con.)	30	40	30	30	30
29 mm baseplate; 6 mm poly. (inf.)	30;35	30;35	30	35	35;40
36 mm glenopshere (lateral eccentric)					
25 mm baseplate; 6 mm poly. (con.)	25;30	30	25;30	30	30
25 mm baseplate; 6 mm poly. (inf.)	30;35	35;40	35	35	30;35
29 mm baseplate; 6 mm poly. (con.)	25;30	25;30	20	30	20
29 mm baseplate; 6 mm poly. (inf.)	25	25	20	30	20
42 mm glenopshere (concentric)					
25 mm baseplate	40;45	40	35;40	*35	*30
29 mm baseplate	25;30	30	30	30	30
42 mm glenopshere (inferior eccentric)					
25 mm baseplate	*30	*25;*30	*15;*20	*15	*15-25
29 mm baseplate	45	40	*40	*35	*25
42 mm glenopshere (lateral eccentric)					
25 mm baseplate	*35	*30	*25	*20-35	*20-40
29 mm baseplate	30;35	35	35	40	40

*There was no adduction deficit.

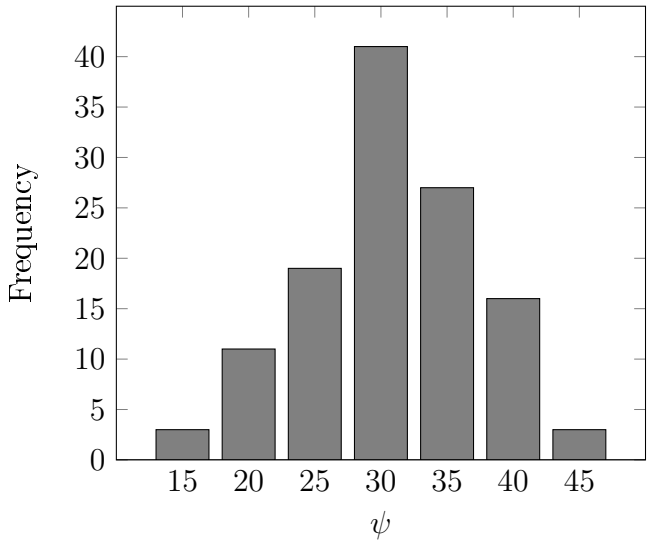

Figure 4.2: ψ Frequency Distribution (Table 4.2)

The ψ that had the smallest combined adduction deficit remained relatively constant for a specific component combination, while φ was changed. Changing the polyethylene insert from a concentric to an inferiorly eccentric option (36 mm glenospheres) only slightly influenced the ψ values. (Table 4.2).

Figure 4.2 shows a normal frequency distribution of the values in Table 4.2. A ψ of 30° was found to be the median and the mode of the distribution, occurring 41 times out of the 120 entries (34.2 %). The ψ values between the 5^{th} and 95^{th} percentiles of the distribution were between 20° and 40°.

Figures B.2 - B.4 display the combined humerothoracic ROM and adduction deficit angles for the 36 mm glenosphere options. Figure B.5 shows the combined humerothoracic ROM and adduction deficit angles for the 42 mm glenosphere options. Refer to Figure 3.4 in Section 3.2.1 for the different glenosphere options. All combinations simulated used the 6 mm polyethylene inserts. Using thicker inserts made no change in the humerothoracic ROM and adduction deficit. The box plots for each of these figures depict the data contained in the tables in Appendix B.1. Figure 4.3 shows an example of the graphical illustration of the simulation data for the concentric 36 mm glenosphere component combinations.

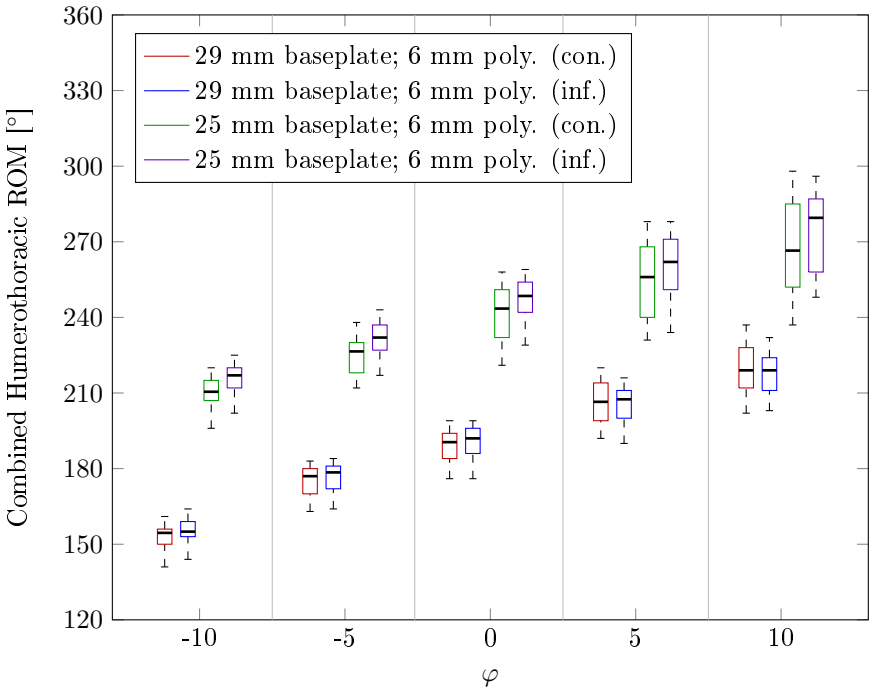

(a) Humerothoracic ROM

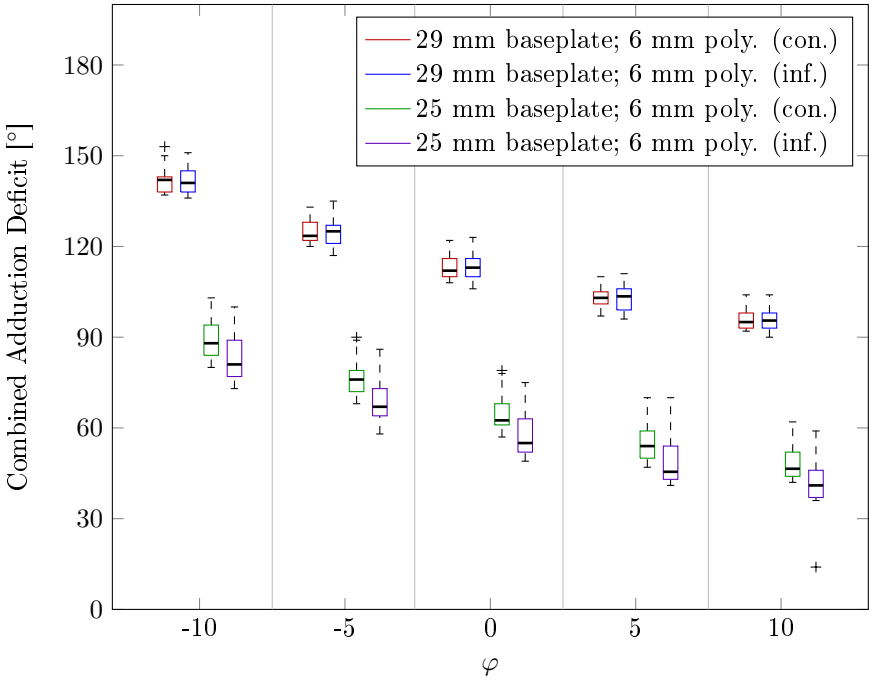

(b) Adduction Deficit

Figure 4.3: 36 mm Glenosphere (concentric) - Humerothoracic ROM and Adduction Deficit

In all cases, increasing φ increased the combined humerothoracic ROM and decreased the combined adduction deficit. For every glenosphere simulated, the 25 mm baseplate option produced a greater combined humerothoracic ROM (40 % to 80 % increase) and a smaller combined adduction deficit compared to the 29 mm option (10 % to 30 % decrease). There was no statistical significant difference ($p < 0.001$) by changing the polyethylene insert from concentric to 2 mm inferiorly eccentric.

Changing the glenosphere options from concentric to either inferiorly eccentric or laterally eccentric improved the combined humerothoracic ROM and adduction deficit by up to 20 % and 80 %, respectively.

There was a 60 % to 80 % increase in the combined humerothoracic ROM and a 20 % to 30 % decrease in the combined adduction deficit when changing the 36 mm glenosphere option (concentric, inferior or lateral) to its corresponding 42 mm glenosphere option. The laterally eccentric glenospheres produced the greatest increase in the combined humerothoracic ROM, whereas the inferiorly eccentric glenospheres produced the greatest decrease in the combined adduction deficit.

The greatest average combined humerothoracic ROM was 355.7° (42 mm glenosphere (lateral); 25 mm baseplate; 10° inclination), whereas the least was 153.2° (36 mm glenosphere (concentric); 29 mm baseplate; 6 mm polyethylene insert (concentric); −10° inclination). The smallest average combined adduction deficit was 0.5° (42 mm glenosphere (inferior); 25 mm baseplate; 10° inclination) and the largest was 141.8° (36 mm glenosphere (concentric); 29 mm baseplate; 6 mm polyethylene insert (inferior); −10° inclination).

4.1.2.2 Prosthesis Design Changes

The results obtained from the previous simulations indicated that laterally eccentric glenospheres produced the greatest combined humerothoracic ROM and inferiorly eccentric glenospheres resulted in the smallest combined adduction deficit. A design change that was postulated to improve the shoulder complex motion of a reverse shoulder component was to combine the laterally and inferiorly eccentric behaviour of the glenospheres. A 36 mm and a 42 mm glenosphere, which were both 3 mm laterally and 4 mm inferiorly eccentric, were simulated with a 25 mm baseplate at 0° inclination for ψ ranging from 0° to 50°. The 36 mm glenosphere simulations included a concentric polyethylene insert.

Another design change implemented was to change the γ). A decrease in adduction deficit was expected for a smaller γ. This should in turn beneficially influence the combined humerothoracic ROM. The simulations for this design change included a γ of 145°, 155° (standard) and 165° (Figure 4.4). The simulations were performed with the concentric 36 mm and 42 mm glenospheres, with a 25 mm baseplate, a concentric polyethylene insert, at 0° inclination and for ψ ranging from 20° to 40°.

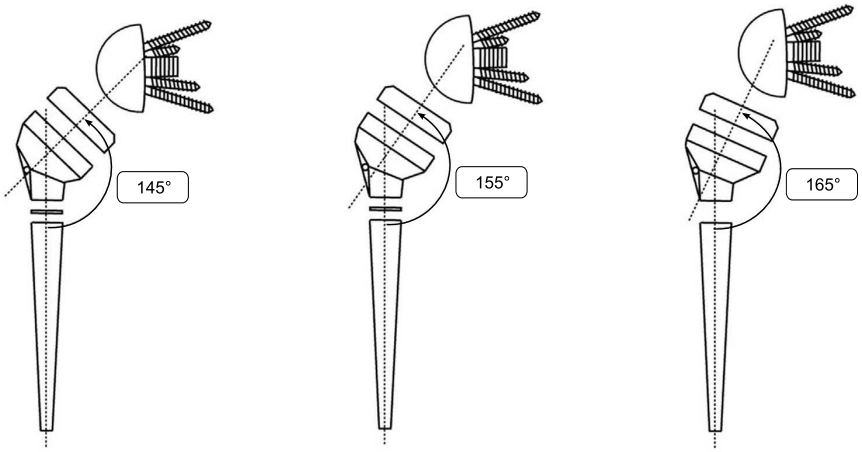

(a) 145 ° (b) 155 ° (c) 165 °

Figure 4.4: Humeral Component Neck-shaft Angle (γ)

The results for the prosthesis design changes can be found in Appendix B.2 and are presented below in Figure 4.5 and Figure 4.6. Figure 4.5 shows the comparison of the different eccentric glenospheres and Figure 4.6 shows the trends obtained for the different γ.

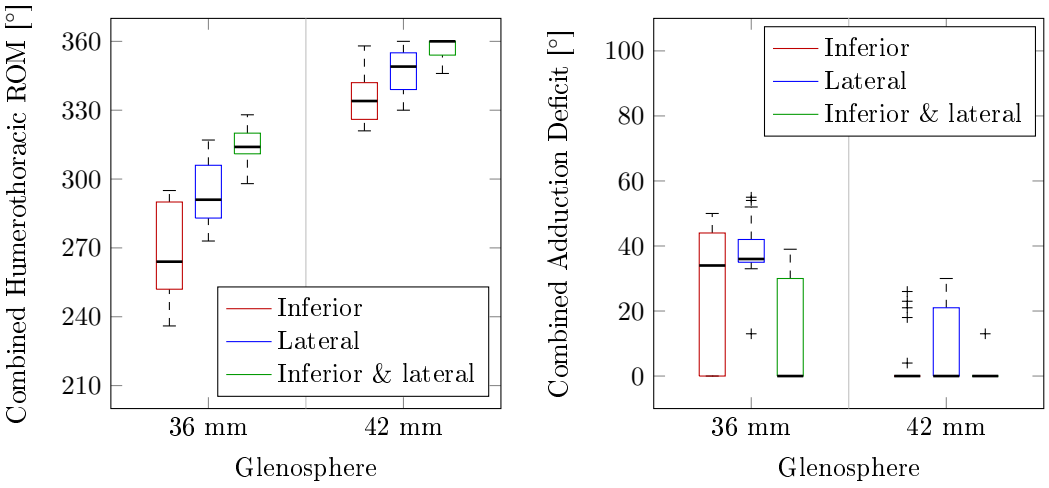

(a) Humerothoracic ROM (b) Adduction Deficit

Figure 4.5: 36 mm and 42 mm Glenosphere Design Change Comparison

The glenospheres with both lateral and inferior eccentricity showed improvement compared to the glenospheres with only lateral or only inferior eccentricity. There was a slight increase of 7.2 % and 2.7 % in the combined humerothoracic ROM of the 36 mm and 42 mm glenospheres, respectively, and

a substantial decrease of 52.9 % and 85.9 % in the combined adduction deficit of the 36 mm and 42 mm glenospheres, respectively.

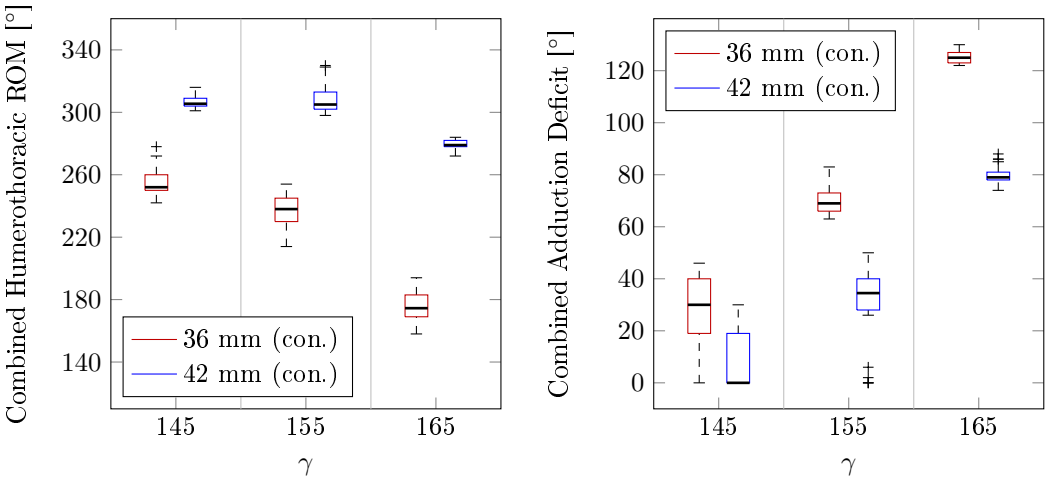

(a) Humerothoracic ROM

(b) Adduction Deficit

Figure 4.6: γ Design Change Comparison

As postulated, the γ of 145° produced a decrease of 61.5 % and 72.4 % in the combined adduction deficit of the 36 mm and 42 mm glenospheres, respectively. This subsequently produced a 7.5 % and 0.8 % increase in the combined humerothoracic ROM of the 36 mm and 42 mm glenospheres, respectively. Increasing the γ to 165° produced the expected results. There was an exponential decrease in the combined humerothoracic ROM, as well as an exponential increase in the combined adduction deficit achieved by the γ of 165°.

4.1.3 Discussion

RSA is increasingly being used in the treatment of arthritic rotator cuff deficient shoulders. There are, however, many complications still associated with this procedure, with scapular notching being the most common. Scapular notching has been clinically shown to have an adverse effect on the long-term outcomes of a RSA and that the impingement might further induce prosthetic wear and osteolysis (Nyffeler *et al.*, 2004; Simovitch *et al.*, 2007). Clinical outcomes of this procedure are dependent on the preoperative diagnosis, the function of the remaining deltoid and remaining rotator cuff muscles, orientation and placement of the reverse shoulder component, and the biomechanical design of the prosthesis.

The purpose of the simulations was to better understand the mechanics of a RSA and the behaviour of the Tornier Aequalis® - Reversed II components

and combinations. Additionally, the biomechanical effect of prosthesis design changes on scapular notching and total ROM was investigated. This will assist the surgeon during pre-operative planning with implant selection and placement to maximize impingement-free coronal, scapula and sagittal ROM and to eliminate scapular notching. It may also provide information for future implant designs.

Previous studies (Section 2.2.3 and 2.2.4) have shown that laterally or inferiorly eccentric glenospheres allow a greater ROM of the arm and a decrease in scapular notching. Placing the glenosphere more inferiorly on the glenoid has also shown to increase the total ROM and decrease the adduction deficit. The simulation results in this study followed the expected trends found in literature. This verifies the simulation software developed. In both the 36 mm and 42 mm glenosphere cases, changing the glenosphere from a concentric to a laterally or inferiorly eccentric COR produced an improvement in ROM, as well as decreasing the adduction deficit. Additionally, changing the baseplate from the 25 mm to the 29 mm, effectively moving the glenosphere inferiorly by 2 mm, also produced up to 80 % improvement in ROM and up to 30 % decrease in the adduction deficit.

The ROM after a RSA has been studied in a limited scope thus far. A clinical study by Seebauer *et al.* (2005), using dynamic fluoroscopic radiographs, observed a maximum active scapula plane ROM of 53° for the DePuy Delta III prosthesis. Another biomechanical study measured a scapula plane ROM of 66° and an adduction deficit of 9° with the Delta III baseplate inferiorly positioned on the glenoid (Nyffeler *et al.*, 2005). These studies were limited to a single elevation plane. The current study looked at virtual shoulder complex motion in the coronal, scapula and sagittal elevation planes. It also provided the ability to simultaneously analyse multiple factors.

Sirveaux *et al.* (2004) and Lévigne *et al.* (2008) have shown that introducing an inferior tilt to the glenoid component decreases scapular notching, whereas Simovitch *et al.* (2007) found that an inferior tilt increased scapular notching. The simulation results show that the combined adduction deficit increases for a more inferiorly tilted glenoid component and decreases for a more superiorly tilted glenoid component, agreeing with Simovitch *et al.* (2007). Scapular notching decreases in some of the elevation planes for an increasing glenoid component inclination angle. The 42 mm glenosphere options even showed a decrease in scapular notching across all three elevation planes, with no combined adduction deficit found. More reaming of the glenoid surface was required for an inferior tilted glenoid component to ensure that the back of the baseplate was properly seated on the glenoid. This moved the COR of the glenosphere medially and would explain the increase in adduction deficit. The glenoid surface is naturally concave. The Delta III and the Aequalis® have a flat-backed baseplate, which require more reaming to place it flush with the glenoid surface to ensure good fixation, stability and osseointegration at the baseplate-bone interface. A convex-backed baseplate would require

less reaming for stable fixation and would allow screws to be placed further apart than with a flat-backed design, which resulted in greater resistance to baseplate-bone interface motion (Hopkins and Hansen, 2009). DePuy have modified their Delta III baseplate design to include a convex-backed baseplate in the Delta XTend^{TM}. Even though the simulations indicated that a superiorly tilted glenoid component produced the least adduction deficit, this might not be the optimal glenoid inclination angle. Gutiérrez *et al.* (2011) showed that for concentric and lateral glenospheres an inferior tilt provides the most even distribution of forces between the superior and inferior screws and a superior tilt provides the most uneven distribution of forces. For inferior eccentric glenospheres, an inferior tilt produced the most uneven distribution of forces and a neutral tilt (0°) produced the most even distribution of forces (refer to Figure 2.19 in 2.2.3). An uneven distribution of forces promotes the 'rocking horse' motion of the baseplate. For the current Tornier Aequalis® - Reversed II system the optimal glenoid inclination is concluded to be a neutral tilt for concentric and lateral glenospheres and a neutral or superior tilt for an inferior glenosphere, where the superior tilted inferior glenosphere produces the greatest combined ROM and least combined adduction deficit.

Stephenson *et al.* (2011) found that for the Tornier Aequalis® Reversed shoulder prosthesis, the optimal version for the humeral component appears to be between 20° and 40° of retroversion. The simulation data correlated very well with these findings. The humeral component retroversion values between the 5^{th} and 95^{th} percentiles of the distribution that produced the smallest combined adduction deficit for a specific component combination were also between 20° and 40°. This validates the simulation software in terms of the humeral component retroversion optimization. The humeral component retroversion that appeared most (34.2 %) in the distribution was 30°. Interesting to note is that the internal rotation of the scapula at rest was 33.3°. Nothing definitive can be said about this, but further studies could be done to identify the relationship between the internal rotation angle and the optimal humeral component retroversion angle.

Combining inferior and lateral eccentricity into one glenosphere was simulated as a suggested improvement to the current Tornier designs that only exhibit one of the two eccentricities in their glenospheres. There was a small improvement in the combined humerothoracic ROM of a maximum of 7.2 %. The combined adduction deficit showed great improvement of up to 85.9 %, where the combined eccentric glenospheres produced almost no combined adduction deficit for the varying humeral component retroversion angles. The findings confirmed that combining both eccentric behaviours would result in an overall improvement compared to the current designs. Gutiérrez *et al.* (2011) did not look at the superior and inferior screw force distribution for a combined eccentric glenosphere. However, taking an average of the most desirable and acceptable tilt positions of the inferior and lateral glenospheres (Figure 2.19 in Section 2.2.3) would suggest that a neutral tilt would favour a combined

eccentric glenosphere. There was no statistical difference between the results obtained from the inferiorly eccentric glenospheres at 10° superior tilt and the combined eccentric glenospheres at neutral tilt ($p < 0.001$). A lateralized COR, however, increases the chances of the 'rocking horse' phenomenon occurring, which means that the inferior glenospheres placed at a 10° superior tilt would seem like the most desirable glenosphere and glenoid component inclination angle.

A humeral neck-shaft angle of 145° produced a decrease of the combined adduction deficit of up to 72.4 % compared to a neck-shaft angle of 145°. Previous studies also found that a decrease in the neck-shaft angle resulted in a decrease in the adduction deficit (Gutiérrez *et al.*, 2007; Oh *et al.*, 2014) . Furthermore, Oh *et al.* (2014) found that although the current neck-shaft angle was more prone to scapular impingement than a smaller neck-shaft angle, it had the advantage of being more stable at the internally rotated position, which was found to be the least stable humeral rotation. More biomechanical and kinematic testing would be required to accurately conclude, whether changing the neck-shaft angle to 145° is indeed advantageous.

The limitations of this study need to be addressed. The shoulder complex motion simulation takes a mechanical approach to determine the combined humerothoracic ROM and combined adduction deficit. In practice, many factors contribute to the decision-making of implant selection and the active ROM. Some of which are the amount of good bone available for fixation, screw placement, soft tissue impingement, soft tissue balance, overall space limitations, and strength of the remaining muscles. These factors have to be considered in conjunction with the results of the simulations when performing the pre-operative surgery planning. By not including these factors in the simulation software, the true ROM values may differ compared to the values of this study.

Only the Tornier Aequalis® - Reversed II system was simulated. A more complete study that considers some of the other existing reverse shoulder systems is required to provide a more comprehensive analysis and comparison.

Finally, the simulations performed were all virtual. A cadaver or a clinical study is needed to fully validate the simulation software. Virtual simulations provide a powerful approach for simultaneous analysis of multiple factors and a reduction of testing time.

4.2 Case Study

The case study consists of the RS^3 pre-operative planning simulation performed on one of Dr De Beer's patients. Unfortunately, due to timing constraints, Dr De Beer could not use the RS^3 as a pre-operative planning tool for this case. A blind experiment could still be performed by performing an

optimal implant selection and placement on the patient files and potentially comparing the results with the actual post-operative analysis of the patient.

4.2.1 Patient Details

The patient was female and qualified for a reverse shoulder arthroplasty on her left shoulder.

A CT scan was taken in accordance with the requirements stated in Section 3.2.2. Mimics software was used to convert the patient data to 3D STL files, which were checked for quality in 3-Matic software.

The scapula had a glenoid height and width of 37.7 mm and 29.1 mm, and superior inclination and retroversion of 8.5° and 5.8°, respectively. The humeral head radius was 24.6 mm. At rest, the sternoclavicular joint was retracted, elevated and anteriorly rotated with 0.4°, 21.0° and 0°, respectively. And the scapulothoracic joint was internally rotated, upwardly rotated and anteriorly tilted with 40.4°, 3.8° and 29.3°, respectively.

4.2.2 Pre-operative Planning Simulation

The 25 mm baseplate was placed at 0° glenoid version and was placed flush with the inferior margin of the glenoid rim. The centre peg showed no perforation of the scapular neck.

The initial simulations were performed with the 42 mm inferior glenosphere at a superior tilt. With the glenoid's anatomical superior inclination of 8.5°, a glenoid component superior tilt of 8° ensured minimal reaming to place the back of the baseplate flush with the glenoid surface.

The humeral component was set at 30° retroversion, which was found to be the optimal retroversion for the majority of the simulations performed in Section 4.1. Simulations were also run with a retroversion of 40° to investigate the relationship between the resting internal rotation of the scapula and the humeral component retroversion. The simulations showed that due to the large resting anterior tilt of the scapula, impingement occurred between the humerus shaft and the coracoid process (see Figure 2.1 in Chapter 2) of the scapula in the sagittal elevation plane. This limited the sagittal humerothoracic ROM. Therefore, a retroversion of 20° was also simulated. The previous simulation results showed that smaller retroversion produced improved sagittal plane motion. The results for the simulations with the inferior glenosphere are contained in Table 4.3. The 20° retroversion showed a slight improvement in the sagittal humerothoracic ROM, but still being very limited with a maximum of 65°.

Thereafter, the 42 mm lateral glenosphere was simulated at a neutral tilt. The simulation results are also shown in Table 4.3. With a lateralized COR of the glenosphere, impingement at the coracoid process occurred later. This increased the sagittal humerothoracic ROM to 71°.

The optimal placement of the Tornier Aequalis® - Reversed II components that maximized the combined humerothoracic ROM and minimized the combined adduction deficit was found to be at 0° glenoid inclination and 20° humeral component retroversion for the 25 mm baseplate and 42 mm lateral glenosphere. There was no combined adduction deficit, therefore no scapular notching found at this placement.

Table 4.3: Case Study Simulation Results

			Coronal Plane		Scapula Plane		Sagittal Plane	
Glenosphere	φ	ψ	**LB [°]**	**UB [°]**	**LB [°]**	**UB [°]**	**LB [°]**	**UB [°]**
42 mm (inferior)	8	20	0	120	0	120	0	65
	8	30	0	120	0	120	0	65
	8	40	0	120	0	120	2	64
42 mm (lateral)	0	20	0	120	0	120	0	71
	0	30	0	120	0	120	0	70
	0	40	0	120	0	120	0	68

LB - Lower Boundary (adduction deficit)
UB - Upper Boundary
Humerothoracic ROM = UB - LB

4.3 Summary

To determine the optimal placement of the reverse shoulder component the influence of component combinations and orientations on humerothoracic ROM and adduction deficit has to be better understood. A series of simulations comparing the effect of glenoid inclination, humeral component retroversion, glenosphere size, glenosphere eccentricity and baseplate position on total ROM and adduction deficit was performed. Additionally, the impact of combining inferior and lateral eccentricity in a glenosphere and changing the humeral component neck-shaft angle was assessed.

A 42 mm inferior glenosphere placed at a 10° superior inclination angle produced the greatest combined humerothoracic ROM and least combined adduction deficit, while taking the superior and inferior screw force distributions and the 'rocking horse' phenomenon into account.

A smaller humeral component neck-shaft angle produced better simulation results compared to the standard 155°, however, a previous study showed that a humeral component with a 155° neck-shaft angle was more stable than with a smaller neck-shaft angle.

Finally, the simulation results were applied to a case study and should be compared to the actual post-operative patient placement results.

5. Conclusions and Recommendations

The purpose of this study was to optimize the patient-specific placement of a reverse shoulder component. This would be achieved through the development of a simulation software package. With the use of the simulation software, the effect of the placement and design of the reverse shoulder prosthesis on total ROM and scapular notching could be thoroughly assessed. This would provide the knowledge required to optimally position the reverse shoulder components for any patients, as well as to observe the shoulder motion.

Chapter 3 describes the development and functionality of the reverse shoulder simulation software. The simulation software package was developed using Matlab software and its GUIDE tools. The chapter clearly shows and explains the work flow and the processes involved in the simulation software. The RS^3 allows the user to upload any patient's shoulder data. The patient data must conform to certain requirements. The data files have to be in STL format, which can be generated from the patient's CT data using Mimics software. One of the processes involved in the RS^3 is the patient setup process. This process is used mainly for anatomical landmark identification, which is necessary to calculate the various shoulder coordinate systems such that the patient-specific simulation can function properly. The patient files consist of the clavicle, the scapula, the humerus, the C7 and T8 vertebrae and the sternum. The simulation motion is not only comprised of the glenohumeral motion, but also includes the sternoclavicular and scapulothoracic motion, together making up the shoulder complex motion. The simulation in the software package is driven by motion equations. These equations were obtained by fitting polynomials to the motion data of Ludewig *et al.* (2009). Ludewig *et al.* (2009) looked at the shoulder complex motion in the coronal, scapula and sagittal elevation planes. The motion equations are patient-specific by taking into account the sternoclavicular and scapulothoracic joint angles at rest, at 0° humerothoracic elevation. Dr De Beer, a leading shoulder specialist in South Africa, worked closely on the development of this software. He makes use of the Tornier Aequalis® - Reversed II implants, therefore this is also used in the simulation software. The RS^3 provides the surgeon the capability to perform 3D pre-operative planning compared to the current 2D radiographic

or CT planning being used. This allows the surgeon to simulate not just the shoulder motion, but also part of the surgery, which may reduce theatre time and cost. Finally, once the user is satisfied with the RS^3 results, a report containing the anatomical angles, the selected implant components, the implant positions and the achievable ROM is generated.

Using the RS^3, a series of simulations was performed to analyse the influence of the Aequalis® - Reversed II component combinations and orientations on humerothoracic ROM and adduction deficit. This is contained in Chapter 4. The shoulder model used throughout the simulations conformed to the typical geometric parameters of patients that have undergone a RSA. This does not take into account the anatomic variations found in patients, but it provides a good reference point to better understand the biomechanics after a RSA using the Aequalis® - Reversed II implants. Moreover, the RS^3 is patient-specific and takes any anatomic variations into consideration during pre-operative simulations. The simulation results agree with observations found in previous studies. Laterally or inferiorly eccentric glenospheres allow a greater ROM of the arm and introduce a decrease in scapular notching. Placing the baseplate more inferiorly on the glenoid also increases the total ROM and decreases the adduction deficit. The effect of the glenoid component inclination angle on the shoulder motion confirmed the results found by Simovitch *et al.* (2007), which say that an inferior tilt increases scapular notching. Additionally, the simulation results show that a superior tilt decreases the adduction deficit and in some cases even scapular notching. Combining the simulation results with the superior and inferior screw force distribution diagram of Gutiérrez *et al.* (2011), the optimal glenoid inclination for the Aequalis® - Reversed II components was found to be a neutral tilt for concentric and lateral glenospheres and a neutral or superior tilt for an inferior glenosphere. The 10° superiorly tilted inferior glenosphere produced the greatest combined ROM and least combined adduction deficit of the optimally tilted glenospheres. The RS^3 simulation results correlated very closely with the findings of Stephenson *et al.* (2011). The optimal retroversion for the humeral component appears to be between 20° and 40°. This validated the simulation software in terms of the humeral component retroversion optimization. The scapula of the shoulder model used for the simulation series was internally rotated at 33.3° and showed that an optimal humeral component retroversion of 30° was found for at least 34 % of the component combinations.

Furthermore, also found in Chapter 4 are the proposed design changes. The design changes for the Tornier Aequalis® - Reversed II reverse shoulder prosthesis included a convex-backed baseplate, a inferiorly and laterally combined eccentric glenosphere, and a humeral component neck-shaft angle of 145°. With the glenoid surface being naturally concave, a convex-backed baseplate would require less reaming until the entire baseplate is fully seated on the glenoid surface. This is required to ensure good fixation, stability and osseointegration. A convex-backed baseplate also allows screws to be placed

further apart than with a flat-backed baseplate, which provides greater resistance to baseplate-bone interface motion. The combined inferior and lateral glenosphere produced improved combined humerothoracic ROM and combined adduction deficit results compared to the glenospheres that are only inferiorly or laterally eccentric. An average of the most desirable and acceptable tilt positions found in force distribution diagram of Gutiérrez *et al.* (2011) would suggest that a neutral tilt would favour a combined eccentric glenosphere. There was no statistical difference found between the results obtained from the inferiorly eccentric glenospheres at 10° superior tilt and the combined eccentric glenospheres at neutral tilt. However, a lateralized COR increases the chances of the 'rocking horse' phenomenon occurring, which meant that the inferior glenospheres placed at a 10° superior tilt seemed like the most desirable glenosphere and glenoid component inclination angle, respectively. Lastly, using a smaller humeral component neck-shaft angle resulted in a decrease in the adduction deficit, as already shown by previous studies (Gutiérrez *et al.*, 2007; Oh *et al.*, 2014). This is not necessarily an improvement, as Oh *et al.* (2014) showed that a smaller neck-shaft angle is less stable at the internally rotated position than the standard neck-shaft angle of 155°.

The outcomes of the objectives mentioned in the first chapter, which are described above, were applied to a case study described in Chapter 4.

5.1 Future Work Recommendations

The simulation software was not fully validated yet. Experimental testing or a cadaver or clinical study is required to perform the validation. It would be complicated to reproduce the complex sternoclavicular and scapulothoracic motion described by the motion equations, either experimentally or in a cadaver study. Therefore, the post-operative active ROM in a clinical study would have to be measured for the different elevation planes and compared to the pre-operative software simulation results. This would only partly validate the software, due to the fact that no soft tissue effects are taken into consideration by the RS^3. Iteratively, the other factors, such as muscle forces, soft tissue impingement and soft tissue balance, could be included in the RS^3 to eventually attain a fully validated software package.

In addition, different types of reverse shoulder components should be included in the RS^3. More surgeons would be able to make use of the RS^3, which would in turn provide more simulation data. This would provide a large enough sample size of shoulders to perform simulations on and produce statistically relevant results for any type of reverse shoulder implant.

The greater number of simulation data may illustrate an interesting relationship between the optimal humeral component retroversion and the scapula internal rotation angle at rest. This could allow a unique humeral component retroversion angle to be found for every patient.

Finally, more testing, apart from ROM, is required to conclusively say whether a smaller humeral component neck-shaft angle, compared to the current angle of 155 °, is indeed more advantageous.

5.2 Conclusion

The objectives presented in Chapter 1 were addressed and successfully achieved throughout this study. The expected contributions of this study will assist surgeons in pre-operative implant selection and placement to determine the optimal positioning of the reverse shoulder components. More inexperienced surgeons will be able to attempt a RSA with greater confidence. Improved pre-operative planning will reduce surgery time and cost. Finally, the implementation of the results of this study and the use of the RS^3 may improve prosthesis survival rates and long-term clinical outcomes.

List of References

Baulot, E., Chabernaud, D. and Grammont, P. (1995). Results of grammont's inverted prosthesis in omarthritis associated with major cuff destruction. apropos of 16 cases]. *Acta orthopaedica Belgica*, vol. 61, p. 112.

Boileau, P., Bicknell, R., Mazzoleni, N., Walch, G. and Urien, J. (2008). Ct scan method accurately assesses humeral head retroversion. *Clinical orthopaedics and related research*, vol. 466, pp. 661–669.

Boileau, P. and Walch, G. (1997). The three-dimensional geometry of the proximal humerus implications for surgical technique and prosthetic design. *Journal of Bone & Joint Surgery, British Volume*, vol. 79, no. 5, pp. 857–865.

Boileau, P., Watkinson, D., Hatzidakis, A. and Balg, F. (2005). Grammont reverse prosthesis: design, rationale, and biomechanics. *Journal of shoulder and elbow surgery*, vol. 14, no. 1, pp. S147–S161.

Boileau, P., Watkinson, D., Hatzidakis, A. and Hovorka, I. (2006). Neer award 2005: The grammont reverse shoulder prosthesis: results in cuff tear arthritis, fracture sequelae, and revision arthroplasty. *Journal of shoulder and elbow surgery*, vol. 15, no. 5, pp. 527–540.

Bokor, D., O'Sullivan, M. and Hazan, G. (1999). Variability of measurement of glenoid version on computed tomography scan. *Journal of Shoulder and Elbow Surgery*, vol. 8, no. 6, pp. 595–598.

Boulahia, A., Edwards, T., Walch, G. and Baratta, R. (2002). Early results of a reverse design prosthesis in the treatment of arthritis of the shoulder in elderly patients with a large rotator cuff tear. *Orthopedics*, vol. 25, no. 2, p. 129.

Bourne, D., Choo, A., Regan, W., MacIntyre, D. and Oxland, T. (2007). Three-dimensional rotation of the scapula during functional movements: an in vivo study in healthy volunteers. *Journal of Shoulder and Elbow surgery*, vol. 16, no. 2, pp. 150–162.

Burke, C., Roberts, C., Nyland, J., Radmacher, P., Acland, R. and Voor, M. (2006). Scapular thickness-implications for fracture fixation. *Journal of shoulder and elbow surgery*, vol. 15, no. 5, pp. 645–648.

Chebli, C., Huber, P., Watling, J., Bertelsen, A., Bicknell, R. and Matsen III, F. (2008). Factors affecting fixation of the glenoid component of a reverse total shoulder prothesis. *Journal of Shoulder and Elbow Surgery*, vol. 17, no. 2, pp. 323–327.

Culham, E. and Peat, M. (1993). Functional anatomy of the shoulder complex. *Journal of Orthopaedic and Sports Physical Therapy*, vol. 18, pp. 342–342.

Dedy, N., Stangenberg, M., Liem, D., Hurschler, C., Simmen, B., Riner, M., Marquardt, B. and Steinbeck, J. (2011). Effect of posterior offset humeral components on range of motion in reverse shoulder arthroplasty. *International orthopaedics*, vol. 35, no. 4, pp. 549–554.

DeFranco, M. and Walch, G. (2011). Current issues in reverse total shoulder arthroplasty: understanding of the inherent limitations and complications is needed. *J Musculoskeletal Med*, vol. 28, no. 3, pp. 85–94.

Ebaugh, D., McClure, P. and Karduna, A. (2005). Three-dimensional scapulothoracic motion during active and passive arm elevation. *Clinical Biomechanics*, vol. 20, no. 7, pp. 700–709.

Edwards, T., Trappey, G., Riley, C., O'Connor, D., Elkousy, H. and Gartsman, G. (2012). Inferior tilt of the glenoid component does not decrease scapular notching in reverse shoulder arthroplasty: results of a prospective randomized study. *Journal of Shoulder and Elbow Surgery*, vol. 21, no. 5, pp. 641–646.

Favard, L., Lautmann, S., Sirveaux, F., Oudet, D., Kerjean, Y. and Huguet, D. (2000). Hemi arthroplasty versus reverse arthroplasty in the treatment of osteoarthritis with massive rotator cuff tear. *Walch G, Boileau P, Molé D, Editors*, pp. 261–8.

Favre, P., Sussmann, P. and Gerber, C. (2010). The effect of component positioning on intrinsic stability of the reverse shoulder arthroplasty. *Journal of Shoulder and Elbow Surgery*, vol. 19, no. 4, pp. 550–556.

Franklin, J., Barrett, W., Jackins, S.E. and Matsen III, F. (1988). Glenoid loosening in total shoulder arthroplasty: association with rotator cuff deficiency. *The Journal of arthroplasty*, vol. 3, no. 1, pp. 39–46.

Friedman, R., Hawthorne, K. and Genez, B. (1992). The use of computerized tomography in the measurement of glenoid. *J Bone Joint Surg Am*, vol. 74, pp. 1032–1037.

Grammont, P. and Baulot, E. (1993). Shoulder update: Delta shoulder prosthesis for rotator cuff rupture. *Orthopedics*, vol. 16, no. 1.

Grammont, P., Trouilloud, P., Laffay, J. and Deries, X. (1987). Design and manufacture of a new shoulder prosthesis. *Rhumatologie*, vol. 39, pp. 407–18.

Gulotta, L., Choi, D., Marinello, P., Knutson, Z., Lipman, J., Wright, T., Cordasco, F., Craig, E. and Warren, R. (2012). Humeral component retroversion in reverse total shoulder arthroplasty: a biomechanical study. *Journal of Shoulder and Elbow Surgery*, vol. 21, no. 9, pp. 1121–1127.

Gutiérrez, S., ComiskeyIV, C., Luo, Z., Pupello, D. and Frankle, M. (2008). Hierarchy of surgical and implant-design-related factors in range of impingement-free abduction and adduction deficit after reverse shoulder arthroplasty. *The Journal of Bone & Joint Surgery*, vol. 90, no. 12, pp. 2606–2615.

Gutiérrez, S., Greiwe, R., Frankle, M., Siegal, S. and Lee III, W. (2007). Biomechanical comparison of component position and hardware failure in the reverse shoulder prosthesis. *Journal of Shoulder and Elbow Surgery*, vol. 16, no. 3, pp. S9–S12.

Gutiérrez, S., Walker, M., Willis, M., Pupello, D. and Frankle, M. (2011). Effects of tilt and glenosphere eccentricity on baseplate-bone interface forces in a computational model, validated by a mechanical model, of reverse shoulder arthroplasty. *Journal of Shoulder and Elbow Surgery*, vol. 20, no. 5, pp. 732–739.

Harman, M., Frankle, M., Vasey, M. and Banks, S. (2005). Initial glenoid component fixation in "reverse" total shoulder arthroplasty: a biomechanical evaluation. *Journal of shoulder and elbow surgery*, vol. 14, no. 1, pp. S162–S167.

Henninger, H., Barg, A., Anderson, A., Bachus, K., Burks, R. and Tashjian, R. (2012). Effect of lateral offset center of rotation in reverse total shoulder arthroplasty: a biomechanical study. *Journal of Shoulder and Elbow Surgery*, vol. 21, no. 9, pp. 1128–1135.

Hopkins, A. and Hansen, U. (2009). Primary stability in reversed-anatomy glenoid components. *Proceedings of the Institution of Mechanical Engineers, Part H: Journal of Engineering in Medicine*, vol. 223, no. 7, pp. 805–812.

Hopkins, A., Hansen, U., Bull, A., Emery, R. and Amis, A. (2008). Fixation of the reversed shoulder prosthesis. *Journal of Shoulder and Elbow Surgery*, vol. 17, no. 6, pp. 974–980.

Huja, S., Litsky, A., Beck, F., Johnson, K. and Larsen, P. (2005). Pull-out strength of monocortical screws placed in the maxillae and mandibles of dogs. *American journal of orthodontics and dentofacial orthopedics*, vol. 127, no. 3, pp. 307–313.

Humphrey, C., Kelly II, J. and Norris, T. (2008). Optimizing glenosphere position and fixation in reverse shoulder arthroplasty, part two: The three-column concept. *Journal of Shoulder and Elbow Surgery*, vol. 17, no. 4, pp. 595–601.

Iannotti, J., Greeson, C., Downing, D., Sabesan, V. and Bryan, J. (2012). Effect of glenoid deformity on glenoid component placement in primary shoulder arthroplasty. *Journal of Shoulder and Elbow Surgery*, vol. 21, no. 1, pp. 48–55.

Koh, T., Grabiner, M. and Brems, J. (1998). Three-dimensional in vivo kinematics of the shoulder during humeral elevation. *Journal of applied biomechanics*, vol. 14, pp. 312–326.

Krekel, P., Botha, C., Valstar, E., de Bruin, P., Rozing, P. and Post, F. (2006). Interactive simulation and comparative visualisation of the bone-determined range of motion of the human shoulder. In: *SimVis*, pp. 275–288.

Krekel, P., Valstar, E., De Groot, J., Post, F., Nelissen, R. and Botha, C. (2010). Visual analysis of multi-joint kinematic data. In: *Computer Graphics Forum*, vol. 29, pp. 1123–1132. Wiley Online Library.

Kwon, Y., Powell, K., Yum, J., Brems, J. and Iannotti, J. (2005). Use of three-dimensional computed tomography for the analysis of the glenoid anatomy. *Journal of shoulder and elbow surgery*, vol. 14, no. 1, pp. 85–90.

Lévigne, C., Boileau, P., Favard, L., Garaud, P., Molé, D., Sirveaux, F. and Walch, G. (2008). Scapular notching in reverse shoulder arthroplasty. *Journal of Shoulder and Elbow Surgery*, vol. 17, no. 6, pp. 925–935.

Ludewig, P., Phadke, V., Braman, J., Hassett, D., Cieminski, C. and LaPrade, R. (2009). Motion of the shoulder complex during multiplanar humeral elevation. *The Journal of Bone & Joint Surgery*, vol. 91, no. 2, pp. 378–389.

McClure, P., Michener, L., Sennett, B. and Karduna, A. (2001). Direct 3-dimensional measurement of scapular kinematics during dynamic movements in vivo. *Journal of Shoulder and Elbow Surgery*, vol. 10, no. 3, pp. 269–277.

Medical MultiMEDIA Group, LLC (2009). *Shoulder Anatomy*. [Online] Available at: `http://www.eorthopod.com/content/shoulder-anatomy` [Accessed 13 February 2014].

Meskers, C., Van der Helm, F., Rozendaal, L. and Rozing, P. (1997). < i> in vivo</i> estimation of the glenohumeral joint rotation center from scapular bony landmarks by linear regression. *Journal of biomechanics*, vol. 31, no. 1, pp. 93–96.

Molé, D. and Favard, L. (2007). Excentered scapulohumeral osteoarthritis. *Revue de chirurgie orthopédique et réparatrice de l'appareil moteur*, vol. 93, no. 6 Suppl, p. 37.

NeerII, C. (1955). Articular replacement for the humeral head. *The Journal of Bone & Joint Surgery*, vol. 37, no. 2, pp. 215–228.

NeerII, C. (1974). Replacement arthroplasty for glenohumeral osteoarthritis. *The Journal of Bone & Joint Surgery*, vol. 56, no. 1, pp. 1–13.

Nyffeler, R., Werner, C. and Gerber, C. (2005). Biomechanical relevance of glenoid component positioning in the reverse delta iii total shoulder prosthesis. *Journal of shoulder and elbow surgery*, vol. 14, no. 5, pp. 524–528.

Nyffeler, R., Werner, C., Simmen, B. and Gerber, C. (2004). Analysis of a retrieved delta iii total shoulder prosthesis. *Journal of Bone & Joint Surgery, British Volume*, vol. 86, no. 8, pp. 1187–1191.

Oh, J., Shin, S., McGarry, M., Scott, J., Heckmann, N. and Lee, T. (2014). Biomechanical effects of humeral neck-shaft angle and subscapularis integrity in reverse total shoulder arthroplasty. *Journal of Shoulder and Elbow Surgery*.

Pollock, R., Deliz, E., McIlveen, S., Flatow, E. and Bigliani, L. (1992). Prosthetic replacement in rotator cuff-deficient shoulders. *Journal of Shoulder and Elbow Surgery*, vol. 1, no. 4, pp. 173–186.

Randelli, M. and Gambrioli, P. (1986). Glenohumeral osteometry by computed tomography in normal and unstable shoulders. *Clinical orthopaedics and related research*, vol. 208, pp. 151–156.

Sanchez-Sotelo, J., Cofield, R. and Rowland, C. (2001). Shoulder hemiarthroplasty for glenohumeral arthritis associated with severe rotator cuff deficiency. *The Journal of Bone and Joint Surgery (American)*, vol. 83, no. 12, pp. 1814–1822.

Seebauer, L., Walter, W. and Keyl, W. (2005). Reverse total shoulder arthroplasty for the treatment of defect arthropathy. *European Journal of Trauma*, vol. 31, no. 5, pp. 508–520.

Simovitch, R., Zumstein, M., Lohri, E., Helmy, N. and Gerber, C. (2007). Predictors of scapular notching in patients managed with the delta iii reverse total shoulder replacement. *The Journal of Bone & Joint Surgery*, vol. 89, no. 3, pp. 588–600.

Sirveaux, F., Favard, L., Oudet, D., Huquet, D., Walch, G. and Mole, D. (2004). Grammont inverted total shoulder arthroplasty in the treatment of glenohumeral osteoarthritis with massive rupture of the cuff. *Journal of Bone & Joint Surgery, British Volume*, vol. 86, no. 3, pp. 388–395.

Sperling, J., Hawkins, R., Walch, G., Mahoney, A., Zuckerman, J. *et al.* (2012). Complications in total shoulder arthroplasty. *Instructional course lectures*, vol. 62, pp. 135–141.

Stephenson, D., Oh, J., McGarry, M., Rick Hatch III, G. and Lee, T. (2011). Effect of humeral component version on impingement in reverse total shoulder arthroplasty. *Journal of Shoulder and Elbow Surgery*, vol. 20, no. 4, pp. 652–658.

Tornier, Inc (). *Surgical Implants*. [Online] Available at: `http://http://www.tornier.com/` [Accessed 2 September 2014].

van der Glas, M., Vos, F., Botha, C. and Vossepoel, A. (2002). Determination of position and radius of ball joints. In: *Medical Imaging 2002*, pp. 1571–1577. International Society for Optics and Photonics.

Van der Merwe, J. (2013). *Development of a patient-specific unicompartmental knee replacement*. Ph.D. thesis, Stellenbosch University.

Virani, N., Harman, M., Li, K., Levy, J., Pupello, D. and Frankle, M. (2008). In vitro and finite element analysis of glenoid bone/baseplate interaction in the reverse shoulder design. *Journal of Shoulder and Elbow Surgery*, vol. 17, no. 3, pp. 509–521.

Wall, B., Nové-Josserand, L., O'Connor, D., Edwards, T. and Walch, G. (2007). Reverse total shoulder arthroplasty: a review of results according to etiology. *The Journal of Bone & Joint Surgery*, vol. 89, no. 7, pp. 1476–1485.

Williams, G. and Rockwood, C. (1996). Hemiarthroplasty in rotator cuff-deficient shoulders. *Journal of Shoulder and Elbow Surgery*, vol. 5, no. 5, pp. 362–367.

Wu, G., Van der Helm, F., Veeger, H., Makhsous, M., Van Roy, P., Anglin, C., Nagels, J., Karduna, A., McQuade, K., Wang, X. *et al.* (2005). Isb recommendation on definitions of joint coordinate systems of various joints for the reporting of human joint motion-part ii: shoulder, elbow, wrist and hand. *Journal of biomechanics*, vol. 38, no. 5, pp. 981–992.

Appendices

A. Shoulder Complex Motion Data

The shoulder complex motion data obtained by Ludewig *et al.* (2009) is contained in this section.

Scapula plane abduction was performed at a plane 40° anterior to the coronal plane.

A.1 Sternoclavicular Motion

All rotations of the clavicle are relative to the thorax, are about the SC joint, and occur around the three axes of the TCS (section 2.1.3). Protraction/retraction is around the superior axis, elevation/depression is around the anterior axis, and anterior/posterior rotation is around the lateral axis of the TCS. Figure A.1 depicts the directions for protraction (a), elevation (b) and posterior rotation (c), respectively.

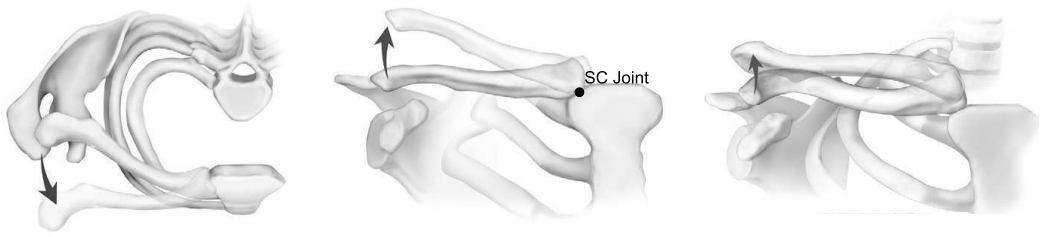

(a) Protraction (b) Elevation (c) Posterior Rotation

Figure A.1: Rotation of the Clavicle (Illustration: Ludewig *et al.* (2009))

The sternoclavicular angular rotation values for the coronal, scapula and sagittal plane elevation are shown in Table A.1 - A.3. The values shown are for the humerothoracic elevation range of 15° - 120°.

Table A.1: Means for Sternoclavicular Retraction Across Different Planes of Elevation (Ludewig *et al.* (2009))

Humerothoracic Elevation [°]	Coronal Plane Abduction [°]	Scapula Plane Abduction [°]	Sagittal Plane Flexion [°]
15	-27.4	-23.4	-19.0
20	-28.8	-23.1	-19.8
25	-29.8	-23.9	-20.1
30	-31.3	-24.6	-20.4
35	-32.5	-25.4	-20.8
40	-33.5	-26.1	-21.3
45	-34.7	-26.9	-21.6
50	-35.7	-27.6	-21.9
55	-36.5	-28.4	-22.3
60	-37.3	-29.0	-22.7
65	-37.9	-29.6	-23.1
70	-38.5	-30.2	-23.4
75	-39.1	-30.6	-23.8
80	-39.6	-31.1	-24.1
85	-40.1	-31.6	-24.5
90	-40.6	-32.0	-24.8
95	-41.5	-32.4	-25.3
100	-42.0	-32.8	-25.9
105	-42.6	-33.2	-26.6
110	-43.0	-33.8	-27.6
115	-43.4	-34.4	-29.6
120	-44.0	-36.4	-31.7

*Negative values indicate a retracted position.

Table A.2: Means for Sternoclavicular Elevation Across Different Planes of Elevation (Ludewig *et al.* (2009))

Humerothoracic Elevation [°]	Coronal Plane Abduction [°]	Scapula Plane Abduction [°]	Sagittal Plane Flexion [°]
15	-13.0	-10.6	-10.8
20	-13.1	-10.7	-9.8
25	-13.6	-11.0	-9.9
30	-14.3	-11.5	-10.1
35	-14.7	-12.2	-10.3
40	-15.2	-12.7	-10.5
45	-15.7	-13.2	-10.8
50	-16.1	-13.6	-11.2
55	-16.5	-14.0	-11.6
60	-16.8	-14.4	-12.0
65	-17.1	-14.7	-12.2
70	-17.3	-15.0	-12.5
75	-17.5	-15.2	-12.7
80	-17.7	-15.4	-13.0
85	-17.9	-15.5	-13.2
90	-18.1	-15.5	-13.5
95	-19.1	-15.7	-13.7
100	-19.1	-15.8	-14.0
105	-19.2	-15.8	-14.1
110	-19.3	-15.8	-14.2
115	-19.4	-15.8	-15.1
120	-19.5	-16.9	-14.5

*Negative values indicate an elevated position.

Table A.3: Means for Sternoclavicular Posterior Rotation Across Different Planes of Elevation (Ludewig *et al.* (2009))

Humerothoracic Elevation [°]	Coronal Plane Abduction [°]	Scapula Plane Abduction [°]	Sagittal Plane Flexion [°]
15	1.3	0.7	-1.3
20	1.3	1.0	-0.9
25	1.9	1.4	-0.6
30	3.1	1.9	0.0
35	4.0	2.6	0.9
40	4.9	3.6	1.9
45	5.9	4.7	2.8
50	6.9	5.8	4.0
55	7.7	7.0	5.3
60	8.6	8.2	6.6
65	9.6	9.4	7.8
70	10.7	10.5	9.0
75	11.8	11.6	10.2
80	13.0	12.8	11.5
85	14.4	14.0	12.8
90	15.8	15.2	14.1
95	16.6	16.5	15.5
100	18.2	17.9	17.1
105	19.9	19.5	19.0
110	21.5	21.2	21.1
115	23.1	22.9	22.8
120	24.8	24.3	25.0

*Negative values indicate an anteriorly rotated position.

A.2 Scapulothoracic Motion

All rotations of the scapula are relative to the thorax, are about the AC and SC joints, and occur around the three axes of the TCS (section 2.1.3). Internal/external rotation is around the superior axis, upward/downward rotation is around the anterior axis, and anterior/posterior tilting is around the lateral axis of the TCS. Figure A.2 depicts the directions for internal rotation (a), upward rotation (b) and posterior tilting (c), respectively.

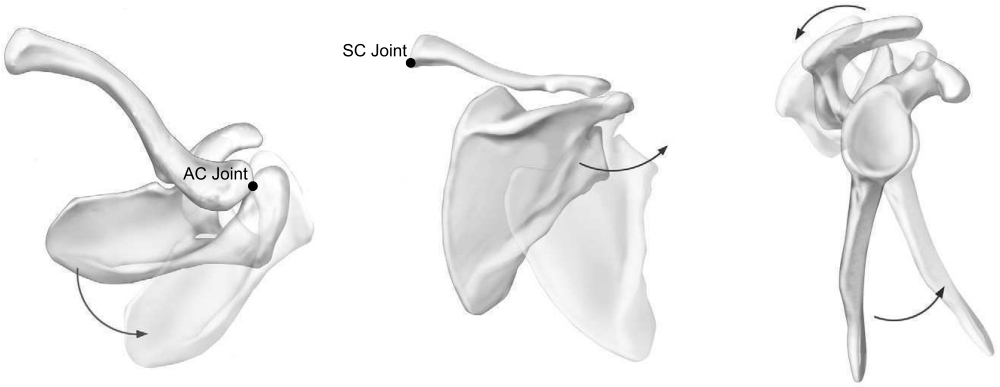

(a) Internal Rotation (b) Upward Rotation (c) Posterior Tilting

Figure A.2: Rotation of the Scapula (Illustration: Ludewig *et al.* (2009))

The scapulothoracic angular rotation values for the coronal, scapula and sagittal plane elevation are shown in Table A.4 - A.6. The values shown are for the humerothoracic elevation range of 15° - 120°.

Table A.4: Means for Scapulothoracic Internal Rotation Across Different Planes of Elevation (Ludewig *et al.* (2009))

Humerothoracic Elevation [°]	Coronal Plane Abduction [°]	Scapula Plane Abduction [°]	Sagittal Plane Flexion [°]
15	31.3	37.0	42.8
20	31.0	38.1	43.2
25	31.3	38.3	43.8
30	31.2	38.5	44.3
35	31.2	38.6	44.8
40	31.0	38.7	45.2
45	30.9	38.7	45.6
50	30.8	38.7	46.1
55	30.6	38.7	46.5
60	30.5	38.8	46.7
65	30.5	38.8	47.0
70	30.5	38.9	47.2
75	30.6	38.9	47.4
80	30.6	39.0	47.5
85	30.6	39.0	47.7
90	30.8	39.0	47.8
95	30.5	39.1	47.9
100	30.5	39.1	47.7
105	30.6	39.1	47.4
110	30.8	38.9	46.8
115	30.8	38.6	45.2
120	30.6	37.2	43.5

Table A.5: Means for Scapulothoracic Upward Rotation Across Different Planes of Elevation (Ludewig *et al.* (2009))

Humerothoracic Elevation [°]	Coronal Plane Abduction [°]	Scapula Plane Abduction [°]	Sagittal Plane Flexion [°]
15	-10.9	-10.3	-11.7
20	-12.0	-11.9	-12.6
25	-13.5	-13.6	-13.8
30	-15.6	-15.5	-15.1
35	-17.5	-17.3	-16.6
40	-19.2	-19.1	-18.1
45	-21.1	-20.9	-19.6
50	-22.9	-22.7	-21.3
55	-24.7	-24.3	-22.9
60	-26.5	-26.0	-24.4
65	-28.2	-27.5	-25.9
70	-29.9	-29.0	-27.3
75	-31.5	-30.5	-28.7
80	-33.1	-31.8	-30.1
85	-34.8	-33.1	-31.4
90	-36.5	-34.4	-32.9
95	-38.3	-35.7	-34.3
100	-40.0	-37.1	-35.9
105	-41.7	-38.6	-37.4
110	-43.4	-40.1	-39.1
115	-44.9	-41.6	-41.0
120	-46.4	-43.5	-43.3

*Negative values indicate an upwardly rotated position.

Table A.6: Means for Scapulothoracic Posterior Tilting Across Different Planes of Elevation (Ludewig *et al.* (2009))

Humerothoracic Elevation [°]	Coronal Plane Abduction [°]	Scapula Plane Abduction [°]	Sagittal Plane Flexion [°]
15	-13.7	-13.0	-12.2
20	-11.9	-12.7	-11.9
25	-11.3	-11.8	-11.2
30	-10.2	-11.2	-10.4
35	-9.5	-10.5	-9.6
40	-8.8	-9.8	-8.7
45	-8.1	-9.0	-8.0
50	-7.4	-8.3	-7.2
55	-6.7	-7.5	-6.5
60	-6.1	-6.8	-5.7
65	-5.5	-6.1	-5.0
70	-4.8	-5.5	-4.3
75	-4.2	-4.9	-3.6
80	-3.5	-4.2	-2.8
85	-2.8	-3.6	-2.1
90	-2.1	-2.8	-1.4
95	-0.6	-2.2	-0.6
100	0.2	-1.5	0.2
105	1.1	-0.7	1.1
110	2.1	0.2	2.1
115	2.9	1.3	4.0
120	3.8	2.7	5.4

*Negative values indicate an anteriorly rotated position.

A.3 Shoulder Complex Motion Equations

The average sternoclavicular and scapulothoracic motion data from Section A.1 and A.2 is contained in Figures A.3 - A.5. Figure A.3 shows the motion data for the coronal elevation plane, Figure A.4 shows the motion data for the scapula elevation plane and Figure A.5 shows the motion data for the sagittal elevation plane. The best fit line, as well as the R^2 values are also shown on each graph. The motion equations (best fit lines) for the different elevation planes are given below.

Coronal Elevation Plane:

Sternoclavicular Motion:

$$y_{PR_a} = -1\text{E-}05x^3 + 0.00290x^2 - 0.390x - c_1 \quad (A.1)$$
$$y_{ED_a} = 4\text{E-}04x^2 - 0.113x - c_2 \quad (A.2)$$
$$y_{APR_a} = 9\text{E-}04x^2 + 0.0961x - c_3 \quad (A.3)$$

Scapulothoracic Motion:

$$y_{IER_a} = 2\text{E-}04x^2 - 0.0272x + c_{10} \quad (A.4)$$
$$y_{UDR_a} = -0.345x - c_{11} \quad (A.5)$$
$$y_{APT_a} = 2\text{E-}04x^2 + 0.130x - c_{12} \quad (A.6)$$

Scapula Elevation Plane:

Sternoclavicular Motion:

$$y_{PR_b} = -5\text{E-}06x^3 + 0.00120x^2 - 0.204x - c_4 \quad (A.7)$$
$$y_{ED_b} = 5\text{E-}04x^2 - 0.130x - c_5 \quad (A.8)$$
$$y_{APR_b} = 0.001x^2 + 0.102x - c_6 \quad (A.9)$$

Scapulothoracic Motion:

$$y_{IER_b} = -2\text{E-}04x^2 + 0.0313x + c_{13} \quad (A.10)$$
$$y_{UDR_b} = 6\text{E-}04x^2 - 0.386x - c_{14} \quad (A.11)$$
$$y_{APT_b} = 2\text{E-}04x^2 + 0.121x - c_{15} \quad (A.12)$$

Sagittal Elevation Plane:

Sternoclavicular Motion:

$$y_{PR_c} = -4\text{E-}07x^4 + 9\text{E-}05x^3 - 0.00650x^2 + 0.105x - c_7 \quad (A.13)$$
$$y_{ED_c} = -7\text{E-}05x^2 - 0.0407x - c_8 \quad (A.14)$$
$$y_{APR_c} = 0.00130x^2 + 0.0822x - c_9 \quad (A.15)$$

Scapulothoracic Motion:

$$y_{IER_c} = -2\text{E-}05x^3 + 0.00250x^2 - 0.0129x + c_{16} \quad \text{(A.16)}$$

$$y_{UDR_c} = -2\text{E-}04x^2 - 0.265x - c_{17} \quad \text{(A.17)}$$

$$y_{APT_c} = 4\text{E-}04x^2 + 0.111x - c_{18} \quad \text{(A.18)}$$

Definitions:

y_{PR}: Sternoclavicular protraction/retraction in degrees at a given humerothoracic elevation.

y_{ED}: Sternoclavicular elevation/depression in degrees at a given humerothoracic elevation.

y_{APR}: Sternoclavicular anterior/posterior in degrees at a given humerothoracic elevation.

y_{IER}: Scapulothoracic internal/external rotation in degrees at a given humerothoracic elevation.

y_{UDR}: Scapulothoracic upward/downward rotation in degrees at a given humerothoracic elevation.

y_{APT}: Scapulothoracic anterior/posterior tilting in degrees at a given humerothoracic elevation.

a: Coronal elevation plane.

b: Scapula elevation plane.

c: Sagittal elevation plane.

x: Humerothoracic elevation ranging from $0\,^\circ$ to $120\,^\circ$.

$c_1 - c_{18}$: Motion values at resting position, with $0\,^\circ$ humerothoracic elevation.

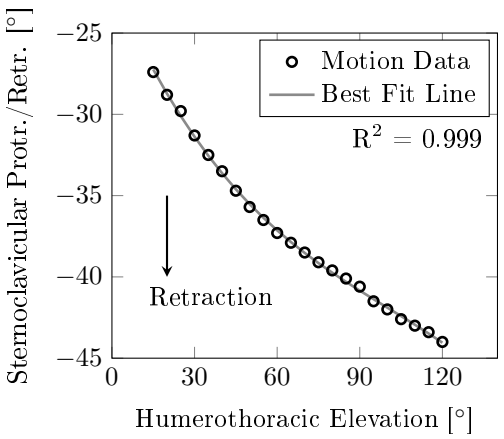

(a) Sternoclavicular Protraction/Retraction Data and Best Fit Line

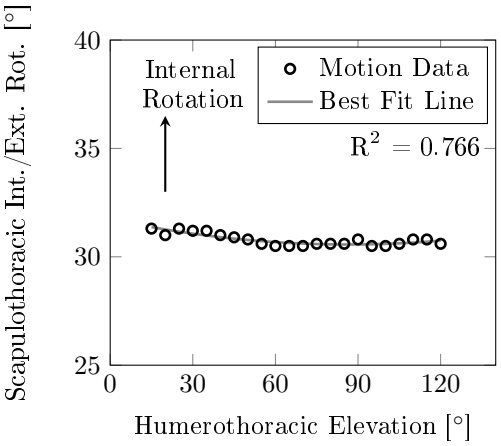

(b) Scapulothoracic Internal/External Rotation Data and Best Fit Line

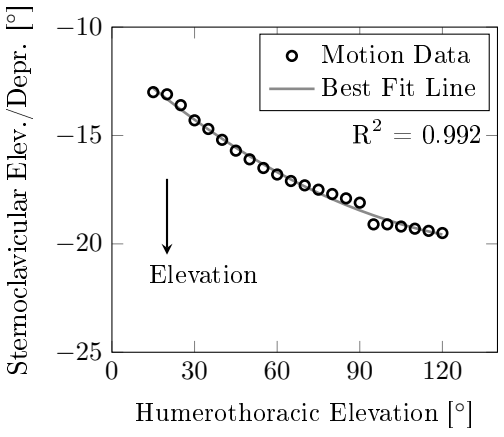

(c) Sternoclavicular Elevation/Depression Data and Best Fit Line

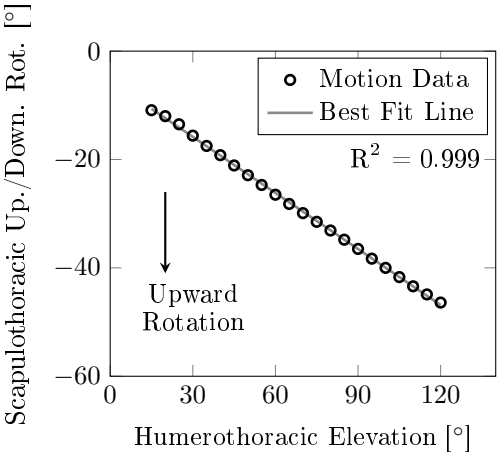

(d) Scapulothoracic Upward/Downward Rotation Data and Best Fit Line

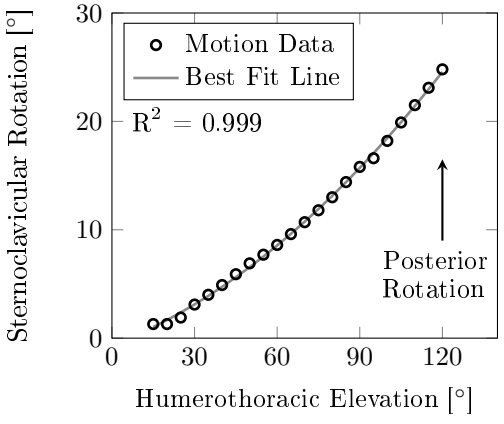

(e) Sternoclavicular Anterior/Posterior Rotation Data and Best Fit Line

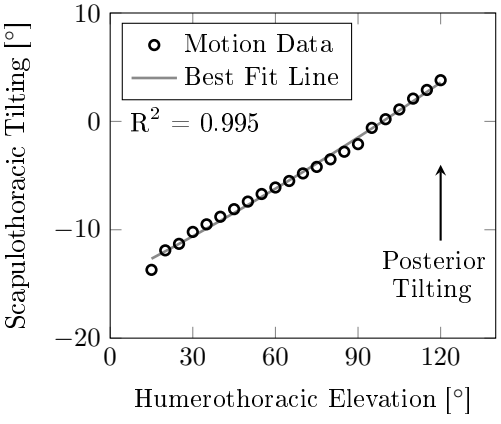

(f) Scapulothoracic Anterior/Posterior Tilting Data and Best Fit Line

Figure A.3: Coronal Plane Elevation - Sternoclavicular and Scapulothoracic Motion

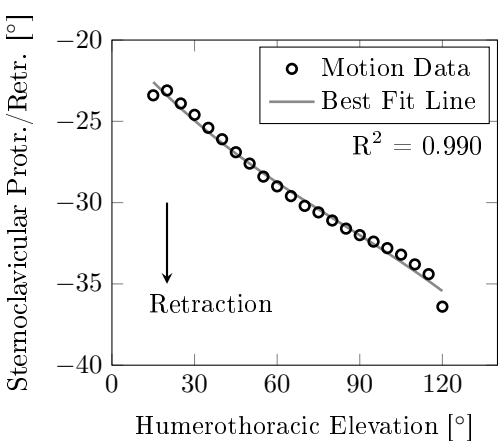

(a) Sternoclavicular Protraction/Retraction Data and Best Fit Line

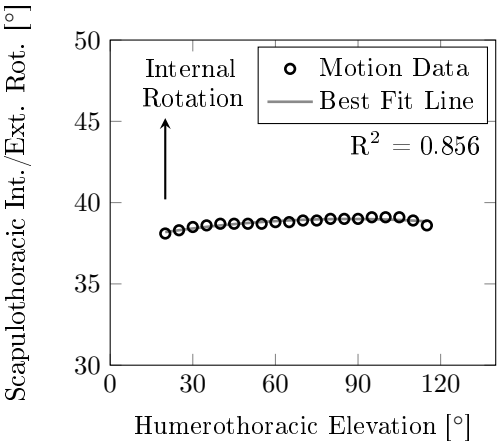

(b) Scapulothoracic Internal/External Rotation Data and Best Fit Line

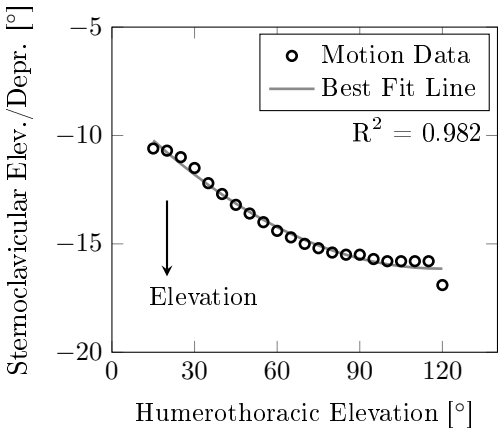

(c) Sternoclavicular Elevation/Depression Data and Best Fit Line

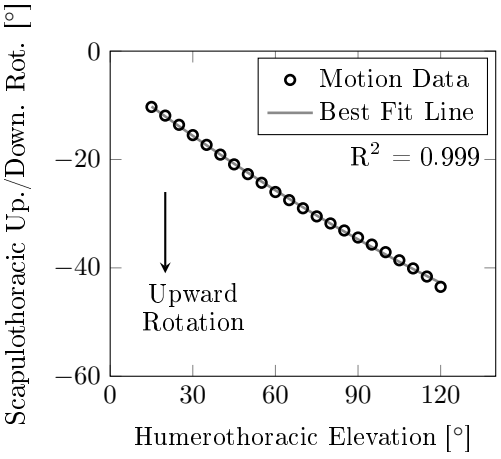

(d) Scapulothoracic Upward/Downward Rotation Data and Best Fit Line

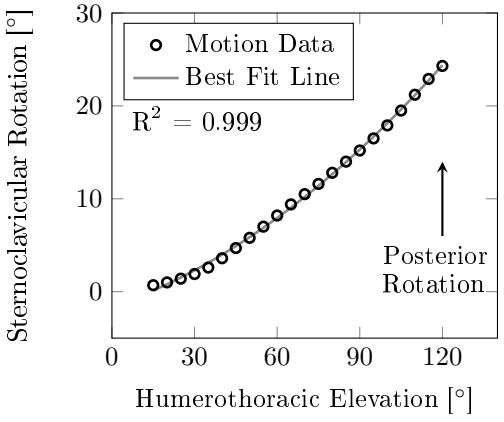

(e) Sternoclavicular Anterior/Posterior Rotation Data and Best Fit Line

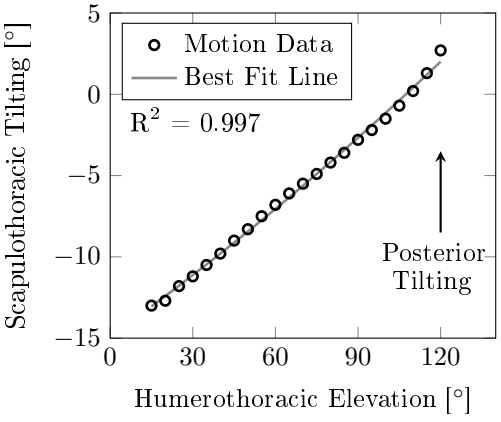

(f) Scapulothoracic Anterior/Posterior Tilting Data and Best Fit Line

Figure A.4: Scapula Plane Elevation - Sternoclavicular and Scapulothoracic Motion

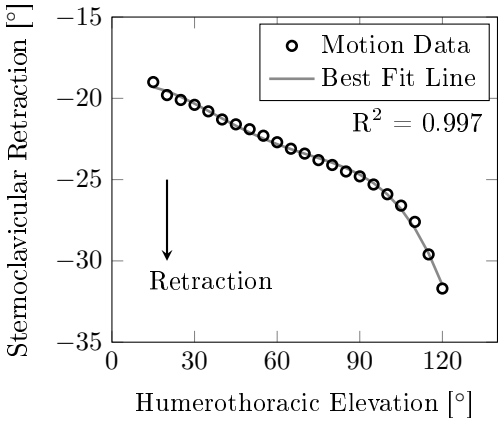

(a) Sternoclavicular Protraction/Retraction Data and Best Fit Line

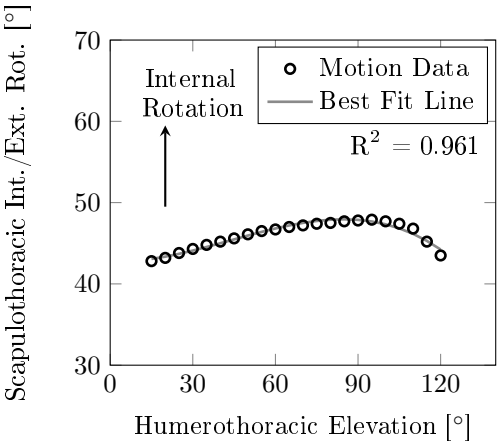

(b) Scapulothoracic Internal/External Rotation Data and Best Fit Line

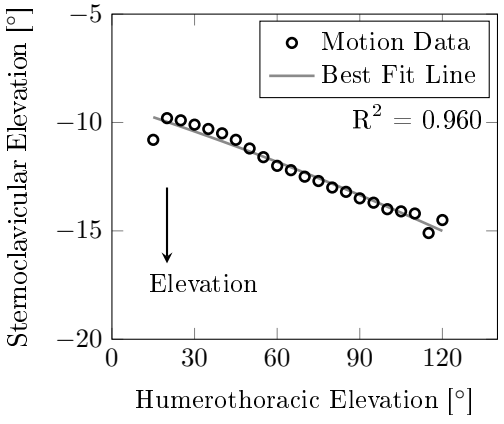

(c) Sternoclavicular Elevation/Depression Data and Best Fit Line

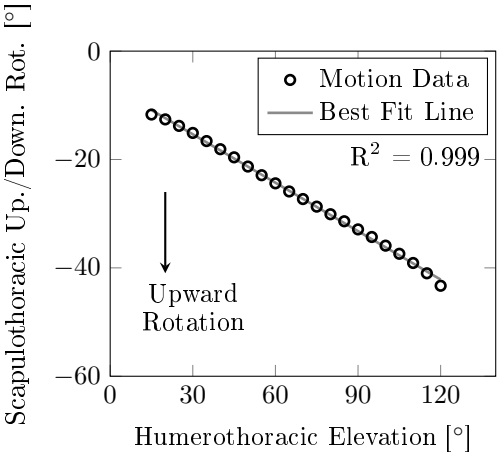

(d) Scapulothoracic Upward/Downward Rotation Data and Best Fit Line

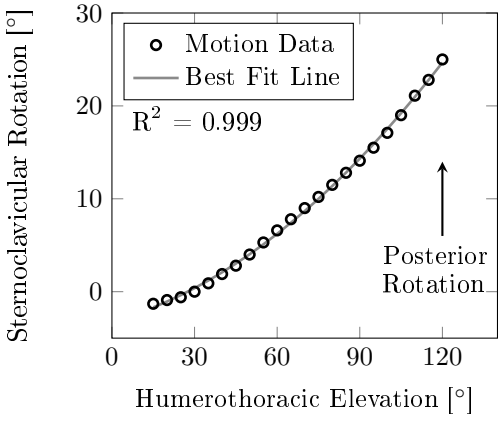

(e) Sternoclavicular Anterior/Posterior Rotation Data and Best Fit Line

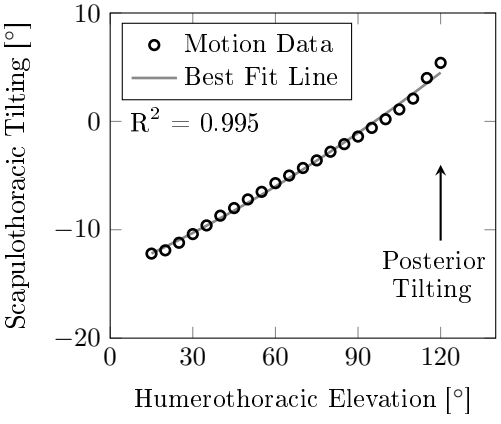

(f) Scapulothoracic Anterior/Posterior Tilting Data and Best Fit Line

Figure A.5: Sagittal Plane Elevation - Sternoclavicular and Scapulothoracic Motion

B. Reverse Shoulder Simulation Software Data

This section contains the data obtained from the RS^3 for different component combinations, varying glenoid component inclination angles (φ) and varying humeral component retroversion angles (ψ).

Appendix B.1 contains the upper and lower boundary averages and standard deviations for ψ ranging from 0° to 50° for the simulations of the Aequalis® - Reversed II system. Appendix B.2 contains the simulation data for the glenosphere and humeral component neck-shaft angle design changes.

B.1 Aequalis® - Reversed II System

The 25 mm baseplate and 36 mm glenosphere (concentric) placement for the different φ is shown in Figure B.1.

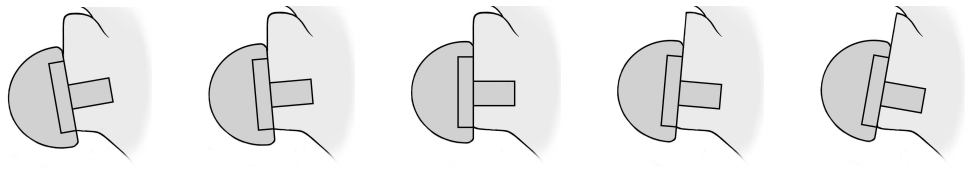

(a) -10° (b) -5° (c) 0° (d) 5° (e) 10°

Figure B.1: Glenoid Component Inclination (φ)

The simulation data for the 36 mm and 42 mm glenospheres is contained in Tables B.1 - B.4. For each table a corresponding figure (Figures B.2 - B.5) illustrates the data graphically.

Table B.1: Simulation Data for the 36 mm Glenosphere (concentric) for Different Elevation Planes and φ

	Coronal Plane		Scapula Plane		Sagittal Plane	
φ	LB [°]	UB [°]	LB [°]	UB [°]	LB [°]	UB [°]
25 mm Baseplate; 6 mm Polyethylene Insert (concentric)						
-10	63.6 ± 1.7	117.7 ± 5.1	19.0 ± 6.4	120	6.5 ± 3.1	61.9 ± 8.9
-5	57.8 ± 2.4	119.7 ± 1.2	13.4 ± 5.8	120	5.7 ± 3.5	61.9 ± 11.5
0	52.9 ± 3.3	120	8.0 ± 6.0	120	4.2 ± 3.9	66.1 ± 15.9
5	47.9 ± 4.3	120	4.5 ± 5.0	120	3.3 ± 4.1	70.5 ± 19.9
10	43.2 ± 5.3	120	2.5 ± 3.7	120	3.6 ± 4.8	77.0 ± 24.2
25 mm Baseplate; 6 mm Polyethylene Insert (2 mm inferior eccentric)						
-10	62.2 ± 1.9	117.9 ± 4.7	16.0 ± 7.2	120	5.0 ± 3.6	61.2 ± 8.4
-5	55.7 ± 3.1	120	9.7 ± 6.8	120	4.0 ± 4.4	60.5 ± 11.3
0	50.0 ± 4.1	120	4.9 ± 5.7	120	3.0 ± 4.3	64.9 ± 13.8
5	43.9 ± 5.9	120	2.5 ± 3.8	120	2.9 ± 4.3	69.6 ± 18.1
10	37.1 ± 10.5	120	1.1 ± 2.3	120	3.5 ± 4.8	76.1 ± 21.6
29 mm Baseplate; 6 mm Polyethylene Insert (concentric)						
-10	78.9 ± 1.7	119.3 ± 2.0	45.3 ± 2.9	120	18.1 ± 3.6	56.2 ± 4.0
-5	73.3 ± 1.9	120	36.2 ± 3.8	120	15.6 ± 4.4	60.7 ± 5.4
0	67.4 ± 2.2	120	30.0 ± 3.8	120	16.0 ± 5.2	63.3 ± 6.8
5	62.5 ± 2.5	120	24.7 ± 3.8	120	15.6 ± 5.7	69.5 ± 8.9
10	58.9 ± 4.0	120	21.0 ± 3.6	120	16.4 ± 6.3	75.6 ± 10.8
29 mm Baseplate; 6 mm Polyethylene Insert (2 mm inferior eccentric)						
-10	78.6 ± 2.0	119.3 ± 1.8	45.2 ± 2.8	120	18.0 ± 3.6	57.6 ± 3.3
-5	73.2 ± 2.0	120	35.9 ± 3.7	120	15.5 ± 4.3	61.8 ± 4.4
0	67.4 ± 2.7	120	29.7 ± 3.5	120	16.0 ± 5.1	64.1 ± 5.5
5	62.8 ± 2.8	120	24.3 ± 3.7	120	15.6 ± 5.7	68.8 ± 6.9
10	58.8 ± 3.6	120	20.7 ± 3.4	120	16.3 ± 6.3	74.0 ± 8.8

LB - Lower Boundary (adduction deficit)
UB - Upper Boundary
Humerothoracic ROM = UB - LB

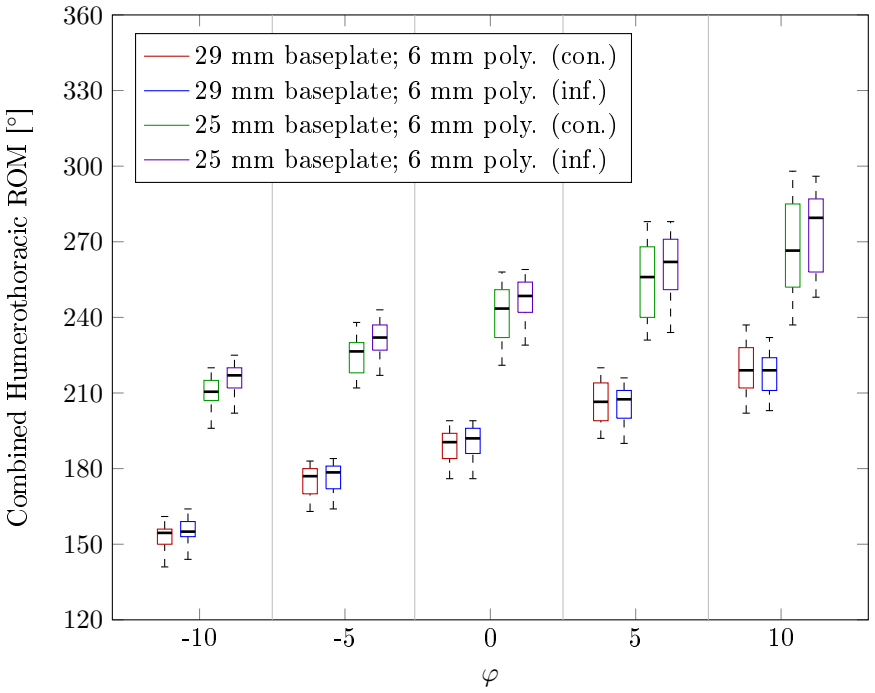

(a) Humerothoracic ROM

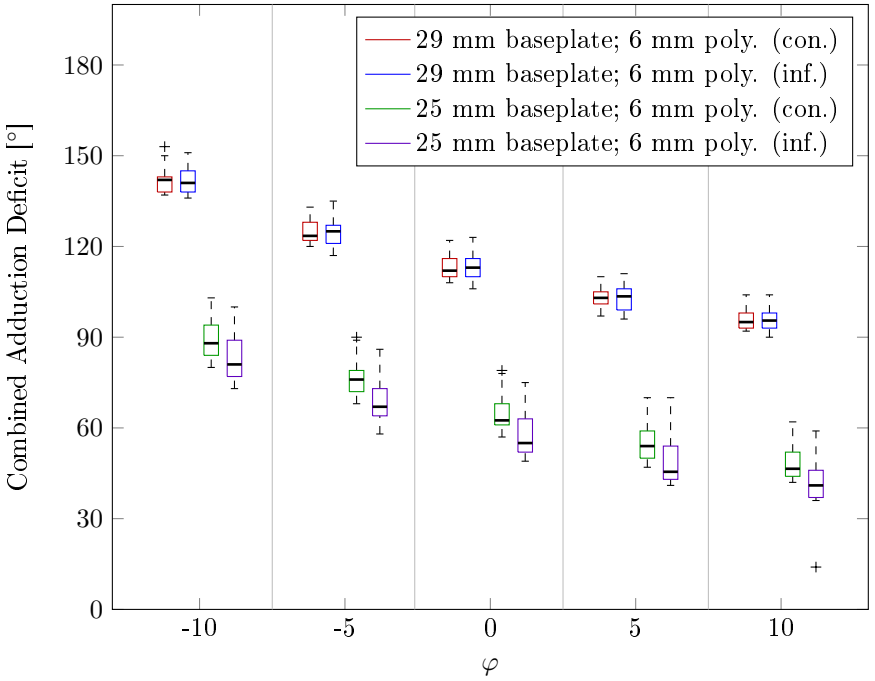

(b) Adduction Deficit

Figure B.2: 36 mm Glenosphere (concentric) - Humerothoracic ROM and Adduction Deficit

Table B.2: Humerothoracic ROM for the 36 mm Glenosphere (4 mm inferior eccentric) for Different Elevation Planes and φ

	Coronal Plane		Scapula Plane		Sagittal Plane	
φ	LB [°]	UB [°]	LB [°]	UB [°]	LB [°]	UB [°]
25 mm Baseplate; 6 mm Polyethylene Insert (concentric)						
-10	51.2 ± 11.4	101.3 ± 16.6	1.5 ± 3.3	120	0.3 ± 1.0	51.5 ± 3.9
-5	38.3 ± 17.2	109.3 ± 13.8	0.4 ± 1.3	120	0.2 ± 0.5	54.7 ± 5.4
0	27.1 ± 20.0	114.5 ± 10.0	0	120	0	60.8 ± 9.5
5	19.7 ± 17.9	118.1 ± 4.6	0	120	0	69.3 ± 14.3
10	12.8 ± 15.7	120	0	120	0	77.3 ± 24.3
25 mm Baseplate; 6 mm Polyethylene Insert (2 mm inferior eccentric)						
-10	50.0 ± 15.3	101.1 ± 16.6	1.5 ± 3.6	120	0.1 ± 0.4	62.8 ± 6.7
-5	35.8 ± 18.7	109.5 ± 13.4	0.2 ± 0.8	120	0	64.0 ± 8.5
0	22.7 ± 19.4	115.2 ± 9.2	0	120	0	68.5 ± 11.9
5	14.3 ± 16.3	119.3 ± 2.6	0	120	0	73.3 ± 17.7
10	8.5 ± 12.5	120	0	120	0	80.8 ± 24.6
29 mm Baseplate; 6 mm Polyethylene Insert (concentric)						
-10	68.4 ± 1.2	109.0 ± 12.6	23.2 ± 6.5	120	6.2 ± 2.7	59.2 ± 3.6
-5	62.3 ± 2.0	112.8 ± 10.1	13.8 ± 7.1	120	3.5 ± 2.6	65.1 ± 5.9
0	54.5 ± 3.0	118.7 ± 3.4	7.0 ± 6.3	120	2.6 ± 3.3	68.0 ± 9.0
5	47.3 ± 4.7	120	2.9 ± 4.1	120	1.8 ± 2.9	73.6 ± 14.0
10	38.7 ± 10.1	120	1.0 ± 2.0	120	1.6 ± 2.8	81.5 ± 20.4
29 mm Baseplate; 6 mm Polyethylene Insert (2 mm inferior eccentric)						
-10	67.5 ± 1.7	108.7 ± 12.8	20.4 ± 8.3	120	4.3 ± 3.2	60.6 ± 3.5
-5	60.4 ± 2.5	113.0 ± 10.7	9.8 ± 8.1	120	1.8 ± 3.2	65.8 ± 5.7
0	51.4 ± 4.2	118.8 ± 3.9	4.5 ± 5.7	120	1.8 ± 3.2	66.9 ± 10.1
5	41.7 ± 10.6	120	1.4 ± 2.9	120	1.5 ± 2.8	72.5 ± 13.9
10	30.8 ± 15.0	120	0.3 ± 1.0	120	1.3 ± 2.6	79.5 ± 17.5

LB - Lower Boundary (adduction deficit)
UB - Upper Boundary
Humerothoracic ROM = UB - LB

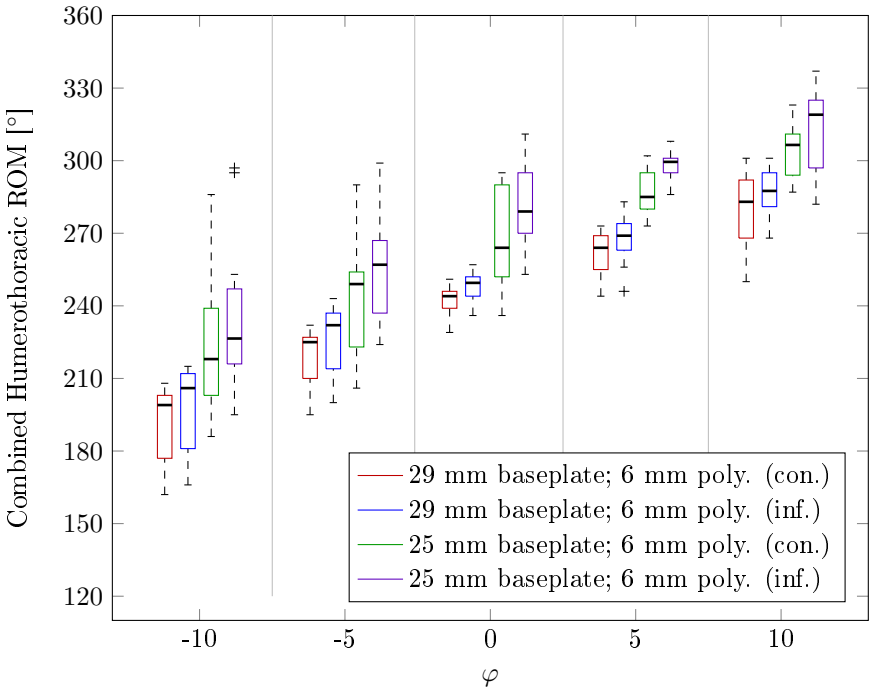

(a) Humerothoracic ROM

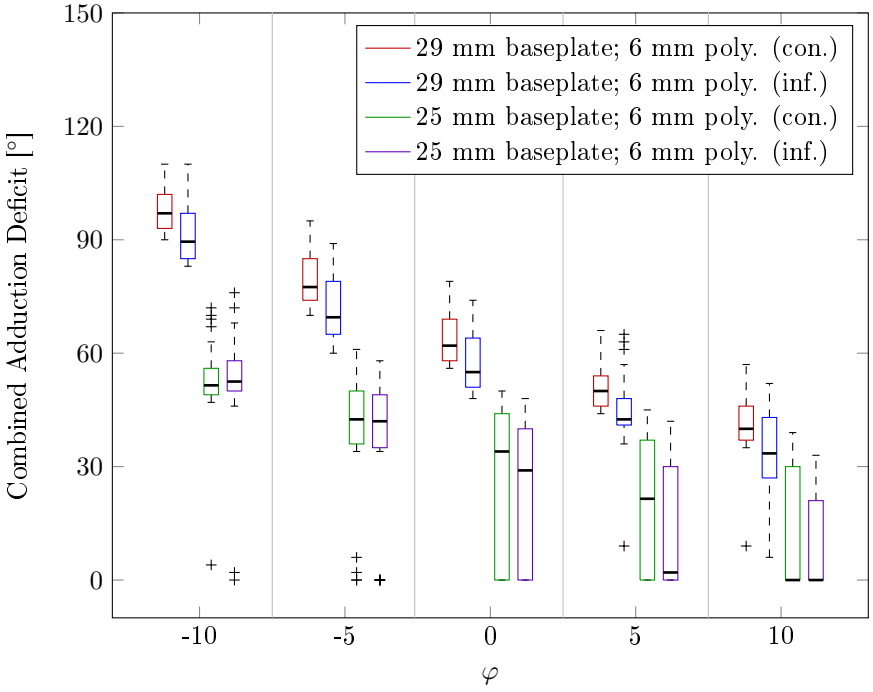

(b) Adduction Deficit

Figure B.3: 36 mm Glenosphere (4 mm inferior eccentric) - Humerothoracic ROM and Adduction Deficit

Table B.3: Humerothoracic ROM for 36 mm Glenosphere (3 mm lateral eccentric) for Different Elevation Planes and φ

	Coronal Plane		Scapula Plane		Sagittal Plane	
φ	LB [°]	UB [°]	LB [°]	UB [°]	LB [°]	UB [°]
25 mm Baseplate; 6 mm Polyethylene Insert (concentric)						
-10	49.2 ± 4.4	120	3.8 ± 4.9	120	2.3 ± 3.4	72.8 ± 15.0
-5	42.0 ± 5.5	120	2.2 ± 3.2	120	3.0 ± 4.3	80.6 ± 18.9
0	34.4 ± 10.5	120	0.8 ± 1.8	120	3.4 ± 4.8	92.5 ± 18.0
5	26.3 ± 15.1	120	0.2 ± 0.9	120	4.2 ± 5.6	103.4 ± 14.4
10	22.0 ± 15.1	120	0.1 ± 0.6	120	6.2 ± 6.9	110.6 ± 10.7
25 mm Baseplate; 6 mm Polyethylene Insert (2 mm inferior eccentric)						
-10	45.0 ± 6.2	120	2.2 ± 3.6	120	2.1 ± 3.6	71.2 ± 13.1
-5	34.8 ± 12.6	120	0.7 ± 1.9	120	2.9 ± 4.4	77.5 ± 16.6
0	25.8 ± 15.3	120	0.1 ± 0.6	120	3.5 ± 5.0	88.8 ± 18.3
5	19.6 ± 16.1	120	0	120	4.3 ± 5.8	98.2 ± 16.3
10	17.3 ± 14.9	120	0	120	6.3 ± 7.0	104.7 ± 14.4
29 mm Baseplate; 6 mm Polyethylene Insert (concentric)						
-10	64.5 ± 3.3	120	24.1 ± 4.1	120	15.1 ± 5.5	69.5 ± 10.0
-5	60.0 ± 4.2	120	19.7 ± 4.1	120	14.3 ± 6.1	77.0 ± 11.9
0	54.5 ± 4.4	120	16.7 ± 3.3	120	16.7 ± 6.8	82.3 ± 14.4
5	50.7 ± 5.4	120	14.7 ± 2.7	120	19.4 ± 6.7	91.6 ± 15.9
10	49.0 ± 6.8	120	15.2 ± 1.9	120	24.8 ± 7.1	98.7 ± 15.8
29 mm Baseplate; 6 mm Polyethylene Insert (2 mm inferior eccentric)						
-10	64.8 ± 3.9	120	23.6 ± 3.8	120	15.1 ± 5.5	69.0 ± 8.2
-5	59.9 ± 3.8	120	19.5 ± 4.1	120	14.3 ± 6.1	75.5 ± 9.5
0	54.6 ± 5.0	120	16.8 ± 3.2	120	16.7 ± 6.8	79.3 ± 11.9
5	50.3 ± 5.1	120	14.7 ± 2.7	120	19.3 ± 6.8	87.0 ± 13.8
10	48.0 ± 6.6	120	15.3 ± 2.0	120	24.7 ± 7.1	93.8 ± 15.1

LB - Lower Boundary (adduction deficit)
UB - Upper Boundary
Humerothoracic ROM = UB - LB

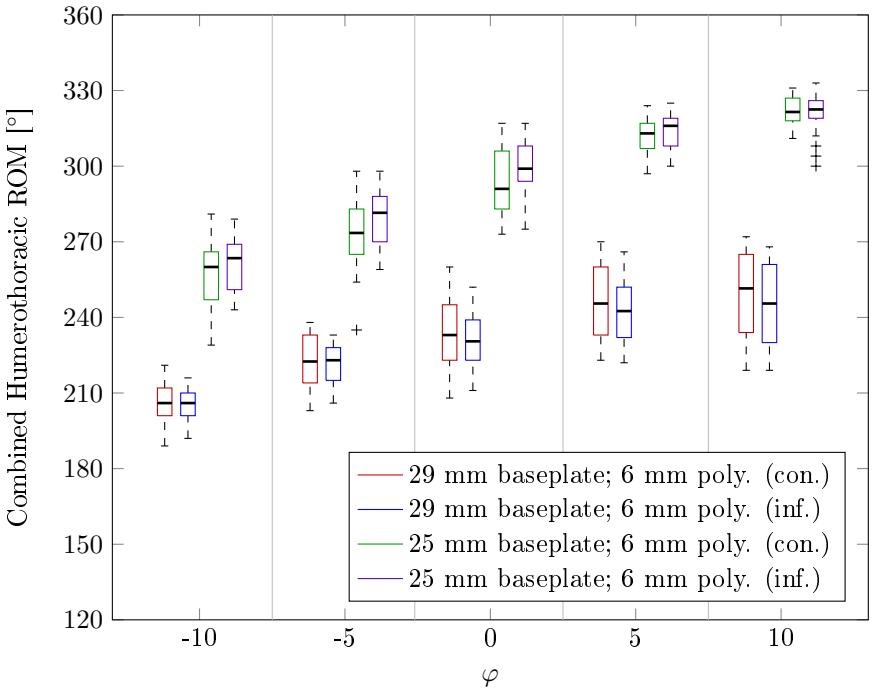

(a) Humerothoracic ROM

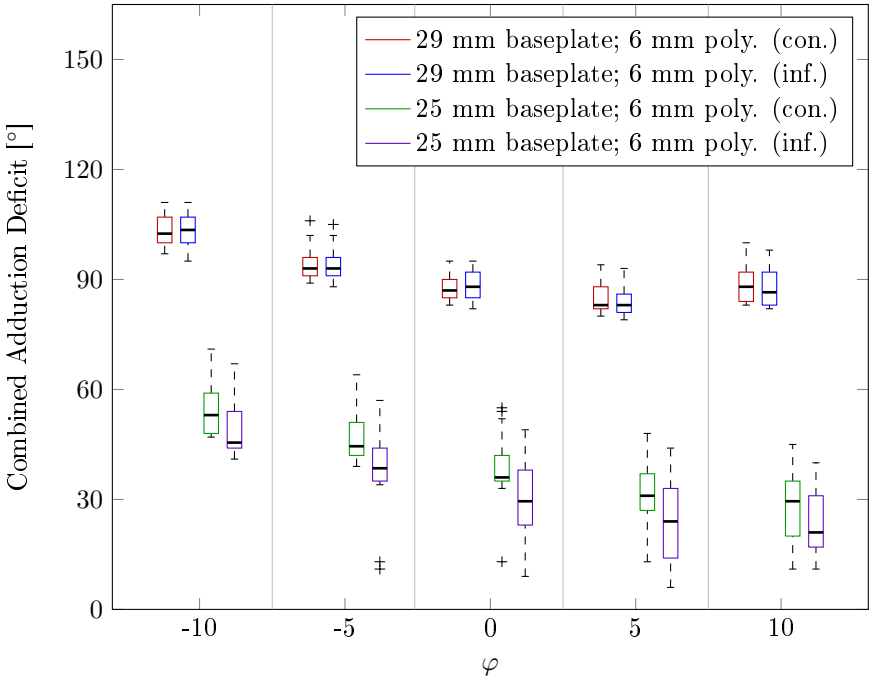

(b) Adduction Deficit

Figure B.4: 36 mm Glenosphere (3 mm lateral eccentric) - Humerothoracic ROM and Adduction Deficit

Table B.4: Humerothoracic ROM for 42 mm Glenospheres for Different Elevation Planes and φ

	Coronal Plane		Scapula Plane		Sagittal Plane	
φ	LB [°]	UB [°]	LB [°]	UB [°]	LB [°]	UB [°]
42 mm Glenosphere (concentric); 25 mm Baseplate						
-10	46.2 ± 3.8	120	1.8 ± 3.6	120	0.1 ± 0.4	88.3 ± 7.4
-5	34.8 ± 13.8	120	0.5 ± 1.7	120	0.2 ± 0.5	93.0 ± 9.6
0	26.2 ± 16.0	120	0.1 ± 0.6	120	0	99.8 ± 10.8
5	19.0 ± 16.1	120	0	120	0	106.3 ± 10.1
10	14.2 ± 14.4	120	0	120	0	111.2 ± 8.3
42 mm Glenosphere (concentric); 29 mm Baseplate						
-10	58.6 ± 1.2	120	18.0 ± 6.3	120	4.5 ± 2.9	77.2 ± 5.5
-5	53.8 ± 1.8	120	10.7 ± 7.4	120	2.2 ± 3.2	83.2 ± 7.0
0	48.1 ± 2.8	120	6.6 ± 6.1	120	2.2 ± 3.3	87.3 ± 8.4
5	43.3 ± 3.6	120	3.6 ± 4.7	120	1.7 ± 3.0	94.3 ± 10.5
10	38.7 ± 4.9	120	1.8 ± 3.1	120	1.7 ± 2.9	100.8 ± 11.2
42 mm Glenosphere (4 mm inferior eccentric); 25 mm Baseplate						
-10	14.7 ± 17.2	120	0	120	0	80.5 ± 9.5
-5	7.7 ± 12.5	120	0	120	0	86.5 ± 12.7
0	3.5 ± 8.1	120	0	120	0	98.2 ± 13.7
5	1.7 ± 5.0	120	0	120	0	108.1 ± 10.8
10	0.5 ± 2.5	120	0	120	0	115.8 ± 6.0
42 mm Glenosphere (4 mm inferior eccentric); 29 mm Baseplate						
-10	49.9 ± 3.4	120	2.3 ± 4.0	120	0.2 ± 0.7	80.4 ± 5.6
-5	35.4 ± 17.9	120	0.3 ± 1.0	120	0	88.2 ± 7.2
0	25.3 ± 18.1	120	0	120	0	94.8 ± 9.3
5	17.4 ± 16.4	120	0	120	0	103.9 ± 10.1
10	11.8 ± 13.9	120	0	120	0	111.2 ± 8.1
42 mm Glenosphere (3 mm lateral eccentric); 25 mm Baseplate						
-10	19.5 ± 16.7	120	0	120	0	107.9 ± 9.2
-5	13.1 ± 13.9	120	0	120	0	111.6 ± 8.2
0	8.5 ± 11.7	120	0	120	0	115.9 ± 5.3
5	5.8 ± 9.3	120	0	120	0	118.8 ± 2.3
10	4.3 ± 7.8	120	0	120	0	120.0 ± 0.2
42 mm Glenosphere (3 mm lateral eccentric); 29 mm Baseplate						
-10	45.0 ± 3.6	120	3.9 ± 4.9	120	1.6 ± 2.9	96.1 ± 10.4
-5	39.7 ± 5.0	120	1.6 ± 3.0	120	1.2 ± 2.4	102.7 ± 10.6
0	30.6 ± 11.1	120	0.7 ± 1.6	120	1.4 ± 2.6	106.9 ± 10.4
5	23.2 ± 13.8	120	0.2 ± 0.7	120	1.9 ± 3.3	111.9 ± 8.0
10	19.2 ± 13.6	120	0	120	2.7 ± 4.1	115.8 ± 5.5

LB - Lower Boundary (adduction deficit)
UB - Upper Boundary
Humerothoracic ROM = UB - LB

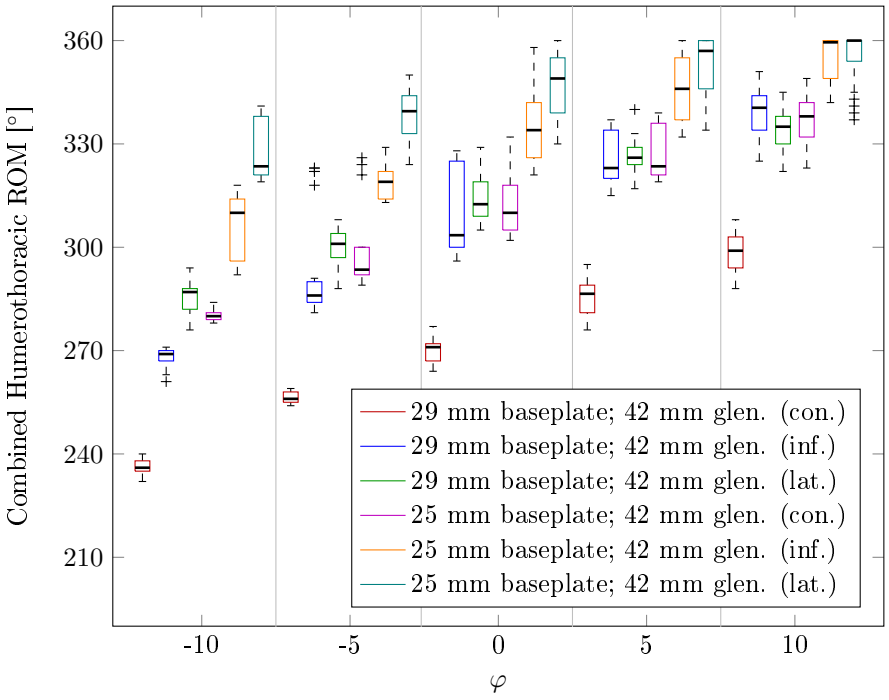

(a) Humerothoracic ROM

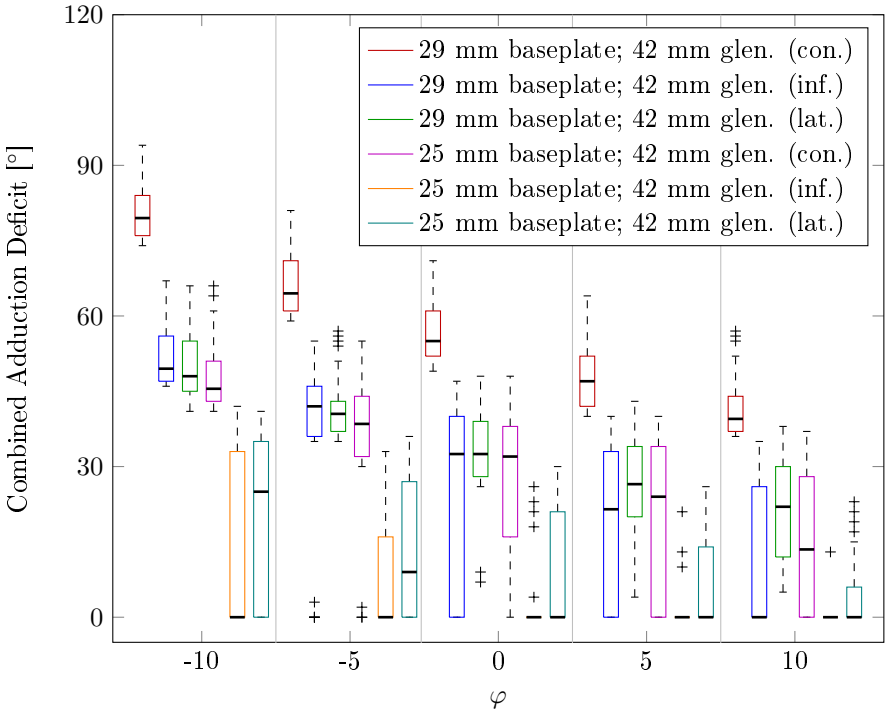

(b) Adduction Deficit

Figure B.5: 42 mm Glenospheres - Humerothoracic ROM and Adduction Deficit

B.2 Prosthesis Design Changes

The prosthesis design changes implemented were a glenosphere with 3 mm inferior and 4 mm lateral eccentricity and a humeral stem with a neck-shaft angle (γ) of 145 ° and 165 °.

B.2.1 Glenosphere Eccentricity

Table B.5 contains the simulation data for glenospheres with different eccentricities. The 36 mm and 42 mm glenospheres (inferior, lateral, inferior and lateral) were simulated with a 25 mm baseplate, a concentric polyethylene insert, at 0 ° inclination and for ψ ranging from 0 ° to 50 °.

Table B.5: Humerothoracic ROM for 36 mm and 42 mm Glenospheres with Different Eccentricities

Coronal Plane		Scapula Plane		Sagittal Plane	
LB [°]	**UB [°]**	**LB [°]**	**UB [°]**	**LB [°]**	**UB [°]**
36 mm Glenosphere (4 mm inferior eccentric)					
27.1 ± 20.0	114.5 ± 10.0	0	120	0	60.8 ± 9.5
36 mm Glenosphere (3 mm lateral eccentric)					
34.4 ± 10.5	120	0.8 ± 1.8	120	3.4 ± 4.8	92.5 ± 18.0
36 mm Glenosphere (4 mm inferior and 3 mm lateral eccentric)					
12.8 ± 15.7	120	0	120	0	87.8 ± 18.4
42 mm Glenosphere (4 mm inferior eccentric)					
3.5 ± 8.1	120	0	120	0	98.2 ± 13.7
42 mm Glenosphere (4 mm lateral eccentric)					
8.5 ± 11.7	120	0	120	0	115.9 ± 5.3
42 mm Glenosphere (4 mm inferior and 3 mm lateral eccentric)					
0.5 ± 2.5	120	0	120	0	117.2 ± 4.3

LB - Lower Boundary (adduction deficit)
UB - Upper Boundary
Humerothoracic ROM = UB - LB

B.2.2 Humeral Component Neck-shaft Angle (γ)

Table B.6 contains the simulation data for different γ. The simulations were performed with the concentric 36 mm and 42 mm glenospheres, with a 25 mm baseplate, a concentric polyethylene insert, at 0 ° inclination and for ψ ranging from 20 ° to 40 °.

Table B.6: Humerothoracic ROM for Different γ

			Coronal Plane		Scapula Plane		Sagittal Plane	
Glenosphere	γ	ψ	**LB [°]**	**UB [°]**	**LB [°]**	**UB [°]**	**LB [°]**	**UB [°]**
36 mm (concentric)	145	20	33	120	0	120	0	41
		25	30	120	0	120	0	30
		30	26	120	0	120	0	29
		35	22	120	0	120	0	28
		40	0	120	0	120	0	32
	155	20	56	120	10	120	3	56
		25	53	120	9	120	4	62
		30	53	120	9	120	4	50
		35	52	120	4	120	6	66
		40	53	120	8	120	9	58
	165	20	73	120	36	120	15	101
		25	74	120	34	120	15	96
		30	72	120	34	120	17	95
		35	74	120	32	120	17	92
		40	74	120	32	120	19	94
42 mm (concentric)	145	20	4	120	0	120	0	73
		25	0	120	0	120	0	69
		30	0	120	0	120	0	67
		35	0	120	0	120	0	65
		40	0	120	0	120	0	65
	155	20	37	120	0	120	0	100
		25	34	100	0	120	0	96
		30	31	120	0	120	0	93
		35	31	120	0	120	0	90
		40	28	120	0	120	0	88
	165	20	59	120	16	120	6	120
		25	57	120	14	120	6	120
		30	58	120	13	120	7	118
		35	57	120	12	120	7	116
		40	57	120	12	120	9	117

LB - Lower Boundary (adduction deficit)
UB - Upper Boundary
Humerothoracic ROM = UB - LB